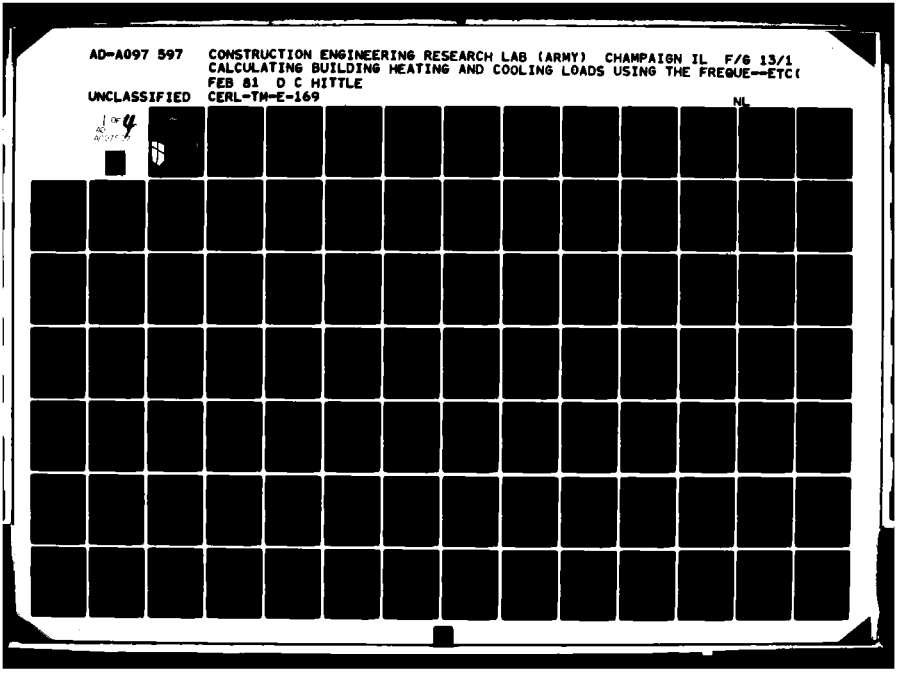
AD-A097 597 CONSTRUCTION ENGINEERING RESEARCH LAB (ARMY) CHAMPAIGN IL F/G 13/1
CALCULATING BUILDING HEATING AND COOLING LOADS USING THE FREQUE--ETC(
FEB 81 D C HITTLE
UNCLASSIFIED CERL-TM-E-169
NL

construction engineering research laboratory

United States Army Corps of Engineers
...Serving the Army
...Serving the Nation

TECHNICAL MANUSCRIPT E-169
February 1981

LEVEL II

(12)

CALCULATING BUILDING HEATING AND COOLING LOADS USING THE FREQUENCY RESPONSE OF MULTILAYERED SLABS

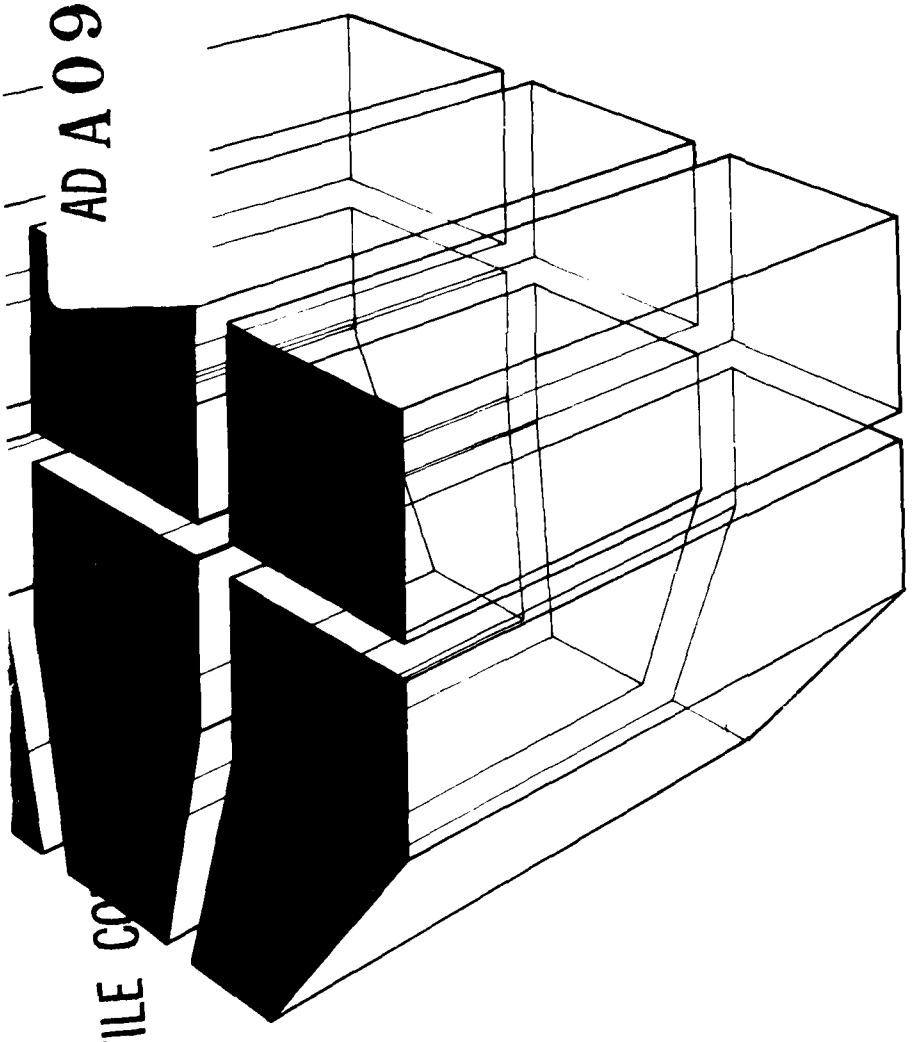

by
D. C. Hittle

CERL

Approved for public release; distribution unlimited.

UNCLASSIFIED

SECURITY CLASSIFICATION OF THIS PAGE (When Data Entered)

REPORT DOCUMENTATION PAGE

READ INSTRUCTIONS BEFORE COMPLETING FORM

1. REPORT NUMBER: CERL-TM-E-169	2. GOVT ACCESSION NO.: AD A097597
3. RECIPIENT'S CATALOG NUMBER:	
4. TITLE (and Subtitle): CALCULATING BUILDING HEATING AND COOLING LOADS USING THE FREQUENCY RESPONSE OF MULTILAYERED SLABS	5. TYPE OF REPORT & PERIOD COVERED: TECHNICAL MANUSCRIPT
	6. PERFORMING ORG. REPORT NUMBER:
7. AUTHOR(s): C. Hittle, Douglas	8. CONTRACT OR GRANT NUMBER(s):
9. PERFORMING ORGANIZATION NAME AND ADDRESS: U.S. ARMY CONSTRUCTION ENGINEERING RESEARCH LABORATORY P.O. Box 4005, Champaign, IL 61820	10. PROGRAM ELEMENT, PROJECT, TASK AREA & WORK UNIT NUMBERS: 4A761102AT43/B-013
11. CONTROLLING OFFICE NAME AND ADDRESS: 1223	12. REPORT DATE: February 1981
	13. NUMBER OF PAGES: 207
14. MONITORING AGENCY NAME & ADDRESS (if different from Controlling Office)	15. SECURITY CLASS. (of this report): Unclassified
	15a. DECLASSIFICATION/DOWNGRADING SCHEDULE

16. DISTRIBUTION STATEMENT (of this Report)
Approved for public release; distribution unlimited.

17. DISTRIBUTION STATEMENT (of the abstract entered in Block 20, if different from Report)

18. SUPPLEMENTARY NOTES
Copies are obtainable from the National Technical Information Service
Springfield, VA 22151

19. KEY WORDS (Continue on reverse side if necessary and identify by block number)
energy consumption
buildings
heating load
cooling load

20. ABSTRACT (Continue on reverse side if necessary and identify by block number)
This thesis describes the development of a method for calculating room heating and cooling loads using frequency response methods to calculate heat flow through multi-layered room walls and roofs.

Existing methods for calculating room loads are discussed and the need to consider the effects of thermal mass are emphasized. A detailed derivation of the solution of the transient one-dimensional heat conduction equation for multi-layered slabs which leads to the -

DD FORM 1 JAN 73 1473 EDITION OF 1 NOV 65 IS OBSOLETE

UNCLASSIFIED

SECURITY CLASSIFICATION OF THIS PAGE (When Data Entered)

4 5279

Block 20 continued.

calculation of response factors and conduction transfer functions is presented. Next, the special case of a fixed temperature on one side of a multi-layered slab and a sinusoidal temperature variation on the other side is examined and the simplifications which result are described. This frequency response method for calculating heat flow can be applied to buildings if the outdoor climate can be represented by a reasonably small number of sinusoidal components.

To determine the extent of sinusoidal variation in climate, time series analysis techniques were applied to hourly measured weather data from four climatically different sites in order to separate the deterministic periodic behavior in the data from its stochastic behavior. A combined deterministic plus stochastic model was found to be adequate for the climate variables studied. This model included as its deterministic component sinusoids with frequencies corresponding to the annual cycle, the diurnal cycle, and the first harmonic of the diurnal cycle.

The effect on building energy calculations of using only the sinusoidal components of climate was determined by comparing the results of energy calculations which used only sinusoidally varying climate to the results obtained when hourly measured climate data was used. Very good agreement was found.

Since ignoring the non-sinusoidal components in climate variation produced little error in calculating building energy use, frequency response methods were judged to be adequate for calculating heat flow through walls and roofs. The use of this method as part of a simplified room load-calculating procedure was compared to results from a more detailed approach, and again, very good agreement was found.

The use of this simplified method for calculating room heating and cooling loads will allow building energy analysis procedures to be implemented on microcomputers, which may enlarge the number of engineers who can use such procedures to improve the energy efficiency of their designs.

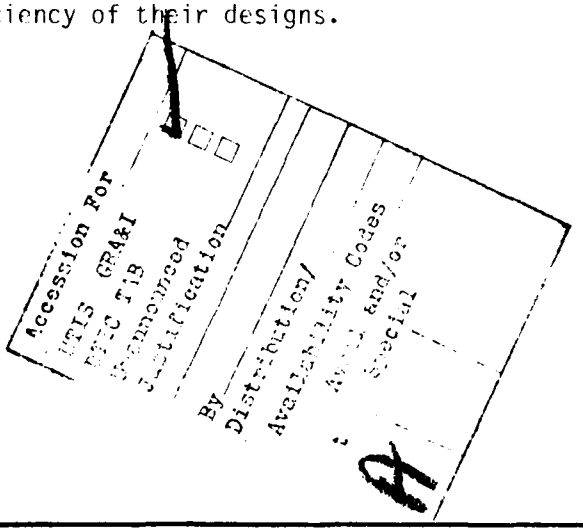

FOREWORD

This research was conducted in partial fulfillment of the requirements for the degree of Doctor of Philosophy in Mechanical Engineering at the University of Illinois at Urbana-Champaign. The work was conducted at the U.S. Army Construction Engineering Research Laboratory (CERL). The work was funded under Project 4A761102AT43, "Basic Research in Military Construction"; Task B, "Energy Systems"; Work Unit 013, "Rapid Building Energy Analysis." COL L. J. Circeo is Commander and Director of CERL, and Dr. L. R. Shaffer is Technical Director.

I wish to express my sincerest appreciation to Dr. C. O. Pedersen for his guidance during the course of this investigation and for his continuous encouragement during my pursuit of a Doctorate in Mechanical Engineering. I am also grateful to Dr. Stoecker, Dr. DeVor, Dr. Kapoor, and Dr. Kuo who served on my doctoral committee.

I am also indebted to Dr. J. J. Stukel for giving me the confidence to continue my education.

CERL made me the recipient of the Year of Advanced Study award which allowed me to pursue my education for 1 year on a fulltime basis. I will always be grateful to the management at CERL for this

award and particularly to Don Leverenz and Richard Donaghy for supporting my nomination.

I am thankful too for the editing of this thesis performed by Terry James and to the professional typing of this manuscript by CERL's Word Processing Center.

This thesis is dedicated to my wife, Anita, whose valuable support made this work possible.

CONTENTS

FIGURES

FIGURES (Cont'd)

FIGURES (Cont'd)

FIGURES (Cont'd)

FIGURES (Cont'd)

TABLES

TABLES (Cont'd)

TABLES (Cont'd)

1 INTRODUCTION

Background

In the past, designers of heating and cooling systems for buildings have focused on two main objectives: (1) insuring comfort in the air-conditioned space, and (2) minimizing the first cost of building mechanical systems. A third, often unstated, objective was (and is) that the designer earn a respectable wage for performing the design task. Furthermore, the designer of building mechanical systems has usually worked under the constraint that his/her work must not influence or affect the building's architecture. With these competing objectives and constraints, the detailed analysis of heat flow and thermodynamics in buildings was economically impractical. Historically, the design of heating and cooling systems for buildings has relied on the most simple calculations. Designers typically applied simple, steady-state heat transfer equations (sometimes adjusted by the use of pretabulated correction factors) to calculate heat gains and losses in buildings. Heating and air-conditioning equipment was selected with sufficient capacity to maintain comfort under peak heating and/or cooling conditions. Suitable control systems were designed to insure that comfort would be maintained during both peak and off-peak conditions. Calculation of building heating or cooling requirements or the expected energy consumption of the

mechanical system under off-peak or part-load conditions was usually not part of the design analysis.

Recent increases in fuel and utility costs, along with new Government energy conservation regulations, have caused a shift in building energy system design objectives and have made building planners more aware of building thermal performance. The effects of architecture on energy use are being considered, and both the annual performance and the peak load performance of building mechanical systems are being evaluated during building design. These more detailed analyses require a much larger number of substantially more complicated calculations. Computers, once used in the building energy system design industry only as research tools or to produce tables of correction factors for simple calculation methods, are gradually being used in the analysis and design of individual buildings.

Detailed energy analyses of buildings have revealed some common trends. For example, building energy systems which are "just big enough" are often much more efficient than systems which are "plenty big enough." Also, estimated annual fuel costs are strongly influenced by thermal mass in buildings and by part-load system performance.

With the increased interest in a more detailed thermal analysis of buildings and their energy systems, a number of building energy analysis computer programs have been developed by Government

laboratories, equipment manufacturers, engineering associations, and private engineering firms. The following two sections discuss the methods used in existing energy analysis programs and a proposed new method for accomplishing part of the energy analysis task.

Existing Building Energy Analysis Procedures

Most modern building energy analysis computer programs perform hourly calculations for a 1-year period, using recorded hourly weather data for a particular site. These calculations are divided into three major parts: (1) space thermal load prediction, (2) air distribution system simulation, and (3) central plant (boiler/chiller) simulation.

Space load prediction involves calculating the amount of heat which must be added to or removed from the space to maintain a desired space temperature. The effects of climate, building construction, space temperature control strategy, occupancy, and lighting use patterns are some of the factors considered in calculating space loads. The need to evaluate the transient response of the space to these load-influencing factors makes space load prediction complicated.

Once space loads are calculated, it is necessary to simulate the performance of the air distribution system which will supply or remove heat from the space. This phase of the building energy

analysis calculation process usually includes steady-state component and control system simulation based on basic principles of thermodynamics and heat transfer. The results from this part of the calculation are the hourly demand for hot and chilled water and electricity.

The final phase of the building energy analysis process is simulating the central plant components which supply energy to the building air distribution system. Components such as boilers and chillers are usually simulated using polynomial expressions; these expressions, which are derived from manufacturers' data, empirically relate component energy inputs to energy outputs.

Note that for the purpose of estimating expected annual energy consumption, transient thermodynamic analysis is necessary only when calculating space loads. This is because the other major elements of buildings (e.g., concrete floors and brick walls) are rarely in steady state. For example, solar energy absorbed by a building exterior wall must be conducted through the wall and convectively transferred to the room air before it becomes a load on the building air-conditioning system (or before it offsets a space heating load).

On the other hand, air distribution systems can be simulated on an hourly basis, using steady-state assumptions, since (1) the energy storage capacity of the circulated air stream is very small compared to the energy being transferred to the air by the mechanical system,

and (2) since the response of the system controls is much faster than 1 hour. Similar reasoning permits the steady-state simulation of central plant components.

Because the transient analysis of heat flow in buildings adds considerable complexity and computational expense to the building energy analysis process, developing improved procedures for performing transient heat flow calculations is a worthwhile goal. The development of an improved procedure is the main subject of this thesis.

Existing Methods for Space Load Prediction

The heat transfer problem in buildings centers around the solution of the heat conduction equation. Almost all computational schemes assume one-dimensional heat transfer for which:

$$\frac{\partial^2 T(x,t)}{\partial x^2} = \frac{1}{\alpha} \frac{\partial T(x,t)}{\partial t} \qquad \text{[Eq 1-1]}$$

where T is temperature, x is the space dimension, t is time, and α is the thermal diffusivity. Given that this differential equation can be solved, a conductive, radiative, and convective heat balance can be computed for interior and exterior surfaces and for the room air volume. In addition to the effects of climate, this heat balance must include energy inputs from people, lights, and equipment, and from the space heating and cooling system.

Existing methods for predicting space loads differ in their approach to solving the heat conduction equation. Gupta, et al. (ref 1), have conveniently divided these methods into three general classes: (1) numerical methods, (2) harmonic methods, and (3) response factor methods.

Numerical methods use lumped parameter approximations to the heat conduction equation and were originally implemented using resistor-capacitor circuits on analog computers; however, digital computer methods now predominate, and both space and time derivatives are approximated as finite differences. As is always the case with finite difference techniques, accuracy, cost, and model stability are all functions of number of nodes, the time step used, and the solution method chosen. Numerical techniques have the advantages of being conceptually simple and able to handle both linear or nonlinear boundary conditions.

Harmonic methods can be used to solve the heat conduction equation if the boundary conditions are represented as periodic functions. (Climate can be reasonably approximated by a limited number of coefficients of a Fourier series; see ref 2.) These methods require that the building heat transfer parameters, including convection coefficients, be constant with time and that radiant heat transfer be linearized.

Mackey and Wright (refs 3,4) first used harmonic methods to calculate the heat gains through building walls and through roofs which separated a room having a fixed constant temperature from a sinusoidally varying outdoor temperature. Walls and roofs were characterized by a decrement factor and a lag factor for the diurnal frequency and its harmonics. (The method was intended for design day calculations only.) Mackey and Wright (ref 5) also devised the so-called sol-air temperature, which allowed solar energy impinging on opaque surfaces to be accounted for as an equivalent convective flux. Van Gorcum (ref 6), Muncey and Spencer (refs 7,8), Pipes (ref 9), Gupta (ref 10), Sonderegger (ref 11), and others have contributed to the enhancement of harmonic methods for space load prediction.

Response factor methods, which represent yet a third approach to solving the heat conduction equation, are in widespread use in the United States and Canada. The major advantages of these methods are that they are not numerical in the sense of finite differences techniques, and they do not require that the heat conduction boundary conditions be periodic and linear.

For constant thermophysical properties, the principle of superposition can be applied to solving the heat conduction equation. Consider the following hypothetical experiment. Suppose that a one-dimensional wall is initially at uniform temperature T_0, and that the outside surface of the wall is suddenly raised to a temperature one

unit above the initial temperature, while the inside surface is maintained at T_0. The resulting heat flux at the inside surface will vary with time, as shown qualitatively in Figure 1-1. Note that if the outside wall temperature had been raised by two units instead of one, the response (heat flux versus time) would simply be twice that shown in Figure 1-1. Similarly, the response to a series of step changes in outside surface temperature occurring at different times is obtained by adding the responses resulting from each step change. By representing the outside surface temperature as a series of positive and negative step changes of appropriate magnitude (rectangular pulses), the flux caused by any arbitrary temperature variation can be determined if the flux resulting from a unit step change is known.

The earliest methods for determining a multilayered slab's heat flux response to a unit step temperature change were numerical (Nessi and Nissole [ref 12], Brisken and Reque [ref 13]). That is, for a given wall or roof section, the response was determined once by solving the lumped parameter resistor-capacitor analog, yielding a set of so-called response factors. Thereafter, any flux was determined by applying the response factors to the actual temperature profile as approximated by rectangular pulses. These methods were extended (by analogy to electrical networks) so that the step response of entire rooms could be determined.

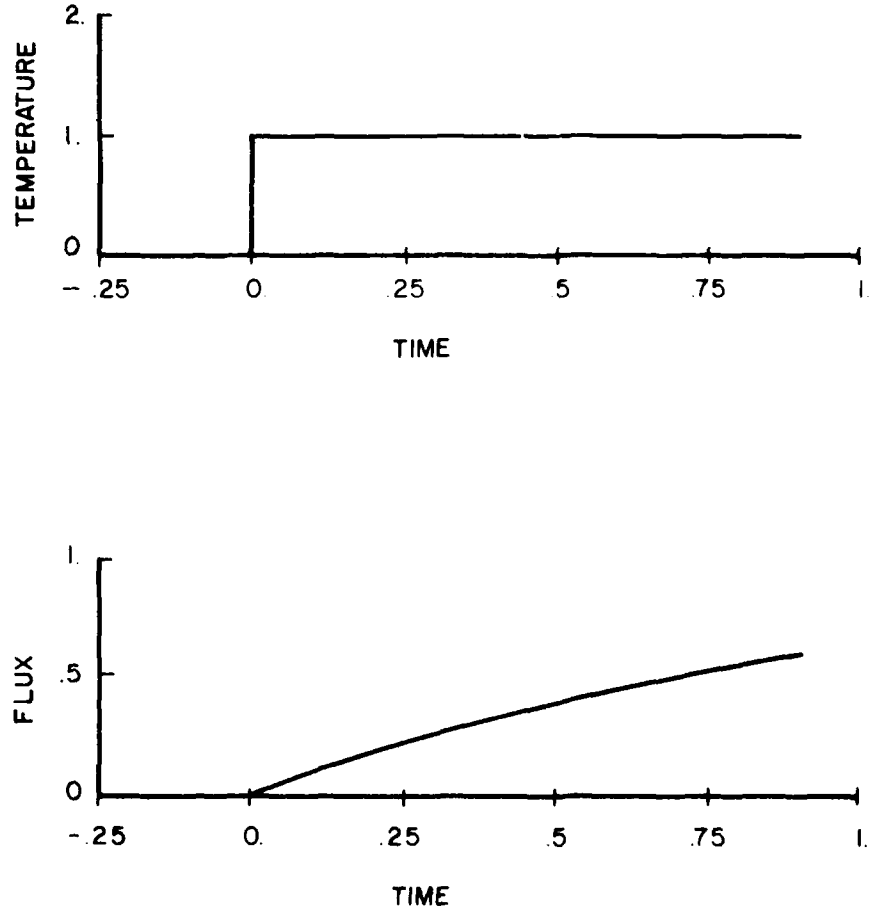

Figure 1-1. Response to step temperature change.

Mitalis and Stephenson (refs 14,15,16), and Kusuda (ref 17) made important improvements in the response factor method by approximating temperature as overlapping triangular pulses (equivalent to a trapezoidal temperature profile approximation) and by treating the multilayered slab by exact analysis rather than by lumped parameter methods. The approach consists of taking the Laplace transform of the heat conduction equation and boundary conditions and solving the equation in the Laplace domain. The required boundary condition matching at the interface of intermediate layers of a multilayered slab yields (in the Laplace domain) an overall transfer function for a multilayered slab. After multiplying the transfer function by the Laplace transform of the triangular temperature pulse, the inverse transform is calculated by numerically solving for roots of the characteristic equation and summing the residues at each of these poles. Carrying out this procedure for heat flow in both directions yields three one-column matrices -- [X], [Y], and [Z] -- called response factors that relate heat flow to surface temperature according to the following formula:

$$q_{o,t} = \sum_{j=0}^{\infty} T_{o,t-j}\, X_j - \sum_{j=0}^{\infty} T_{i,t-j}\, Y_j \qquad \text{[Eq 1-2]}$$

$$q_{i,t} = \sum_{j=0}^{\infty} T_{o,t-j}\, Y_j - \sum_{j=0}^{\infty} T_{i,t-j}\, Z_j \qquad \text{[Eq 1-3]}$$

where:

$q_{o,t}$ is the outer surface heat flux at time t

$q_{i,t}$ is the inner surface heat flux at time t

$T_{o,t-j}$ and $T_{i,t-j}$ are the current and past outside and inside surface temperatures.

Note that as j increases, the response factors converge to a common ratio. This fact and other algebraic manipulations developed by Peavy (ref 18) allow surface heat fluxes to be calculated, using current surface temperatures and a modest number (fewer than 20) of surface temperature and surface flux histories. Chapter 2 provides a thorough exposition of response factor methods for solving transient multilayered slab heat conduction problems.

This response factor conduction model is used as part of a surface-by-surface, hour-by-hour heat balance load-predicting method in the BLAST (ref 19) and NBSLD (ref 20) computer programs.

A final extension of this method, also from Mitalis (see Appendix B of ref 20), allows for decoupling of surface heat fluxes by using weighting factors. If the heat transfer in a room is assumed to be linear (linearized radiant heat transfer) and invariant (constant thermophysical and convective heat transfer coefficients), then the room load due to a unit heat flux pulse can be determined by applying detailed heat balance computer techniques such as those used

in BLAST or NBSLD. Weighting factors can then be calculated which relate the room load at time t, t+1, t+2,.... to a unit flux at time t. Mitalis applied Z-transform methods to the calculation of weighting factors for conduction, transmitted solar radiation, internal radiation, and space temperature drift for light, medium, and heavy buildings (ref 21). Cumali, et al. (ref 22), have recently studied the sensitivity of weighting factors to variations in room geometry, mass, and other variables.

Proposed Method for Space Load Prediction

Calculating hourly loads over a 1-year period, although accurate, can be time-consuming and somewhat costly. Yet for design of building mechanical systems, comparative analyses are usually more important than absolute accuracy. Hence, we will propose a streamlined load-predicting procedure which will characterize the important dynamics of building heat transfer, but will not require detailed hourly heat balance calculations. Such a procedure must be able to produce a time series of predicted loads which capture the general effects of local climate, building use, and building construction without necessarily predicting building response for a specific recorded weather data set.

The following combination and extension of earlier harmonic and weighting factor methods appears to minimize required calculations, yet still considers dynamic response.

Step 1

Using hourly climatological records (on computer tape) and fast Fourier transforms or other time series analysis techniques, determine the most significant coefficients and frequencies of a Fourier series approximation to weather data variables. A set of coefficients will be required for: (1) dry-bulb temperature, (2) sol-air temperature for surfaces of various solar absorptivities and facing directions, (3) incident solar radiation on windows facing different directions, and (4) dew point or specific humidity.

Step 2

For each different wall and roof construction and for each different exposure and for each different frequency judged to be important in step 1, determine the conductive heat flux resulting from unit sinusoidal and cosinusoidal sol-air temperature variation.

Step 3

For each exposure and frequency, multiply the conductive heat flux coefficients from step 2 by the area of the surface and then by the sol-air temperature coefficients determined from step 1. This

will provide the frequency domain representation of conductive heat flux into the space (assuming the space is at constant temperature).

Step 4

Evaluate the function obtained in step 3 at equally spaced points in time. In addition, determine the solar heat gain transmitted through windows and the scheduled heat gain from people, lights, and equipment.

Step 5

Apply appropriate weighting factors to each heat gain and sum to determine space loads.

The following very simple example illustrates this method.

Suppose a room has a south-facing wall of area A_s and a west-facing wall of area A_w. The rest of the room surfaces are interior partitions, a ceiling, and a floor. (Assume a second story above the room and a basement below.) Suppose that from step 1 of the above procedure, the sol-air temperature for south-facing surfaces with absorptivity corresponding to the absorptivity of the south wall of the room can be approximated by:

$$T_{\text{sol-air south}} = C_{0ss} + S_{1s}\sin(\omega_1 t) + C_{1s}\cos(\omega_1 t) + S_{365s}\sin(\omega_{365} t) + C_{365s}\cos(\omega_{365} t) \qquad \text{[Eq 1-4]}$$

where t is time, and the Cs and Ss are constant coefficients corresponding to important weather frequencies, ω (the mean, one cycle per year, and 365 cycles per year in the above example). Similarly, suppose that the sol-air temperature for the west wall is:

$$T_{\text{sol-air west}} = C_{0w} + S_{1w}\sin(\omega_1 t) + C_{1w}\cos(\omega_1 t) + S_{365w}\sin(\omega_{365} t) + L_{365w}\cos(\omega_{365} t) \qquad \text{[Eq 1-5]}$$

If, from step 2, the heat flux coefficients for the two walls at the various important frequencies are U_0, U_{1ss}, U_{1cs}, U_{365ss}, U_{365cs}, U_{0w}, U_{1sw}, U_{1cw}, U_{365sw}, and U_{365cw}, then the heat gain through the exterior walls as a function of time is:

$$\begin{aligned} Q_w(t) = {} & A_s U_{0s} (C_{0s} - T_R) + A_w U_{0w} (C_{0w} - T_R) \\ & + (A_s U_{1ss} S_{1s} + A_w U_{1sw} S_{1w})\sin(\omega_1 t) \\ & + (A_s U_{1cs} C_{1s} + A_w U_{1cw} C_{1w})\cos(\omega_1 t) \\ & + (A_s U_{365ss} S_{365s} + A_w U_{365ws} S_{365w})\sin(\omega_{365} t) \\ & + (A_s U_{365cs} C_{365s} + A_w U_{365cw} C_{365w})\cos(\omega_{365} t) \end{aligned} \qquad \text{[Eq 1-6]}$$

This function can be evaluated at any time t to determine the heat flux through exterior walls (step 4).

The heating or cooling load in the room at time t for the assumed constant room temperature, T_R, is obtained by adding the contributions of wall conductive flux, solar energy transmitted through glass, lighting energy, and the energy emanating from people, with each weighted according to step 5. For example, if the lighting energy flux into the room is Q_L (t), then the contribution to room load from the lights is:

$$L_L(t) = V_0\, Q_L(t) + V_1\, Q_L(t-\Delta t) + V_2\, Q_L(t-2\Delta t)\ldots$$

$$- W_1\, L_L(t-\Delta t) - W_2\, L_L(t-2\Delta t) - W_3\, L_L(t-3\Delta t)\ldots \qquad \text{[Eq 1-7]}$$

where $Q_L(t- n\Delta t)$ are past values of lighting flux, and $L_L(t- n\Delta t)$ are past contributions of lighting energy to the space load.

The total load at time t is therefore:

$$L(t) = \sum_{k=1}^{m} L_K(t) \qquad \text{[Eq 1-8]}$$

where the sum is taken over the number of heat gain components.

The loads from step 5, along with a matching weather data time series (obtained by inverting the transforms obtained in step 1), will provide the input necessary to simulate air distribution systems and boiler/chiller plants.

The proposed load calculation procedure has several advantages over existing hour-by-hour methods. The number of calculations required is reduced substantially, particularly since step 1 -- the processing of weather data -- need only be accomplished once for any given location. The major part of the load calculation procedure -- the evaluation of sine and cosine terms -- is simple enough to be implemented on modern microcomputers (for example, as a subprogram in a larger system simulation program). This should substantially enlarge the number of engineers and architects having the resources and skill to apply the method routinely. The graphic portrayal of the frequency response of wall and roof sections may, in itself, prove to be a valuable design aid.

The proposed method also has limitations. First, the approximation of weather data by a few terms of a Fourier series necessarily "filters out" climate extremes. Hence, energy use estimates based on this filtered data can be expected to be low (ref 2). Second, the method is less, rather than more, detailed and therefore suffers from at least as many simplifying assumptions as the hour-by-hour method.

Objective

The objective of this research was to develop the necessary mathematical techniques to implement and test the new method for space load prediction described in the previous section. Because

much of the complexity of space load calculation stems from the need to deal with transient heat flow through multilayered slabs, a second objective was to provide a comprehensive mathematical development of response factor theory.

Approach

Four main tasks were performed to achieve the objective:

1. A procedure was developed to calculate the frequency response of multilayered slabs.

2. Various procedures were applied to the analysis of weather data, and the best method for determining the periodic components of the data was selected.

3. Errors associated with the use of synthesized weather data which contained only sinusoidal components were assessed.

4. The proposed method for space load prediction was tested.

Outline

The results of this research are described sequentially in Chapters 2 through 7. Chapter 2 provides a detailed development of transfer function methods applied to heat conduction in multilayered

slabs. It provides the necessary background for the study of the frequency response of multilayered slabs described in Chapter 3.

Chapter 4 describes a thorough analysis of important weather data variables. Chapter 5 describes tests performed to determine the error in estimated, annual building energy use associated with using only the sinusoidal components of weather data instead of actual weather data. Chapter 6 presents an hour-by-hour comparison between results of the proposed load calculation method and more detailed methods.

Chapter 7 summarizes the results of the research and outlines a procedure for implementing the new load-predicting procedure in a microprocessor-based building energy analysis program.

2 ONE-DIMENSIONAL HEAT CONDUCTION THROUGH MULTILAYERED SLABS

The Heat Conduction Equation

Heat conduction through a one-dimensional homogeneous slab is governed by the following second-order partial differential equation (see Figure 2-1):

$$\frac{\partial^2 T(x,t)}{\partial x^2} = \frac{1}{\alpha} \frac{\partial T(x,t)}{\partial t} \qquad \text{[Eq 2-1]}$$

where T is the temperature at position x and time t, and α is the thermal diffusivity $\alpha = \frac{k}{\rho C_p}$, where k is the thermal conductivity ($W/m^{o}K$), ρ is density (kg/m^3), and C_p is the specific heat ($J/kg^{o}K$). The heat flux at any position x and time t is given by:

$$q(x,t) = -k \frac{\partial T(x,t)}{\partial x} . \qquad \text{[Eq 2-2]}$$

In both the above relations, k, p, and C_p were assumed to be constant.

A common approach to the solution of the above equations is to use the Laplace transform, which is defined for any transformable function f(t) as

$$\mathcal{L}[f(t)] = F(s) = \int_0^\infty f(t)\, e^{-st} dt \qquad \text{[Eq 2-3]}$$

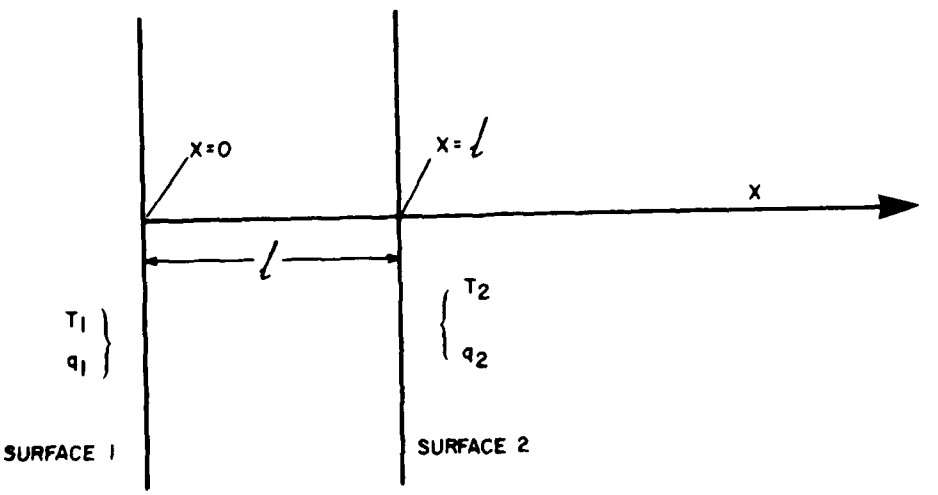

Figure 2-1. One-dimensional homogeneous slab.

where s is a complex number. The utility of the Laplace transform stems from the following property:

$$\mathcal{L}\left[\frac{\partial f(t)}{\partial t}\right] = sF(s) - f(t)\Big|_{t=0} . \qquad \text{[Eq 2-4]}$$

Hence, the Laplace transform of Equation 2-1 transforms this partial differential equation into an ordinary differential equation:

$$\frac{d^2T(x,s)}{dx^2} = \frac{1}{\alpha} sT(x,s) \qquad \text{[Eq 2-5]}$$

where we have assumed that $T(x,0) = 0$. The solution of this transformed differential equation is

$$T(x,s) = A \cosh(x \sqrt{s/\alpha}) + B \sinh(x \sqrt{s/\alpha}) \qquad \text{[Eq 2-6]}$$

The transform of Equation 2-2 is:

$$q(x,s) = -k \frac{dT(x,s)}{dx} \qquad \text{[Eq 2-7]}$$

where we have again assumed that $T(x,0) = 0$. On differentiation of Equation 2-6 with respect to x and substitution into Equation 2-7, we have:

$$q(x,s) = -k \sqrt{s/\alpha}\ A \sinh(x \sqrt{s/\alpha}) - k \sqrt{s/\alpha}\ B \cosh(x \sqrt{s/\alpha}) \qquad \text{[Eq 2-8]}$$

If we now consider only the temperature and heat flux at the surfaces of the slab (at $x = 0$ and $x = \ell$ where ℓ is the thickness of the slab in meters), we can write from Equations 2-6 and 2-8:

$$T_1(s) = A \qquad \text{[Eq 2-9]}$$

$$q_1(s) = -kB\sqrt{s/\alpha} \qquad \text{[Eq 2-10]}$$

$$T_2(s) = A\cosh(\ell\sqrt{s/\alpha}) + B\sinh(\ell\sqrt{s/\alpha}) \qquad \text{[Eq 2-11]}$$

$$q_2(s) = -k\sqrt{s/\alpha}\,A\sinh(\ell\sqrt{s/\alpha}) - k\sqrt{s/\alpha}\,B\cosh(\ell\sqrt{s/\alpha}) \qquad \text{[Eq 2-12]}$$

where $T_1(s) = T(0,s)$, which is the transform of the temperatures at surface 1

$q_1(s) = q(0,s)$, which is the transform of the flux at surface 2

$T_2(s)$ and $q_2(s)$ are corresponding transforms of temperature and flux at surface 2 [i.e., $T(\ell, s)$ and $q(\ell, s)$].

We may now specify any two of $T_1(s)$, $q_1(s)$, $T_2(s)$, or $q_2(s)$ as boundary conditions (transforms of the appropriate time-dependent boundary conductions) in order to complete the solution. While the physical problem will dictate which boundary conditions are known, we will temporarily assume that both $T_2(s)$ and $q_2(s)$ are known. Proceeding with this assumption, we can use Equations 2-11 and 2-12 to find A and B in terms of the physical constants of the slab and the Laplace transform parameter, s.

$$A = \frac{T_2(s) - B \sinh(\ell \sqrt{s/\alpha})}{\cosh(\ell \sqrt{s/\alpha})} \qquad \text{[Eq 2-13]}$$

$$B = \frac{-q_2(s) - k \sqrt{s/\alpha}\, A \sinh \ell(\sqrt{s/\alpha})}{k \sqrt{s/\alpha} \cosh(\ell \sqrt{s/\alpha})} \qquad \text{[Eq 2-14]}$$

A few algebraic manipulations and hyperbolic trigonometric identities yield:

$$A = (\cosh(\ell \sqrt{s/\alpha}))\, T_2(s) + \left(\frac{\sinh(\ell \sqrt{s/\alpha})}{k \sqrt{s/\alpha}}\right) q_2(s) \qquad \text{[Eq 2-15]}$$

$$B = (-\sinh(\ell \sqrt{s/\alpha}))\, T_2(s) - \frac{\cosh(\ell \sqrt{s/\alpha})}{k \sqrt{s/\alpha}} \qquad \text{[Eq 2-16]}$$

Substituting for A and B in Equations 2-9 and 2-10 yields the required solution in the Laplace domain:

$$T_1(s) = (\cosh(\ell \sqrt{s/\alpha}))\, T_2(s) + \left(\frac{1}{k\sqrt{s/\alpha}} \sinh(\ell \sqrt{s/\alpha})\right) q_2(s) \qquad \text{[Eq 2-17]}$$

$$q_1(s) = (k\sqrt{s/\alpha} \sinh(\ell \sqrt{s/\alpha}))\, T_2(s) + (\cosh(\ell \sqrt{s/\alpha}))\, q_2(s) \qquad \text{[Eq 2-18]}$$

For notational convenience, we may now define new variables as follows:

$$A(s) = \cosh(\ell \sqrt{s/\alpha})$$

$$B(s) = \frac{1}{k\sqrt{s/\alpha}} \sinh(\ell \sqrt{s/\alpha})$$

$$C(s) = k\sqrt{s/\alpha} \sinh(\ell \sqrt{s/\alpha})$$

$$D(s) = \cosh(\ell \sqrt{s/\alpha})$$

where A(s) and B(s) should not be confused with A and B used previously. With these new variables, Equations 2-17 and 2-18 become:

$$T_1(s) = A(s)\ T_2(s) + B(s)\ q_2(s) \qquad \text{[Eq 2-19]}$$

$$q_1(s) = C(s)\ T_2(s) + D(s)\ q_2(s) \qquad \text{[Eq 2-20]}$$

Note that these two equations can be solved for any two unknowns in terms of the two knowns which arise from the physical boundary conditions of the problem. For example, if the transforms of temperature variation with time are known for both surfaces, then the fluxes are:

$$q_1(s) = \frac{D(s)}{B(s)}\ T_1(s) - \frac{1}{B(s)}\ T_2(s), \quad B(s) \neq 0 \qquad \text{[Eq 2-21]}$$

$$q_2(s) = \frac{1}{B(s)}\ T_1(s) - \frac{A(s)}{B(s)}\ T_2(s), \quad B(s) \neq 0 \qquad \text{[Eq 2-22]}$$

At least in theory, if Laplace transforms exist for the two required boundary conditions, the unknown fluxes or temperatures can be determined by finding the inverse Laplace transforms of equations like 2-19, 2-20, 2-21, or 2-22.

We may now extend the treatment of one-dimensional heat flow to include multilayered slabs. Notice that Equations 2-19 and 2-20 describe the transform of heat flow and temperature on one surface in terms of the transform of the heat flow and temperature on the <u>other</u> surface. We can rewrite these equations in matrix form as:

$$\begin{bmatrix} T_1(s) \\ q_1(s) \end{bmatrix} = \begin{bmatrix} A(s) & B(s) \\ C(s) & D(s) \end{bmatrix} \begin{bmatrix} T_2(s) \\ q_2(s) \end{bmatrix} \qquad \text{[Eq 2-23]}$$

Suppose now that we have a two-layer slab (see Figure 2-2), where $T_1(s)$ and $q_1(s)$ are the transforms of temperature and flux at the inner surface of slab 1, and $T_2(s)$ and $q_2(s)$ refer to the interface between slabs 1 and 2. $T_3(s)$ and $q_3(s)$ refer to the outer surface -- surface 3. We may treat each slab individually and apply Equation 2-23 to each. Noting that surface 2 is both the "outside" of slab 1 and the "inside" of slab 2, we have for slab 1:

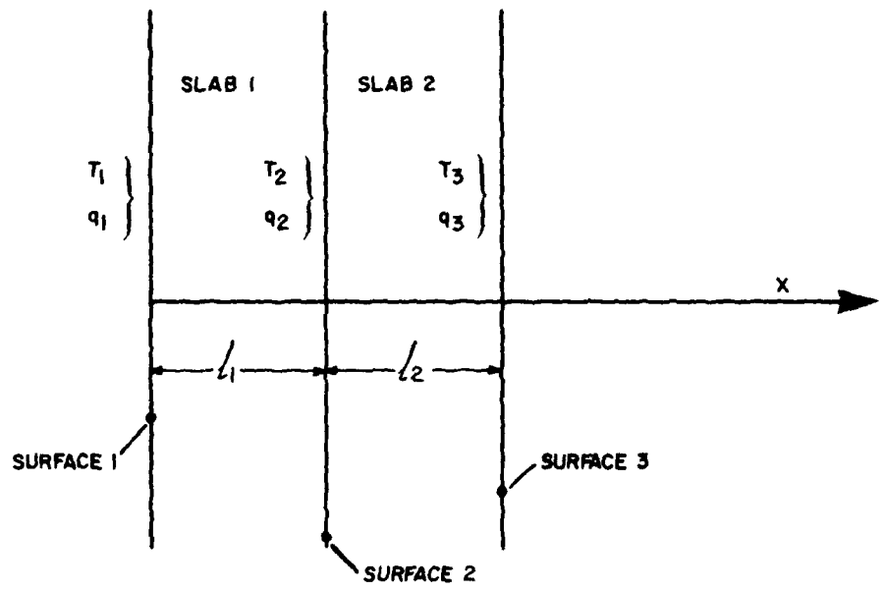

Figure 2-2. One-dimensional two-layer slab.

$$\begin{bmatrix} T_1(s) \\ q_1(s) \end{bmatrix} = \begin{bmatrix} A_1(s) & B_1(s) \\ C_1(s) & D_1(s) \end{bmatrix} \begin{bmatrix} T_2(s) \\ q_2(s) \end{bmatrix} \qquad \text{[Eq 2-24]}$$

and for slab 2:

$$\begin{bmatrix} T_2(s) \\ q_2(s) \end{bmatrix} = \begin{bmatrix} A_2(s) & B_2(s) \\ C_2(s) & D_2(s) \end{bmatrix} \begin{bmatrix} T_3(s) \\ q_3(s) \end{bmatrix} \qquad \text{[Eq 2-25]}$$

where

$$A_1(s) = \cosh(\ell_1 \sqrt{s/\alpha_1})$$
$$B_1(s) = (1/k_1\sqrt{s/\alpha_1}) \sinh(\ell_1 \sqrt{s/\alpha_1})$$
$$C_1(s) = k_1 \sqrt{s/\alpha_1} (\sinh(\ell_1 \sqrt{s/\alpha_1}))$$
$$D_1(s) = \cosh(\ell_1 \sqrt{s/\alpha_1})$$

are all dependent on the properties of slab 1 and the Laplace transform variable, s. $A_2(s)$, $B_2(s)$, $C_2(s)$, and $D_2(s)$ are similarly defined based on the properties of slab 2.

We may now simply substitute the right-hand side of Equation 2-25 for $\begin{bmatrix} T_2(s) \\ q_2(s) \end{bmatrix}$ in Equation 2-24, yielding

$$\begin{bmatrix} T_1(s) \\ q_1(s) \end{bmatrix} = \begin{bmatrix} A_1(s) & B_1(s) \\ C_1(s) & D_1(s) \end{bmatrix} \begin{bmatrix} A_2(s) & B_2(s) \\ C_2(s) & D_2(s) \end{bmatrix} \begin{bmatrix} T_3(s) \\ q_3(s) \end{bmatrix} \quad \text{[Eq 2-26]}$$

The recursive extension of Equation 2-26 to an n-layered slab is now obvious:

$$\begin{bmatrix} T_1(s) \\ q_1(s) \end{bmatrix} = \begin{bmatrix} A_1(s) & B_1(s) \\ C_1(s) & D_1(s) \end{bmatrix} \begin{bmatrix} A_2(s) & B_2(s) \\ C_2(s) & D_2(s) \end{bmatrix} \begin{bmatrix} A_3(s) & B_3(s) \\ C_3(s) & D_3(s) \end{bmatrix} \cdots\cdots \begin{bmatrix} A_n(s) & B_n(s) \\ C_n(s) & D_n(s) \end{bmatrix} \begin{bmatrix} T_{n+1}(s) \\ q_{n+1}(s) \end{bmatrix} \quad \text{[Eq 2-27]}$$

This fundamental equation permits the calculations of the so-called "transmission matrix," defined as

$$\begin{bmatrix} A(s) & B(s) \\ C(s) & D(s) \end{bmatrix} = \begin{bmatrix} A_1(s) & B_1(s) \\ C_1(s) & D_1(s) \end{bmatrix} \begin{bmatrix} A_2(s) & B_2(s) \\ C_2(s) & D_2(s) \end{bmatrix} \cdots\cdots$$

$$\begin{bmatrix} A_{n-1}(s) & B_{n-1}(s) \\ C_{n-1}(s) & D_{n-1}(s) \end{bmatrix} \begin{bmatrix} A_n(s) & B_n(s) \\ C_n(s) & D_n(s) \end{bmatrix} \qquad \text{[Eq 2-28]}$$

With A(s), B(s), C(s), and D(s) now <u>redefined</u> as elements of the above overall transmission matrix, the multilayered slab problem takes the same form as that of a single-layer slab. Equations 2-19, 2-20, 2-21, and 2-22, for example, can be written for a multilayered slab as:

$$\begin{bmatrix} T_1(s) \\ q_1(s) \end{bmatrix} = \begin{bmatrix} A(s) & B(s) \\ C(s) & D(s) \end{bmatrix} \begin{bmatrix} T_{n+1}(s) \\ q_{n+1}(s) \end{bmatrix} \qquad \text{[Eq 2-29]}$$

$$\begin{bmatrix} q_1(s) \\ q_{n+1}(s) \end{bmatrix} = \begin{bmatrix} \frac{D(s)}{B(s)} & -\frac{1}{B(s)} \\ \frac{1}{B(s)} & -\frac{A(s)}{B(s)} \end{bmatrix} \begin{bmatrix} T_1(s) \\ T_{n+1}(s) \end{bmatrix} \qquad \text{[Eq 2-30]}$$

While Equations 2-29 and 2-30 are conceptually simple, their practical use is mathematically tedious for all but the simplest of cases. We will therefore first consider single-layer slab applications and then extend these results to multilayered slabs.

Before proceeding with an example, let us note some of the properties of the transmission matrix for a single-layer slab.

$$\begin{bmatrix} A_1(s) & B_1(s) \\ C_1(s) & D_1(s) \end{bmatrix} = \begin{bmatrix} \cosh(\ell_1 \sqrt{s/\alpha_1}), & \frac{1}{k_1\sqrt{s/\alpha_1}} \sinh(\ell_1 \sqrt{s/\alpha_1}) \\ k_1 \sqrt{s/\alpha_1} \sinh(\ell_1 \sqrt{s/\alpha_1}), & \cosh(\ell_1 \sqrt{s/\alpha_1}) \end{bmatrix} \qquad \text{[Eq 2-31]}$$

We can also write this matrix in terms of the thermal resistance, R_1, and thermal capacitance, C_1, defined as follows:

$$R_1 = \frac{\ell_1}{k_1} \text{ and, in general, } R_n = \frac{\ell_n}{k_n} \qquad \text{[Eq 2-32]}$$

$$C_1 = \ell_1 \rho_1 C_{p1} \text{ and, in general, } C_n = \ell_n \rho_n C_{pn} \qquad \text{[Eq 2-33]}$$

Notice that $R_n C_{pn} = \frac{\ell_n^2}{\alpha_n}$. Thus, the single-layer transmission matrix becomes:

$$\begin{bmatrix} A_1(s) & B_1(s) \\ C_1(s) & D_1(s) \end{bmatrix} = \begin{bmatrix} \cosh \sqrt{sR_1C_1} & \frac{R_1}{\sqrt{sR_1C_1}} \sinh \sqrt{sR_1C_1} \\ \frac{\sqrt{sR_1C_1}}{R_1} \sinh \sqrt{sR_1C_1} & \cosh \sqrt{sR_1C_1} \end{bmatrix} \qquad \text{[Eq 2-34]}$$

The determinant of this matrix is $\cosh^2(\sqrt{sR_1C_1}) - \sinh^2(\sqrt{sR_1C_1}) = 1$. The multilayered slab transmission matrix therefore also has a determinant of one. Also, as the capacitance of the material goes to zero, $\cosh\sqrt{sR_1C_1} = 1$ and $\frac{\sqrt{sR_1C_1}}{R_1}\sinh\sqrt{sR_1C_1} = 0$. $\frac{\sqrt{R_1}}{sR_1C_1} \sinh \sqrt{sR_1C_1}$ can be expanded to reveal its limit as $C_1 \to 0$.

$$\frac{R_1}{\sqrt{sR_1C_1}} \sinh \sqrt{sR_1C_1} = \frac{R_1}{\sqrt{sR_1C_1}} \left(\sqrt{sR_1C_1} + \frac{\sqrt{sR_1C_1}^3}{3!} + \frac{\sqrt{sR_1C_1}^5}{5!} \ldots \right) \qquad \text{[Eq 2-35]}$$

As $C_1 \to 0$, $\frac{R_1}{\sqrt{sR_1C_1}} \sinh\sqrt{sR_1C_1} = R_1$. Thus, for a lightweight slab:

$$\begin{bmatrix} A_1(s) & B_1(s) \\ C_1(s) & D_1(s) \end{bmatrix} = \begin{bmatrix} 1 & R_1 \\ 0 & 1 \end{bmatrix} \qquad \text{[Eq 2-36]}$$

This means that air layers or other light material can be routinely included in the calculation of the multilayered transmission matrix.

Let us now consider the case of a single layer exposed on one side to a temperature "ramp" while the temperature on the other side is fixed. This case is of practical interest, because an arbitrary surface temperature variation can be approximated by a series of such ramps with alternating positive and negative slopes. Figures 2-3 and 2-4 show how three ramps can be used to form a triangular pulse and how overlapping triangular pulses form a trapezoidal approximation to an arbitrary surface temperature.

The Laplace transform of a ramp with unit slope is $\frac{1}{s^2}$. Hence, if this transformed boundary condition is applied to side 2 of a single-layer slab while the temperature on side 1 is held at zero, Equation 2-25 (or Equation 2-30) becomes:

$$\begin{bmatrix} q_1(s) \\ q_2(s) \end{bmatrix} = \begin{bmatrix} \frac{D_1(s)}{B_1(s)} & -\frac{1}{B_1(s)} \\ \frac{1}{B_1(s)} & -\frac{A_1(s)}{B_1(s)} \end{bmatrix} \begin{bmatrix} 0 \\ \frac{1}{s^2} \end{bmatrix} \qquad \text{[Eq 2-37]}$$

If we are interested in the conductive flux at surface 1 due to the ramp boundary condition on surface 2, we have

$$q_1(s) = -\frac{1}{s^2}\left(\frac{1}{B_1(s)}\right) = -\frac{1}{s^2}\,\frac{\sqrt{sR_1C_1}}{R_1 \sinh \sqrt{sR_1C_1}} \qquad \text{[Eq 2-38]}$$

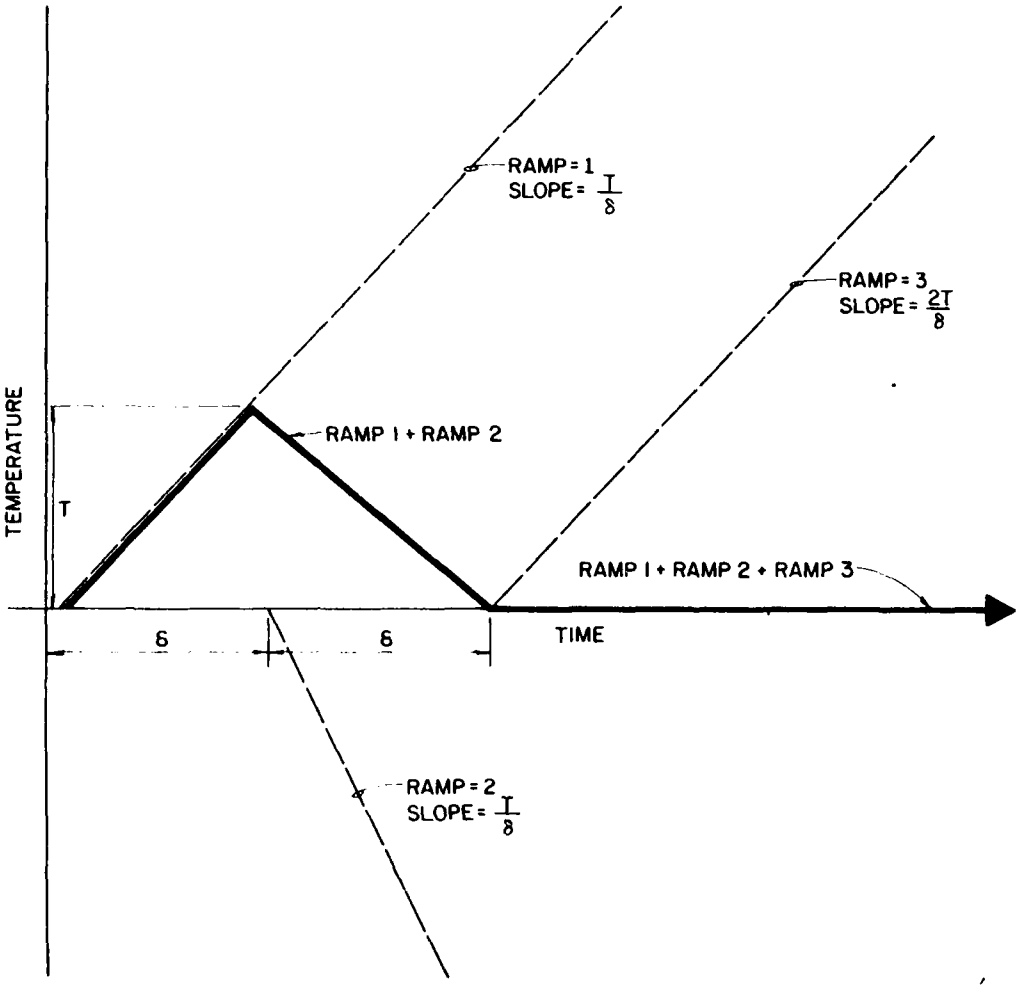

Figure 2-3. The triangular pulse as the sum of the three ramps.

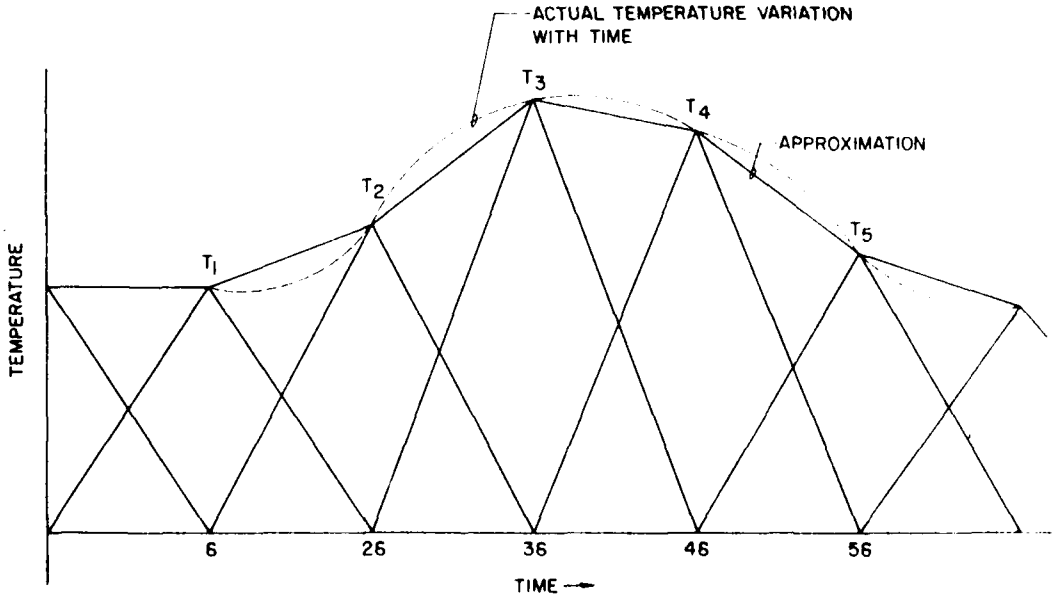

Figure 2-4. Overlapping triangular pulses as an approximation to a continuous function.

The inverse Laplace transform yields flux variation at surface 1 as a function of time.

$$\mathcal{L}^{-1}[q_1(s)] = q_1(t) = \mathcal{L}^{-1}\left[-\frac{1}{s^2}\,\frac{\sqrt{sR_1C_1}}{R_1 \sinh\sqrt{sR_1C_1}}\right] \qquad \text{[Eq 2-39]}$$

Applying the general formula for finding inverse Laplace transforms, we have:

$$q_1(t) = \frac{1}{2\pi j}\int_{a-j\infty}^{a+j\infty} q_1(s)e^{st}ds \qquad \text{[Eq 2-40]}$$

where $j = \sqrt{-1}$ and a is a very large real number. From complex variable theory, the above integral is equal to the sum of the residues at the poles of $q_1(s)e^{st}$. Poles are points where s assumes a value so as to make $q_1(s)e^{st}$ undefined. In our case, any time the denominator of the right side of Equation 2-38 is zero, the function is undefined. Hence, poles exist at $s = 0$ and at $\sqrt{sR_1C_1} = n\pi j$ or $s = -n^2\pi^2/R_1C_1$, where $n = 1,2,3,\ldots$. Notice that the second-order pole at zero is due to $\frac{1}{s^2}$, the boundary condition, and that $\sinh\sqrt{sR_1C_1}$ does not represent a pole at zero, since, as we have already shown, $\lim_{s \to 0} \frac{\sqrt{sR_1C_1}}{\sinh\sqrt{sR_1C_1}} = 1$. All other poles lie on the negative real axis in the s-plane.

The residue at s = 0 is (see ref 23 for details of residue calculation methods):

$$r_o = \lim_{s\to 0}\left[\frac{d}{ds}\left(\frac{-\sqrt{sR_1C_1}\ e^{st}}{R_1 \sinh \sqrt{sR_1C_1}}\right)\right] = \frac{1}{R_1}\left(\frac{R_1C_1}{6} - t\right) \qquad \text{[Eq 2-41]}$$

The residues at $s = -n^2\pi^2/R_1C_1$ are

$$r_n = \left.\frac{-\sqrt{sR_1C_1}\ e^{st}}{\frac{d}{ds}[R_1S^2 \sinh \sqrt{sR_1C_1}}\right|_{s=\frac{-n^2\pi^2}{R_1C_1}} = \frac{-\sqrt{-n^2\pi^2}\ e^{-tn^2x^2/R_1C_1}}{R_1 \frac{n^4\pi^4}{R_1C_1} \frac{\cosh \sqrt{-n^2\pi^2}}{2\sqrt{-n^2n^2}}} \qquad \text{[Eq 2-42]}$$

$$= \frac{2C_1e^{-tn^2\pi^2/R_1C_1}}{n^2\pi^2 \cosh \sqrt{-n^2\pi^2}}$$

Now, $\cosh \sqrt{-n^2\pi^2} = \cos(jn\pi) = (-1)^n$

Thus,

$$r_n = \frac{2(-1)^nC_1e^{-tn^2\pi^2/R_1C_1}}{n^2\pi^2} \qquad \text{[Eq 2-43]}$$

Summing all residues, we have:

$$q_1(t) = \frac{C_1}{6} - \frac{t}{R_1} + 2\sum_{n=1}^{\infty} \frac{(-1)^nC_1e^{-tn^2\pi^2/R_1C_1}}{n^2\pi^2} \qquad \text{[Eq 2-44]}$$

which is the conductive heat flux at surface 1 at time t due to a ramp temperature increase of unit slope applied to surface 2 at time zero while maintaining surface 1 at zero temperature.

We are now ready to calculate the flux due to the triangular pulse of Figure 2-3. The flux at time δ is:

$$q_1(\delta) = \frac{T}{\delta}\left[\frac{C_1}{6} - \frac{\delta}{R_1} + 2\sum_{n=1}^{\infty}\frac{(-1)^n C_1 e^{-\delta n^2\pi^2/R_1C_1}}{n^2\pi^2}\right] \qquad \text{[Eq 2-45]}$$

where we have simply replaced t by δ in Equation 2-41 and replaced the unit ramp with a ramp of slope T/δ. At $t = 2\delta$, both ramp 1 and ramp 2 of Figure 2-3 contribute to the flux. The contribution of ramp 1 is:

$$q_1(2\delta)\Big|_{\substack{\text{due to}\\ \text{ramp 1}}} = \frac{T}{\delta}\left[\frac{C_1}{6} - \frac{2\delta}{R_1} + 2\sum_{n=1}^{\infty}\frac{(-1)^n C_1 e^{-2\delta n^2\pi^2/R_1C_1}}{n^2\pi^2}\right] \qquad \text{[Eq 2-46]}$$

Ramp 2 starts at time δ and has a slope of $-2T/\delta$. Hence, its contribution to the flux is:

$$q_1(2\delta)\Big|_{\substack{\text{due to}\\ \text{ramp 2}}} = -\frac{2T}{\delta}\left[\frac{C_1}{6} - \frac{2\delta-\delta}{R_1} + 2\sum_{n=1}^{\infty}\frac{(-1)^n C_1 e^{-(2\delta-\delta)n^2\pi^2/R_1C_1}}{n^2\pi^2}\right] \qquad \text{[Eq 2-47]}$$

The principles of superposition allow us to add these two contributions to yield

$$q_1(2\delta) = -\frac{T}{\delta}\left[\frac{C_1}{6} + 2\sum_{n=1}^{\infty}\frac{(-1)^n C_1\left(2e^{-\delta n^2\pi^2/R_1C_1} - e^{2\delta n^2\pi^2/R_1C_1}\right)}{n^2\pi^2}\right] \quad \text{[Eq 2-48]}$$

Applying the same procedures for $t = 3\delta$ and including the effect of ramp 3, which starts at 2δ and has a slope of T/δ, we have:

$$q_1(3\delta) = \frac{T}{\delta}\left[2\sum_{n=1}^{\infty}\frac{(-1)^n C_1\left(e^{-3\delta n^2\pi^2/R_1C_1} - 2e^{-2\delta n^2\pi^2/R_1C_1} + e^{-\delta n^2\pi^2/R_1C_1}\right)}{n^2\pi^2}\right] \quad \text{[Eq 2-49]}$$

Similarly, for any incremental time, $m\delta$, where m is greater than or equal to 3:

$$q_1(m\delta) = \frac{T}{\delta}\left[2\sum_{n=1}^{\infty}\frac{(-1)^n C_1\left(e^{-m\delta\beta_n} - 2e^{-(m-1)\delta\beta_n} + e^{-(m-2)\delta\beta_n}\right)}{n^2\pi^2}\right] \quad \text{[Eq 2-50]}$$

where $\beta_n = n^2\pi^2/R_1C_1$.

Equations 2-45, 2-48, and 2-50 can be used together to calculate the flux at surface 1. Figure 2-5 illustrates typical variations in

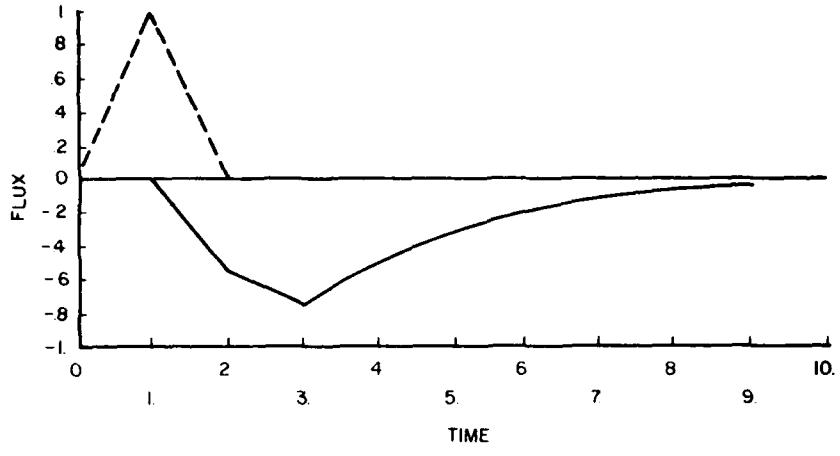

Figure 2-5a. Heat flux (solid line) at surface one due to a triangular temperature pulse (dashed line) at surface two for a heavy slab.

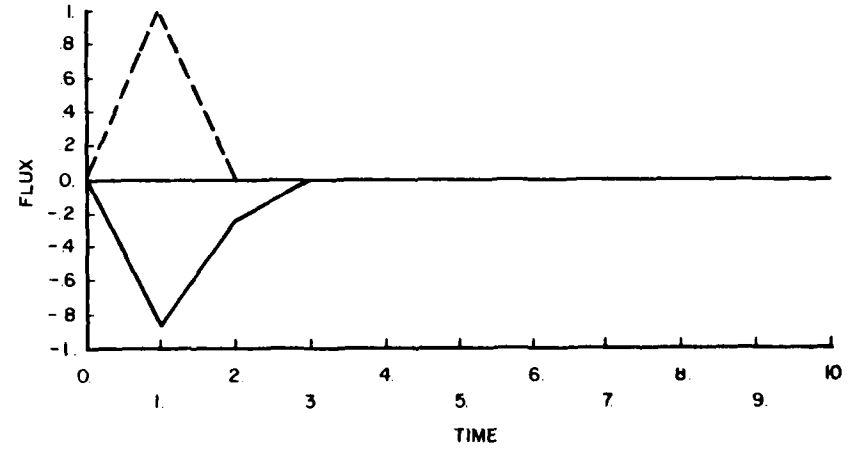

Figure 2-5b. Heat flux (solid line) at surface one due to a triangular temperature pulse (dashed line) at surface two for a light slab.

flux with time for a heavy and light slab subjected to a triangular pulse starting at t = 0. Note that flux is defined to be positive if it flows in the positive x direction; hence, q_1 is the heat flux out of surface 1.

Suppose now that we wish to calculate the conductive flux at surface 1 due to a change in the temperature of surface 1 itself, while surface 2 is held at constant temperature. Following the same procedure of approximating the temperature as a series of ramps, Equation 2-30 becomes:

$$\begin{bmatrix} q_1(s) \\ q_2(s) \end{bmatrix} = \begin{bmatrix} \frac{D_1(s)}{B_1(s)} & -\frac{1}{B_1(s)} \\ \frac{1}{B_1(s)} & -\frac{A_1(s)}{B_1(s)} \end{bmatrix} \begin{bmatrix} \frac{1}{s^2} \\ 0 \end{bmatrix} \qquad \text{[Eq 2-51]}$$

Substituting for $D_1(s)$ and $B_1(s)$ yields the counterpart to Equation 2-38.

$$q_1(s) = \frac{1}{s^2}\left(\frac{D_1(s)}{B_1(s)}\right) = \frac{1}{s^2} \frac{(\cosh \sqrt{sR_1C_1})\ \sqrt{sR_1C_1}}{R_1 \sinh \sqrt{sR_1C_1}} \qquad \text{[Eq 2-52]}$$

The poles of this function are again at s = 0 and $s = -n^2\pi^2/R_1C_1$. Applying the inverse Laplace transform formula and the residue theorem as before, we have:

$$r_o = \lim_{s \to 0} \left[\frac{d}{ds} \left(\frac{(\cosh \sqrt{sR_1C_1})\ \sqrt{sR_1C_1}\ e^{st}}{R_1 \sinh \sqrt{sR_1C_1}} \right) \right] = \frac{1}{R_1} \left(\frac{R_1C_1}{3} + t \right) \qquad \text{[Eq 2-53]}$$

$$r_n = \left. \frac{(\cosh \sqrt{sR_1C_1})\ \sqrt{sR_1C_1}\ e^{st}}{\frac{d}{ds} \left[R_1 s^2 \sinh \sqrt{sR_1C_1} \right]} \right|_{s = \frac{-n^2\pi^2}{R_1C_1}} = - \frac{2C_1 e^{-tn^2\pi^2/R_1C_1}}{n^2\pi^2} \qquad \text{[Eq 2-54]}$$

The counterpart to Equation 2-44 is therefore

$$q_1(t) = \frac{C_1}{3} + \frac{t}{R_1} - 2 \sum_{n=1}^{\infty} \frac{C_1 e^{-tn^2\pi^2/R_1C_1}}{n^2\pi^2} \qquad \text{[Eq 2-55]}$$

which is the conductive heat flux at surface 1 at time t due to a ramp temperature increase of unit slope applied to surface 1 at time zero while maintaining surface 2 at zero temperature.

The flux due to a triangular pulse applied to surface 1 is obtained in the same manner as the derivation of Equations 2-45 through 2-50. Hence:

$$q_1(\delta) = \frac{T}{\delta} \left[\frac{C_1}{3} + \frac{\delta}{R_1} - 2 \sum_{n=1}^{\infty} \frac{C_1 e^{-\delta n^2\pi^2/R_1C_1}}{n^2\pi^2} \right] \qquad \text{[Eq 2-56]}$$

$$q_1(2\delta) = -\frac{T}{\delta}\left[\frac{C_1}{3} + 2\sum_{n=1}^{\infty}\frac{C_1\left(e^{-2\delta n^2\pi^2/R_1C_1} - 2e^{-\delta n^2\pi^2/R_1C_1}\right)}{n^2\pi^2}\right] \qquad \text{[Eq 2-57]}$$

$$q_1(m\delta) = -\frac{T}{\delta}\left[2\sum_{n=1}^{\infty}\frac{C_1\left(e^{-m\delta\beta_n} - 2e^{-(m-1)\delta\beta_n} + e^{-(m-2)\delta\beta_n}\right)}{n^2\pi^2}\right] \qquad \text{[Eq 2-58]}$$

for $m \geq 3$ and $\beta_n = n^2\pi^2/R_1C_1$.

Applying these equations produces Figure 2-6, the counterpart to Figure 2-5, showing variations in conductive flux surface at 1 when a triangular temperature pulse is applied to surface 1 (surface 2 is at zero temperature).

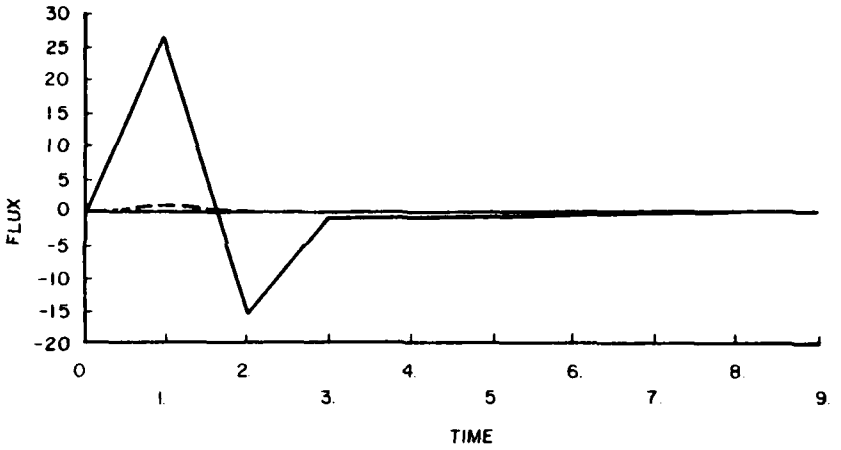

Figure 2-6a. Heat flux (solid line) at surface one due to a triangular pulse (dashed line) at surface one for a heavy slab.

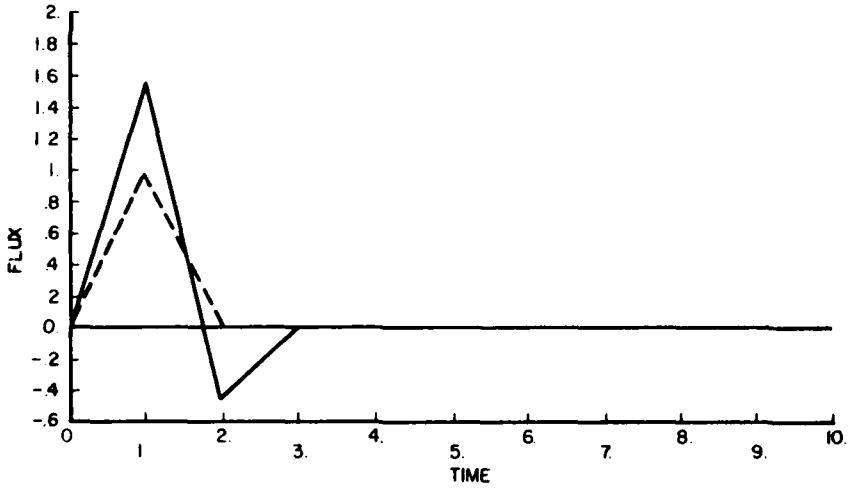

Figure 2-6b. Heat flux (solid line) at surface one due to a triangular pulse (dashed line) at surface one for a light slab.

Response Factors

Let us abbreviate Equations 2-56, 2-57, and 2-58 by defining the following variables:*

$$X_1 = \frac{1}{\delta}\left[\frac{C_1}{3} + \frac{\delta}{R_1} - 2\sum_{n=1}^{\infty}\frac{C_1 e^{-\delta\beta_n}}{n^2\pi^2}\right] \qquad \text{[Eq 2-59]}$$

$$X_2 = -\frac{1}{\delta}\left[\frac{C_1}{3} + 2\sum_{n=1}^{\infty}\frac{C_1\left(e^{-2\delta\beta_n} - 2e^{-\delta\beta_n}\right)}{n^2\pi^2}\right] \qquad \text{[Eq 2-60]}$$

$$X_m = -\frac{1}{\delta}\left[2\sum_{n=1}^{\infty}\frac{C_1\left(e^{-m\delta\beta_n} - 2e^{-(m-1)\delta\beta_n} + e^{-(m-2)\delta\beta_n}\right)}{n^2\pi^2}\right] \qquad \text{[Eq 2-61]}$$

$$= -\frac{1}{\delta}\left[2\sum_{n=1}^{\infty}\frac{C_1\left(e^{-m\delta\beta_n}(1-e^{\delta\beta_n})^2\right)}{n^2\pi^2}\right], \quad m = 3,4,5 \ldots.$$

Next we abbreviate Equations 2-45, 2-48, and 2-50 by defining the following variables.

* In some of the literature, X_1, X_2,... may be defined starting with the subscript zero, i.e., X_0, X_1, X_2...

$$Y_1 = -\frac{1}{\delta}\left[\frac{C_1}{6} - \frac{\delta}{R_1} + 2\sum_{n=1}^{\infty}\frac{(-1)^n C_1 e^{-\delta\beta_n}}{n^2\pi^2}\right] \qquad \text{[Eq 2-62]}$$

$$Y_2 = \frac{1}{\delta}\left[\frac{C_1}{6} + 2\sum_{n=1}^{\infty}\frac{(-1)^n C_1\left(2e^{-\delta\beta_n} - e^{-2\delta\beta_n}\right)}{n^2\pi^2}\right] \qquad \text{[Eq 2-63]}$$

$$Y_m = -\frac{1}{\delta}\left[2\sum_{n=1}^{\infty}\frac{(-1)^n C_1\left(e^{-m\delta\beta_n} - 2e^{-(m-1)\delta\beta_n} + e^{-(m-2)\delta\beta_n}\right)}{n^2\pi^2}\right]$$

$$= -\frac{1}{\delta}\left[2\sum_{n=1}^{\infty}\frac{(-1)^n C_1\left(e^{-m\delta\beta_n}\left(1-e^{\delta\beta_n}\right)^2\right)}{n^2\pi^2}\right], \quad m = 3,4,5 \ldots \qquad \text{[Eq 2-64]}$$

Notice that we have introduced a sign change in defining Y_1, Y_2, and Y_m.

We may now apply the superposition principles to find the conductive flux at surface 1 due to the <u>combined</u> effect of a triangular pulse of height T_i applied to the inside surface (surface 1) <u>and</u> a triangular pulse of height T_o applied at the outside surface (surface 2), where both pulses start at time zero (their apex is at $t = \delta$).

$$q_1(\delta) = T_i X_1 - T_o Y_1 \qquad \text{[Eq 2-65]}$$

$$q_1(2\delta) = T_i X_2 - T_o X_2 \qquad \text{[Eq 2-66]}$$

$$q_1(m\delta) = T_i X_m - T_o Y_m, \quad m = 3,4,5..... \qquad \text{[Eq 2-67]}$$

Remembering that q_1 is the flux in the positive direction, the above equations define the flux leaving surface 1 due to conduction.

By simply changing our point of reference, we can write an equation for the flux leaving surface 1 in terms of present and past surface temperature pulses. Suppose we are sitting at a point in time coincident with the apex of inside and outside triangular temperature pulses of height $T_{i,t}$ and $T_{o,t}$, respectively. Part of the flux leaving surface 1 is due to the upward part of the ramps with slopes $T_{i,t}/\delta$ and $T_{o,t}/\delta$. This contribution is:

$$q_1(t)_t = T_{i,t} X_1 - T_{o,t} Y_1 \qquad \text{[Eq 2-68]}$$

Another contribution is due to two of the three ramps which make up the pulses centered at t-1 (time is in units of δ). This contribution is:

$$q_1(t)_{t-1} = T_{i,t-1}X_2 - T_{o,t-1}Y_2 \qquad \text{[Eq 2-69]}$$

Similarly, all three ramps of the pulses centered at t-2 contribute to the flux at t as do the ramps making up the pulses at t-3, t-4, t-5, and so on. The sum of all these contributions gives the flux leaving surface 1:

$$q_{i,t} = q_1(t) = \sum_{m=1}^{\infty} T_{i,t-m+1}X_m - \sum_{m=1}^{\infty} T_{o,t-m+1}Y_m \qquad \text{[Eq 2-70]}$$

The infinite series of Xs and Ys above forms two parts of a set of three series known as X,Y,Z response factors. Although we have only shown how X and Y response factors are calculated for a single-layer slab, they are equally well defined for multilayered slabs. Repeating Equation 2-30 will help make their definition clear.

$$\begin{bmatrix} q_1(s) \\ q_{n+1}(s) \end{bmatrix} = \begin{bmatrix} \frac{D(s)}{B(s)} & -\frac{1}{B(s)} \\ \frac{1}{B(s)} & -\frac{A(s)}{B(s)} \end{bmatrix} \begin{bmatrix} T_1(s) \\ T_{n+1}(s) \end{bmatrix} \qquad \text{[Eq 2-71]}$$

The X series of response factors is defined as the inverse Laplace transform of the quantity D(s)/B(s) times the Laplace transform of a triangular pulse of unit height. We have already shown that this pulse is made up of three ramps, which leads to a three-part form for the required inverse transform. If, for notational convenience, we define the transform of the pulse as P(s),* we can formally define the set of X response factors as:

$$X_m = {}^{-1}\left[P(s)\,\frac{D(s)}{B(s)}\right]\Bigg|_{t=m\delta,\ m=1,2,3....} \qquad \text{[Eq 2-72]}$$

This series is sometimes referred to as the set of <u>internal</u> response factors, since it represents the flux response of the inside surface to changes in inside surface temperature.

The Y series of response factors is defined as

---

* The Laplace transform of a triangular pulse of unit height and base 2δ is:

$$P(s) = \frac{1}{\delta s^2} \qquad 0 \le t \le \delta$$

$$P(s) = (1-2e^{-s\delta})/\delta s^2 \qquad \delta \le t \le 2\delta$$

$$P(s) = (1-2e^{-s\delta} + e^{-2s\delta})/\delta s^2 \qquad t \ge 2\delta$$

We could equally well have found the inverse of $P(s)\,\frac{D(s)}{B(s)}$ or $\frac{P(s)}{B(s)}$ instead of $\frac{D(s)}{s^2B(s)}$ and $\frac{1}{s^2B(s)}$.

$$Y_m = \mathcal{L}^{-1}\left[P(s)\,\frac{1}{B(s)}\right]\Bigg|_{t=m\delta,\ m=1,2,3.....} \qquad \text{[Eq 2-73]}$$

This series is sometimes referred to as the set of cross response factors, since it characterizes both the flux response of the inside surface to outside temperature variation and the flux response of the outside surface to inside temperature variation.

Finally, the Z series of response factors is defined as:

$$Z_m = \mathcal{L}^{-1}\left[P(s)\,\frac{A(s)}{B(s)}\right]\Bigg|_{t=m\delta,\ m=1,2,3....} \qquad \text{[Eq 2-74]}$$

This series is sometimes referred to as the set of external response factors, since it represents the flux response of the outside surface to changes in the outside surface temperature. For a single-layer slab or a symmetric multilayered slab, A(s) = D(s) and therefore, $Z_m = X_m$. In all other cases they are not equal.

With this definition of the Z response factor series, we can develop an equation for $q_{n+1}(t)$, the outside flux, in exactly the same way we derived Equation 2-70. The final result is:

$$q_{o,t} = q_{n+1}(t) = \sum_{m=1}^{\infty} T_{i,t-m+1} Y_m - \sum_{m=1}^{\infty} T_{o,t-m+1} Z_m \qquad \text{[Eq 2-75]}$$

This is the positive X-directed flux at the outside surface. It is therefore the conductive flux into the outside surface.

We now take note of the complexity involved in finding response factors for a multilayered slab. Equations 2-72, 2-73, and 2-74 have a deceivingly simple form. However, for a multilayered slab, each of the terms A(s), B(s), C(s), and D(s) represents complicated sums and products of hyperbolic functions of s and the properties of each layer. Recall particularly that we must find the poles of the various Laplace transformed expressions in order to find the inverse transforms. Since B(s) is in the denominator of each response factor expression, we must find the roots of B(s) = 0 in order to find the required poles. The problem is complicated even for a two-layered slab for which

$$B(s) = \frac{R_2}{\sqrt{sR_2C_2}} \cosh \sqrt{sR_1C_1} \sinh \sqrt{sR_2C_2} + \frac{R_1}{\sqrt{R_1C_1}} \cosh \sqrt{sR_2C_2} \sinh \sqrt{sR_1C_1}$$

[Eq 2-76]

We are quickly forced to rely on numerical techniques to find the roots of B(s). All of these techniques, however, require that we try various values of s in the appropriate expression for B(s) until we find s such that B(s) = 0. Each time we change the value of s we must perform the matrix multiplication necessary to calculate each

element of the transmission matrix (see Equation 2-28). Furthermore (theoretically), an infinite number of roots must be found. (As a practical matter, we may need to find 20 or more, depending on the properties of the layers in the slab.) Even after the roots are found, we must find the derivative of B(s) with respect to s evaluated at each of the roots (analogously to Equations 2-42 and 2-54). For a multilayered slab, we must carry out a series of matrix manipulations for each root as we apply the chain rule to find the required derivatives. Finally, for each mth response factor, we must carry out the sum of the exponential series illustrated by the right-hand sides of Equations 2-59 through 2-64. Again, in theory, there is an infinite number of X, Y, and Z response factors. In practice, 20 or more response factors may be required to calculate heat flow through heavy masonry walls accurately.

As a practical matter, the calculation of response factors for multilayered slabs requires the use of a computer.

We now conclude our discussion of response factors by presenting the general formula for calculating each term for a multilayered slab.

First, let $-\beta_n$ be the nth root of $B(s) = 0$.

The X response factor series is:

$$X_1 = \left[\frac{D(s)}{B(s)} + \frac{D'(s)}{\delta B(s)} - \frac{D(s)B'(s)}{\delta(B(s))^2}\right]\Bigg|_{s=0} + \sum_{n=1}^{\infty} \frac{e^{-\delta\beta_n} D(s)}{\delta\beta_n^2 B'(s)}\Bigg|_{s=-\beta_n} \qquad \text{[Eq 2-77]}$$

$$X_2 = -\left[\frac{D'(s)}{\delta B(s)} - \frac{D(s)B'(s)}{\delta(B(s))^2}\right]\Bigg|_{s=0} + \sum_{n=1}^{\infty} \frac{e^{-2\delta\beta_n}(1-2e^{\delta\beta_n}) \quad D(s)}{\delta\beta_n^2 B'(s)}\Bigg|_{s=-\beta_n} \qquad \text{[Eq 2-78]}$$

$$X_m = \sum_{n=1}^{\infty} \frac{D(s)e^{-m\delta\beta_n}(1-e^{\delta\beta_n})^2}{\delta\beta_n^2 B'(s)}\Bigg|_{s=-\beta_n} \qquad \text{[Eq 2-79]}$$

where $B'(s) = \frac{d(B(s))}{ds}$; $D'(s) = \frac{d(D(s))}{ds}$

The y response factor series is:

$$Y_1 = \left[\frac{1}{B(s)} + \frac{1}{\delta B(s)} - \frac{B'(s)}{\delta(B(s))^2}\right]\Bigg|_{s=0} + \sum_{n=1}^{\infty} \frac{e^{-\delta\beta_n}}{\delta\beta_n^2 B'(s)}\Bigg|_{s=-\beta_n} \qquad \text{[Eq 2-80]}$$

$$Y_2 = -\left[\frac{1}{\delta B(s)} - \frac{B'(s)}{\delta(B(s))^2}\right]\Bigg|_{s=0} + \sum_{n=1}^{\infty} \frac{e^{-2\delta\beta_n}(1-2e^{\delta\beta_n})}{\delta\beta_n^2 B'(s)}\Bigg|_{s=-\beta_n} \qquad \text{[Eq 2-81]}$$

$$Y_m = \sum_{n=1}^{\infty} \left. \frac{e^{-m\delta\beta_n}(1-e^{\delta\beta_n})^2}{\delta\beta_n^2 B'(s)} \right|_{s=-\beta_n} \qquad \text{[Eq 2-82]}$$

The z response factor series is:

$$Z_1 = \left[\frac{A(s)}{B(s)} + \frac{A'(s)}{\delta B(s)} - \frac{A(s)B'(s)}{\delta(B(s))^2}\right]\Bigg|_{s=0} + \sum_{n=1}^{\infty} \left. \frac{e^{-\delta\beta_n}A(s)}{\delta\beta_n^2 B'(s)} \right|_{s=-\beta_n} \qquad \text{[Eq 2-83]}$$

$$Z_2 = -\left[\frac{A'(s)}{\delta B(s)} - \frac{A(s)B'(s)}{\delta(B(s))^2}\right]\Bigg|_{s=0} + \sum_{n=1}^{\infty} \left. \frac{e^{-2\delta\beta_n}(1-2e^{\delta\beta_n})\quad A(s)}{\delta\beta_n^2 B'(s)} \right|_{s=-\beta_n} \qquad \text{[Eq 2-84]}$$

$$Z_m = \sum_{n=1}^{\infty} \left. \frac{A(s)\, e^{-m\delta\beta_n}(1-e^{\delta\beta_n})^2}{\delta\beta_n^2 B'(s)} \right|_{s=-\beta_n} \qquad \text{[Eq 2-85]}$$

where $A'(s) = \frac{d(A(s))}{ds}$

The derivatives A'(s), B'(s), and D'(s) are found by applying the chain rule as follows:

$$\frac{d}{ds}\begin{bmatrix} A(s) & B(s) \\ C(s) & D(s) \end{bmatrix} = \begin{bmatrix} \frac{dA(s)}{ds} & \frac{dB(s)}{ds} \\ \frac{dc(s)}{ds} & \frac{dD(s)}{ds} \end{bmatrix} = \begin{bmatrix} A'(s) & B'(s) \\ C'(s) & D'(s) \end{bmatrix}$$

$$= \begin{bmatrix} A_1'(s) & B_1'(s) \\ C_1'(s) & D_1'(s) \end{bmatrix} \begin{bmatrix} A_2(s) & B_2(s) \\ C_2(s) & D_2(s) \end{bmatrix} \cdots \begin{bmatrix} A_n(s) & B_n(s) \\ C_n(s) & D_n(s) \end{bmatrix}$$

[Eq 2-86]

$$+ \begin{bmatrix} A_1(s) & B_1(s) \\ C_1(s) & D_1(s) \end{bmatrix} \begin{bmatrix} A_2'(s) & B_2'(s) \\ C_2'(s) & D_2'(s) \end{bmatrix} \cdots \begin{bmatrix} A_n(s) & B_n(s) \\ C_n(s) & D_n(s) \end{bmatrix}$$

$$+ \quad \cdots \quad + \begin{bmatrix} A_1(s) & B_1(s) \\ C_1(s) & D_1(s) \end{bmatrix} \begin{bmatrix} A_2(s) & B_2(s) \\ C_2(s) & D_2(s) \end{bmatrix} \cdots \begin{bmatrix} A_n'(s) & B_n'(s) \\ C_n'(s) & D_n'(s) \end{bmatrix}$$

Finally, we note two properties of response factors which are important in their calculation and use. First, the sum of each of the X, Y, or Z series is equal to the U value of the composite slab ($U = 1/[R_1 + R_2 + R_3 \ldots R_n]$). The steady-state limiting case requires these sums to be the U value as seen by Equations 2-70 and 2-75. In Equation 2-75, for example, if both T_i and T_o are constant with time, then

$$q_{o,t} = T_i \sum_{m=1}^{\infty} y_m - T_o \sum_{m=1}^{\infty} Z_m = (T_i - T_o)U \qquad \text{[Eq 2-87]}$$

Hence,

$$\sum_{m=1}^{\infty} Y_m = \sum_{m=1}^{\infty} Z_m = U \qquad \text{[Eq 2-88]}$$

Similarly, from Equation 2-70,

$$\sum_{m=1}^{\infty} X_m = U. \qquad \text{[Eq 2-89]}$$

This has proved to be a useful check in calculating response factors.

The second useful property of response factors is that later terms in each series are made up exclusively of exponential functions (see Equations 2-79, 2-82, and 2-85). Furthermore, each of these terms is of diminishing importance, since the roots of $B(s) = 0$ are sequentially more negative. We will make immediate use of this property in defining conduction transfer functions.

Conduction Transfer Functions

If we now carefully examine the response factor equations, we see that the higher-order terms have the same basic form. For the Y response factor, for example:

$$Y_m = \sum_{n=1}^{\infty} \frac{e^{-m\delta\beta_n}(1-e^{\delta\beta_n})^2}{\delta\beta_n^2 B'(s)}\Bigg|_{s=-\beta_n} \qquad \text{[Eq 2-90]}$$

for $m \geq 3$.

We can write this equation as

$$Y_m = \sum_{n=1}^{\infty} g_n \lambda_n^m \qquad \text{[Eq 2-91]}$$

where $\lambda_n = e^{-\delta\beta_n}$ and $g_n = \frac{(1-e^{\delta\beta_n})^2}{\delta\beta_n^2 B'(s)}\Big|_{s=-\beta_n}$

Recall that n is the index of the roots of B(s) = 0, all of which lie on the negative real axis and which increase in absolute value as n increases. For a heavy single-layer slab with R_1 = .4 m^2 - $^oK/w$ and C_1 = 704000 J/m^2 - ^oK, the roots of B(s) = 0 are shown below, along with $-\delta\beta_n$, λ_n and g_n for δ = 3600 sec.

n	Roots of B(s)=0 or $-\beta_n$	$-\delta\beta_n$	$\lambda_n = e^{-\delta\beta_n}$	g_n
1	-3.504×10^{-5}	-.126	.8815	+.7166
2	-14.02×10^{-5}	-.505	.6037	-4.270
3	-31.54×10^{-5}	-1.136	.3212	19.66
4	-56.08×10^{-5}	-2.019	.1328	-105.6
5	-87.62×10^{-5}	-3.154	.0427	798.0
6	-126.17×10^{-5}	-4.5423	.0149	-9500.7

Notice that for m = 20, $g_1 \lambda_1^{20}$, = .0575, but $g_2\lambda_2^{20}$ = -.00018 and $g_3\lambda_3^{20} \simeq 0.0000$. Hence, for $m \geq 20$, $Y_m \simeq g_1\lambda_1^m$. Similarly, for m = 10, $g_1\lambda_1^{10}$ = .2030, $g_2\lambda_2^{10}$ = -0.274, but $g_3\lambda_3^{10}$ = .00023 and $g_4\lambda_4^{10} \simeq$ 0.0000. Hence, for $10 \leq m \leq 20$, Y_m is approximately equal to the contribution caused by the two largest roots, i.e., $Y_m \simeq g_1 \lambda_1^m + g_2\lambda_2^m$. The general pattern is clear. For large m, only λ_1 is important. As m decreases, λ_2, then λ_3, then λ_4 and so on, become important. λ_1 takes its value from the root of B(s) = 0 which is nearest the origin, λ_2 from the next nearest root, and so on. While our example is for a single-layer slab, it is but a special case of this general behavior of later terms in the response factor series for multilayered slabs.

We now make use of above expressions to reduce the number of response factors needed to calculate heat flux. Consider the case where the heat flow at the inside surface is to be calculated under varying outside surface temperature, while the inside surface is at zero temperature.

$$q_{i,t} = - \sum_{m=1}^{\infty} Y_m T_{o,t-m+1} \qquad \text{[Eq 2-92]}$$

If, for m greater than or equal to some m', $Y_m \simeq g_1\lambda_1^m$, we may write, for times t and t-1:

$$q_{i,t} = -Y_1 T_{o,t} - Y_2 T_{o,t-1} - Y_3 T_{o,t-2} - \cdots - Y_{m'-1} T_{o,t-m'+2}$$
$$-g_1 \lambda_1^{m'} T_{o,t-m'+1} - g_1 \lambda_1^{m'+1} T_{o,t-m'} - g_1 \lambda_1^{m'+2} T_{o,t-m-1} \cdots \quad \text{[Eq 2-93]}$$

$$q_{i,t-1} = Y_1 T_{o,t-1} - Y_2 T_{o,t-2} - Y_3 T_{o,t-3} - \cdots - Y_{m'-2} T_{o,t-m'+2} - Y_{m'-1} T_{o,t-m'}$$
$$- g_1 \lambda_1^{m'} T_{o,t-m'} - g_1 \lambda_1^{m'+1} T_{o,t-m-1} - \cdots \quad \text{[Eq 2-94]}$$

We can multiply $q_{i,t-1}$ by λ_1 and subtract the result from $q_{i,t}$. After collecting coefficients, we have:

$$q_{i,t} - \lambda_1 q_{i,t-1} = - Y_1 T_{o,t} - (Y_2 - \lambda_1 Y_1) T_{o,t-1} - (Y_3 - \lambda_1 Y_2) T_{o,t-2} - \cdots$$
$$- (Y_{m'-1} - \lambda_1 Y_{m'-2}) T_{o,t-m'+2} - (Y_{m'} - \lambda_1 Y_{m'-1}) T_{o,t-m'+1}$$
$$-(g_1 \lambda_1^{m'+1} - g_1 \lambda_1 \lambda_1^{m'}) T_{o,t-m'} - (g_1 \lambda_1^{m'+2} - g_1 \lambda_1 \lambda_1^{m'+1}) T_{o,t-m'-1}$$
$$- \cdots \quad \text{[Eq 2-95]}$$

Notice that the coefficients for all temperatures preceding $T_{o,\ t-m+1}$ (i.e., $T_{o,t-m'}$, $T_{o,t-m'-1}$, $T_{o,t-m'-2}$...) are zero. We may therefore define a finite series of first-order conduction transfer coefficients or first-order conduction transfer function as follows:

$$Y_{1,1} = Y_1, \qquad \text{[Eq 2-96]}$$

$$Y_{1,m} = Y_m - \lambda_1 Y_{m-1} \quad \text{for } m \geq 2 \qquad \text{[Eq 2-97]}$$

We may now rearrange Equation 2-95 as:

$$q_{i,t} = - \sum_{m=1}^{m'} Y_{1,m} T_{o,t-m+1} + \lambda_1 q_{i,t} \qquad \text{[Eq 2-98]}$$

Applying the same procedure for X and Z response factors yields first-order X and Z conduction transfer functions:

$$X_{1,1} = X_1 \qquad \text{[Eq 2-99]}$$

$$X_{1,m} = X_m - \lambda_1 X_{m-1} \quad \text{for } m \geq 2 \qquad \text{[Eq 2-100]}$$

$$Z_{1,1} = Z_1 \qquad \text{[Eq 2-101]}$$

$$Z_{1,m} = Z_m - \lambda_1 Z_{m-1} \quad \text{for } m \geq 2 \qquad \text{[Eq 2-102]}$$

The counterparts to Equations 2-70 and 2-75 then become:

$$q_{i,t} = \sum_{m=1}^{m'} X_{1,m} T_{i,t-m+1} - \sum_{m=1}^{m'} Y_{1,m} T_{o,t-m+1} + \lambda_1 q_{i,t-1} \qquad \text{[Eq 2-103]}$$

$$q_{o,t} = \sum_{m=1}^{m'} Y_{1,m} T_{i,t-m+1} - \sum_{m=1}^{m'} Z_{1,m} T_{o,t-m+1} + \lambda_1 q_{o,t-1} \qquad \text{[Eq 2-104]}$$

λ_1 is often termed the "common ratio" since, for large m, it equals the ratio of successive terms in the response factor series (i.e., Y_{m+1}/Y_m). It is neither necessary nor advisable, however, to

calculate λ_1 as the ratio of successive terms, since λ_1 is known from calculations which precede the final step used to calculate response factors. It is also not necessary to decide, a priori, on a value for m'. Instead, a reasonable procedure is to calculate response factors until their values are some very small function of the overall U value for the multilayered slab. Conduction transfer functions can then be calculated and the series may be truncated when the mth conduction transfer function is some very small fraction of the U value times $(1 - \lambda_1)$. Figure 2-7 shows a plot of the results of such a procedure for the Y conduction transfer function, using the heavy, single-layer slab of our previous example. The upper solid line shows the Y response factors, and the upper dashed line shows the first-order conduction transfer function.

The lower solid and dashed lines of Figure 2-7 are second- and third-order conduction transfer functions, a logical extension of first-order conduction transfer functions. In going from response factors to first-order conduction transfer functions, we have accounted for the effects of all response factors from m' to infinity in one flux history term and removed the effects of λ_1 from the remaining conduction transfer functions. We are left with first-order conduction transfer functions whose later terms (as $m \rightarrow m'$) are now dominated by λ_2. We now remove the effect of λ_2 in a completely analogous way. The necessary sample equation, similar to Equation 2-95, is:

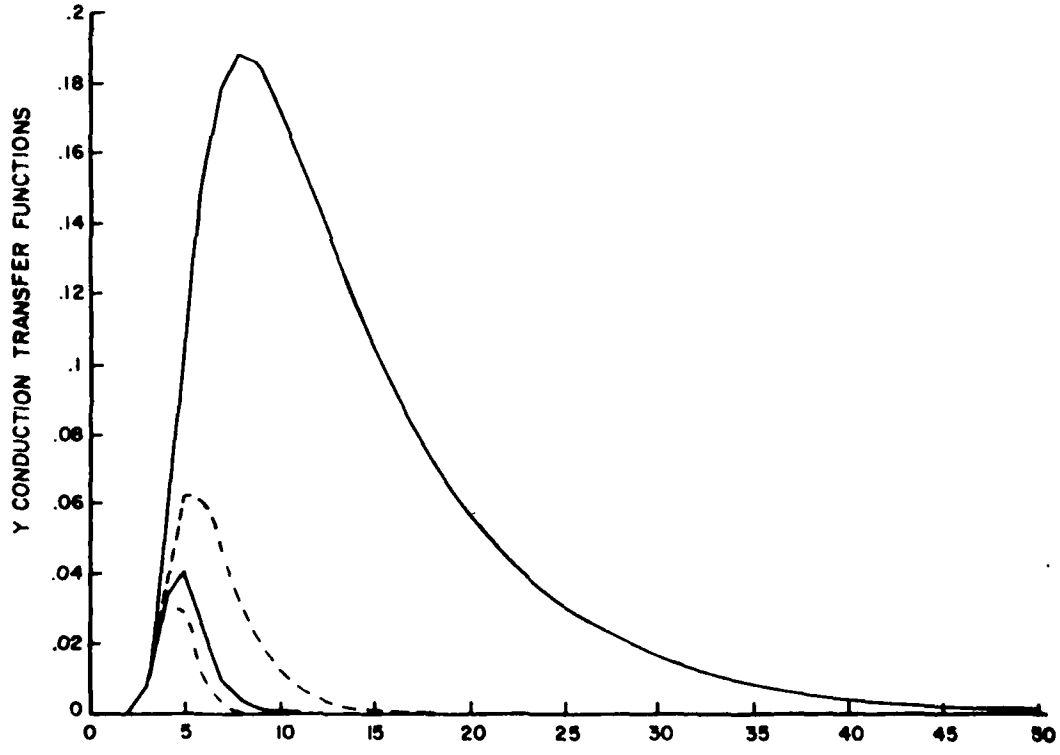

Figure 2-7. Y conduction transfer functions for single-layer slab.

$$(q_{i,t}-\lambda_1 q_{i,t-1}) - \lambda_2(q_{i,t-1}-\lambda_1 q_{i,t-2}) =$$

$$-Y_{1,1}T_{o,t} - (Y_{1,2}-\lambda_2 Y_{1,1})T_{o,t-1} - (Y_{1,3}-\lambda_2 Y_{1,2})T_{o,t-1}$$

$$- \ldots - (Y_{1,m''}-\lambda_2 Y_{1,m''-1})T_{o,t-m''+1} \qquad \text{[Eq 2-105]}$$

where m'' is the point after which $Y_{1,m} \simeq g_2\lambda_2^m$. Second-order conduction transfer functions can now be defined completely analogously to first-order, conduction transfer functions, as can third-, fourth-, or kth-order conduction transfer functions.

$$X_{2,1} = X_{1,1} \qquad \text{[Eq 2-106]}$$

$$X_{2,m} = X_{1,m}-\lambda_2 X_{1,m-1} \quad \text{for } m \geq 2 \qquad \text{[Eq 2-107]}$$

$$Y_{2,1} = Y_{1,1} \qquad \text{[Eq 2-108]}$$

$$Y_{2,m} = Y_{1,m} - \lambda_2 Y_{1,m-1} \quad \text{for } m \geq 2 \qquad \text{[Eq 2-109]}$$

$$Z_{2,1} = Z_{1,1} \qquad \text{[Eq 2-110]}$$

$$Z_{2,m} = Z_{1,m} - \lambda_2 Z_{1,m-1} \quad \text{for } m \geq 2 \qquad \text{[Eq 2-111]}$$

The counterparts to Equations 2-103 and 2-104 for second-order conduction transfer functions are:

$$q_{i,t} = \sum_{m=1}^{m''} X_{2,m} T_{i,t-m+1} - \sum_{m=1}^{m''} Y_{2,m} T_{o,t-m+1} + (\lambda_1+\lambda_2) q_{i,t-1} - \lambda_1 q_{i,t-2} \qquad \text{[Eq 2-112]}$$

$$q_{o,t} = \sum_{m=1}^{m''} Y_{2,m} T_{2,t-m+1} - \sum_{m=1}^{m''} Z_{2,m} T_{o,t-m+1} + (\lambda_1+\lambda_2) q_{o,t-1} - \lambda_1 q_{o,t-2} \qquad \text{[Eq 2-113]}$$

For kth-order conduction transfer functions, we have

$$q_{1,t} = \sum_{m=1}^{M} X_{k,m} T_{i,t-n+1} - \sum_{m=1}^{M} Y_{k,m} T_{o,t-m+1} + \sum_{m=1}^{k} F_m q_{i,t-k} \qquad \text{[Eq 2-114]}$$

$$q_{o,t} = \sum_{m=1}^{M} Y_{k,m} T_{i,t-m+1} - \sum_{m=1}^{M} Z_{k,m} T_{o,t-m+1} + \sum_{m=1}^{k} F_m q_{i,t-k} \qquad \text{[Eq 2-115]}$$

where M is the value of m, above which the kth conduction transfer function is proportional to λ_k^m. F_m values are flux history coefficients defined as follows:

$$F_1 = \sum_{n=1}^{k} \lambda_n \qquad \text{[Eq 2-116]}$$

$$F_2 = - \text{[sum of the products of } \lambda_n \text{ taken two at a time]} \qquad \text{[Eq 2-117]}$$

$$F_3 = + \text{[sum of the products of } \lambda_n \text{ taken three at a time]} \qquad \text{[Eq 2-118]}$$

$$F_k = (-1)^{k+1} \prod_{n=1}^{k} \lambda_n \qquad \text{[Eq 2-119]}$$

For k = 4, for example (fourth-order conduction transfer functions):

$$F_1 = \lambda_1 + \lambda_2 + \lambda_3 + \lambda_4 \qquad \text{[Eq 2-120]}$$

$$F_2 = - [\lambda_1\lambda_2 + \lambda_1\lambda_3 + \lambda_1\lambda_4 + \lambda_2\lambda_3 + \lambda_2\lambda_4 + \lambda_3\lambda_4] \qquad \text{[Eq 2-121]}$$

$$F_3 = + [\lambda_1\lambda_2\lambda_3 + \lambda_1\lambda_2\lambda_4 + \lambda_1\lambda_3\lambda_4 + \lambda_2\lambda_3\lambda_4] \qquad \text{[Eq 2-122]}$$

$$F_4 = - \lambda_1\lambda_2\lambda_3\lambda_4 \qquad \text{[Eq 2-123]}$$

The practical value of conduction transfer function and a general scheme for determining the order of the transfer function to use

are both illustrated by Figure 2-7. First, we see that by using one flux history term, we can use about 20 temperature history terms instead of about 50. Thus, to calculate fluxes using first-order conduction transfer functions, we must perform about 86 multiplications and additions and keep track of about 40 temperature and flux histories, compared to about 200 multiplications and additions and about 98 temperature histories if we had used response factors. For second-order transfer functions, about 10 past temperatures are required, along with two past fluxes (46 operations and 22 histories). For third-order, about eight past temperatures are needed, along with three past fluxes (42 operation and 20 histories). Obviously, the reduction in the number of terms required is diminishing at this point, but we have already reduced the needed calculations and storage to about 20 percent of what would be required if we had used response factors directly. Our efforts would be half of what would be required with first-order conduction transfer functions.

If, in the example shown in Figure 2-7, we proceed to fourth- or fifth- or higher-order transfer functions, we will first simply trade one pair of past temperatures for a pair of past fluxes. Soon, however, the number of flux terms required will increase more rapidly than the reduction in the number of required temperature histories. In the limit, we will need an infinite number of flux terms, along with the current temperature. The selection of the appropriate number and order of conduction transfer function coefficients to use

for a given wall section has been addressed by Mitalis (ref 24), and by Peavy (ref 18) and Walton (ref 25). (The mathematical development of the procedures used by Mitalis, Kusuda [ref 17], and Peavy are fundamentally identical.)

To determine the appropriate number of terms for kth-order conduction transfer functions, we recall that for zero-order conduction transfer functions (i.e., response factors), the sum of the coefficients of the infinite X, Y, or Z series equals the U value. For first-order conduction transfer functions,

$$\sum_{m=1}^{M_1} X_{1,m} = \sum_{m=1}^{M_1} Y_{1,m} = \sum_{m=1}^{M_1} Z_{1,m} = (1-\lambda_1)U \qquad \text{[Eq 2-124]}$$

(approximately). Similarly, for second-order conduction transfer functions,

$$\sum_{m=1}^{M_2} X_{2,m} = \sum_{m=1}^{M_2} Y_{2,m} = \sum_{m=1}^{M_2} Z_{2,m} = (1-\lambda_1)(1-\lambda_2)U \qquad \text{[Eq 2-125]}$$

In general,

$$\sum_{m=1}^{M} Y_{k,m} = \sum_{m-1}^{M} Y_{k,m} = \sum_{m=1}^{M} Z_{k,m} = U \prod_{i=1}^{k} (1-\lambda_i) \qquad \text{[Eq 2-126]}$$

M can be determined by requiring that the sum of the first M terms of each of the X, Y, or Z conduction transfer functions be equal to a large fraction (say 99 percent) of the right side of Equation 2-125.

Two approaches for determining k -- the order of the transfer functions -- have been proposed. Mitalis suggests that the order of the conduction transfer functions should be one less than M (i.e., k = M-1).* Extensive tabulations of conduction transfer functions of order k = M-1 can be found in the ASHRAE Handbook of Fundamentals (ref 21). Peavy (ref 18) suggests that k need be no larger than 5 for common (even massive) walls, roofs, and floors. Using 5 as an upper limit, Walton (ref 25) suggests that first values of X, Y, and Z conduction transfer function coefficients be calculated for all six possible orders (i.e., M = 1, k = 0, 1, 2, 3, 4, and 5; then M = 2, k = 0, 1, 2, 3, 4, and 5, and so on). Each time M is incremented, the test of Equation 2-125 is applied for successively increasing

* This approach is a natural consequence of Mitalis' use of the Z transform (not to be confused with the Z conduction transfer function) and polynomial arithmetic. It does not necessarily lead to a minimum number of coefficients for a given precision requirement.

values of k. (As a refinement, we note that the test need only be made for $k < M$.) As soon as Equation 2-125 is satisfied to the required precision, k and M are both known. Figure 2-8 shows a flow diagram of the process. For a given precision, Walton's procedure yields the smallest possible set of conduction transfer functions and, therefore, results in the minimum number of calculations when flux calculations are made using the conduction transfer functions.

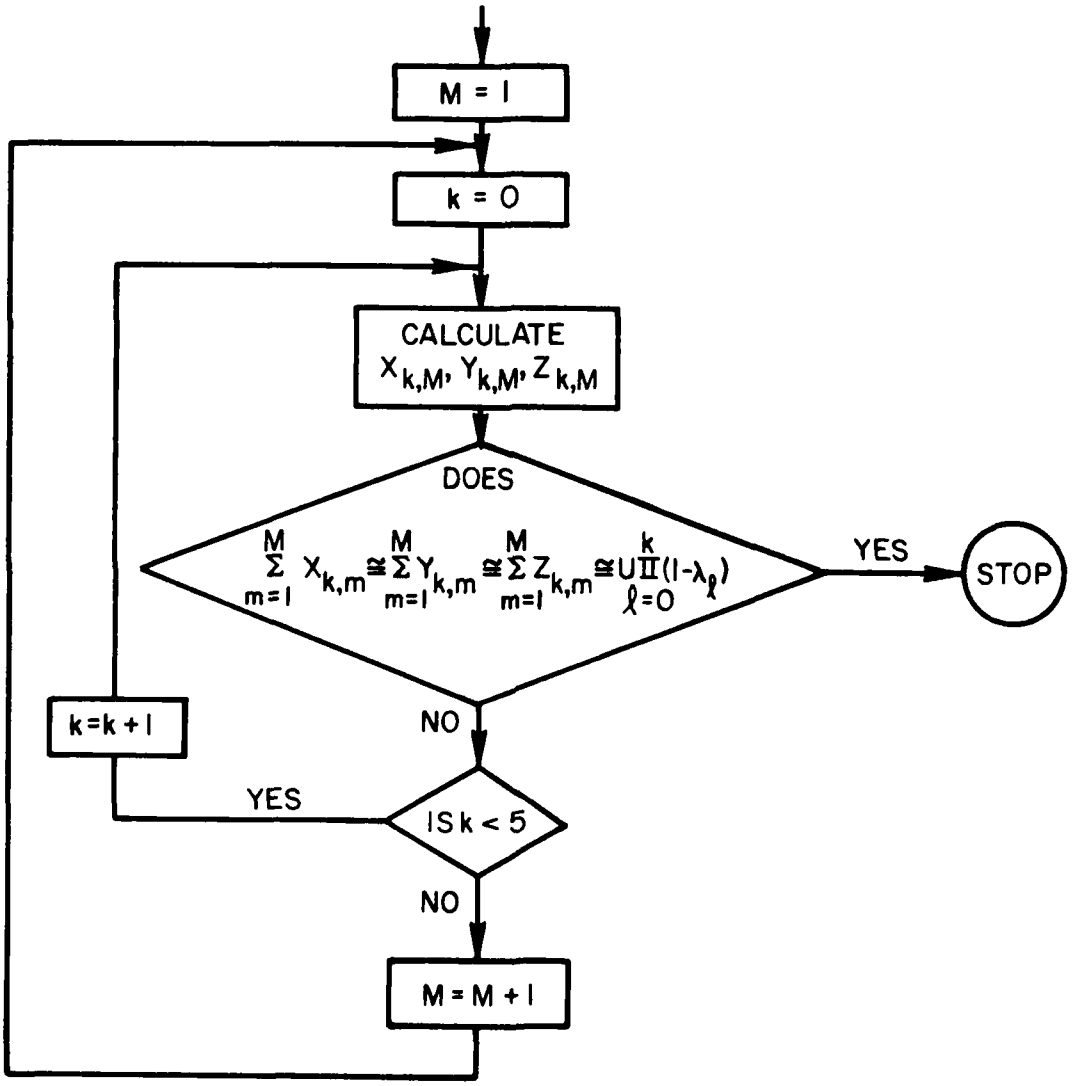

Figure 2-8. Procedure for determining the order of conduction transfer functions.

3 FREQUENCY RESPONSE OF MULTILAYERED SLABS

Exact Solution From the Transmission Matrix

We now examine the special case of a wall with fixed (zero) inside surface temperature and sinusoidally varying outside temperatures. This case is examined for two reasons. First, a large portion of the variation in ambient outdoor temperature and solar radiation is periodic and sinusoidal in character. These two climate variables can be used, along with the absorptivity of the outside surface of a wall or roof, to establish the so-called sol-air temperature. If we treat the thermal resistance of the air film adjoining the outside surface of a multilayered slab as another layer of the slab, then the sol-air temperature becomes the "outside surface" boundary condition. The annual variation in the sol-air temperature for a given location and exposure can be approximated as the sum of a relatively few sine and cosine terms at various fixed frequencies. This simplicity is in sharp contrast to the use of hourly discrete time series containing 8760 hourly values per year.

The second reason for examining this case is that the special instance of one sinusoidal and one fixed temperature boundary condition allows us to solve the heat conduction equation much more easily, as will be demonstrated in subsequent paragraphs.

Recall the general matrix form of the Laplace transform solution of the heat conduction equation for multilayered slabs [Equation 2-27]:

$$\begin{bmatrix} T_1(s) \\ q_1(s) \end{bmatrix} = \begin{bmatrix} A(s) & B(s) \\ C(s) & D(s) \end{bmatrix} \begin{bmatrix} T_{n+1}(s) \\ q_{n+1}(s) \end{bmatrix} \qquad \text{[Eq 3-1]}$$

Since we are interested in the resulting fluxes when temperature boundary conditions are specified, we rewrite Equation 3-1 as follows:

$$\begin{bmatrix} q_1(s) \\ q_{n+1}(s) \end{bmatrix} = \begin{bmatrix} \frac{D(s)}{B(s)} & -\frac{1}{B(s)} \\ \frac{1}{B(s)} & -\frac{A(s)}{B(s)} \end{bmatrix} \begin{bmatrix} T_1(s) \\ T_{n+1}(s) \end{bmatrix} \qquad \text{[Eq 3-2]}$$

For the special case of $T_1(s) = 0$, we may find $q_1(s)$ as:

$$q_1(s) = -\frac{T_{n+1}(s)}{B(s)} \qquad \text{[Eq 3-3]}$$

The transfer function for the wall becomes:

$$\frac{q_1(s)}{T_{n+1}(s)} = -\frac{1}{B(s)} \qquad \text{[Eq 3-4]}$$

We now wish to find $q_1(s)$ under steady periodic state when

$$T_{n+1}(t) = \sin(\omega t) \qquad \text{[Eq 3-5]}$$

where ω = angular frequency of temperature variation of surface T_{n+1}. A well-known property of the Laplace transform is that if $s = j\omega$, the Laplace transform becomes the Fourier transform. Under the special case that $T_{n+1}(t) = \sin(\omega t)$(for $-\infty \leftarrow t \leftarrow +\infty$) and $T_1(t) = 0.0$,

the inverse transform of Equation 3-3 is:

$$q_1(t) = \left[\mathrm{Re}\left[-\frac{1}{B(j\omega)} \right] \sin(\omega t) + \mathrm{Im}\left[-\frac{1}{B(j\omega)} \right] \cos(\omega t) \right] \qquad \text{[Eq 3-6]}$$

where $\mathrm{Re}\left[-\frac{1}{B(j\omega)} \right]$ = the real part of $-\frac{1}{B(s)}$ when $s = j\omega$

$\mathrm{Im}\left[-\frac{1}{B(j\omega)} \right]$ = the imaginary part of $-\frac{1}{B(s)}$ when $s = j\omega$.

Alternately,

$$q_1(t) = \left| -\frac{1}{B(j\omega)} \right| \sin(\omega t - \phi) \qquad \text{[Eq 3-7]}$$

where $\left| -\frac{1}{B(j\omega)} \right|$ = the magnitude of the complex valued function $-\frac{1}{B(j\omega)}$

ϕ = the argument of $-\frac{1}{B(j\omega)}$.

Thus, $q_1(t)$ can be viewed as a weighted sum of $\sin(\omega t)$ and $\cos(\omega t)$ or as a sine wave of amplitude $\left| -\frac{1}{B(j\omega)} \right|$ and phase lag ϕ. We can write $q_1(t)$ for a unit sinusoidal outside surface temperature variation of frequency ω as either:

$$q_1(t) = U_{\omega s} \sin(\omega t) + U_{\omega c} \cos(\omega t) \qquad \text{[Eq 3-8]}$$

where $U_{\omega s} = \mathrm{Re}\left[-\frac{1}{B(j\omega)} \right]$

$U_{\omega c} = \mathrm{Im}\left[-\frac{1}{B(j\omega)} \right]$

or

$$q_1(t) = \bar{U}_{\omega} \sin(\omega t - \phi) \qquad \text{[Eq 3-9]}$$

$$\text{where } \bar{U}_\omega = \sqrt{U_{\omega S}^2 + U_{\omega C}^2} = \left| -\frac{1}{B(j\omega)} \right|$$

$$\phi = \tan^{-1}\left(\frac{U_{\omega C}}{U_{\omega S}}\right)$$

We immediately see how much easier it is to calculate heat flux in this special case. To find $U_{\omega S}$ and $U_{\omega C}$, we simply substitute $j\omega$ for s in each term of the transmission matrix expressions for each layer, carrying out the complex matrix multiplications to find $B(j\omega)$, and find the real and imaginary parts of $-\frac{1}{B(j\omega)}$. For example, for a two-layered slab:

$$\begin{bmatrix} A(j\omega) & B(j\omega) \\ C(j\omega) & D(j\omega) \end{bmatrix} = \begin{bmatrix} \cosh\sqrt{j\omega R_1 C_1} & \frac{R_1}{\sqrt{j\omega R_1 C_1}} \sinh\sqrt{j\omega R_1 C_1} \\ \frac{\sqrt{j\omega R_1 C_1}}{R_1} \sinh\sqrt{j\omega R_1 C_1} & \cosh\sqrt{j\omega R_1 C_1} \end{bmatrix}$$

$$\begin{bmatrix} \cosh\sqrt{j\omega R_2 C_2} & \frac{R_2}{\sqrt{j\omega R_2 C_2}} \sinh\sqrt{j\omega R_2 C_2} \\ \frac{\sqrt{j\omega R_2 C_2}}{R_2} \sinh\sqrt{j\omega R_2 C_2} & \cosh\sqrt{j\omega R_2 C_2} \end{bmatrix} \qquad \text{[Eq 3-10]}$$

$$B(j\omega) = \left(\cosh\sqrt{j\omega R_1 C_1}\right)\left(\frac{R_2}{\sqrt{j\omega R_2 C_2}} \sinh\sqrt{j\omega R_2 C_2}\right)$$

$$+\left(\frac{R_1}{\sqrt{j\omega R_1 C_1}} \sinh\sqrt{j\omega R_1 C_1}\right)\left(\cosh\sqrt{j\omega R_2 C_2}\right) \qquad \text{[Eq 3-11]}$$

Expressions for slabs of more than two layers become complicated, but $B(j\omega)$ can easily be calculated with simple computer algorithms.

Compared to the response factor calculation, the frequency response of multilayered slabs can be calculated without (1) numerically searching for the roots of $B(s) = 0$, (2) finding derivatives of $B(s)$ at the roots of $B(s) = 0$, and (3) evaluating and summing residues at $B(s) = 0$.

Figure 3-1 shows $\overline{U}_\omega$, the frequency-dependent conductance or U-value, and the phase lag, ϕ, versus frequency for a heavy, single-layer slab with inside and outside air film resistances of .12 $\frac{m^{2\circ}K}{\omega}$ and .029 $\frac{m^{2\circ}K}{\omega}$, respectively (essentially three-layered slabs). Figure 3-2 shows similar plots for a heavy, multilayered wall section with insulation separating the heavy layers.

Equivalent Single-Layer Thermal Properties

One of the objectives of this research was to determine whether multilayered slabs could be approximated as single-layer homogeneous slabs having "equivalent" thermal properties. To this end, the error associated with such an approximation was studied. There were two reasons for considering multilayered slabs as having equivalent single-layer resistance, R_e, and equivalent single-layer capacitance, C_e: (1) the potential for simplifying the calculation of $B(j\omega)$, and (2) the potential for experimentally determining values for C_e and R_e for complicated wall sections.

We now consider a two-layered slab and define R_e and C_e for this case, arguing that if these equivalent parameters can be found for a two-layered slab, the procedure can be recursively applied to find R_e and C_e for n layers.

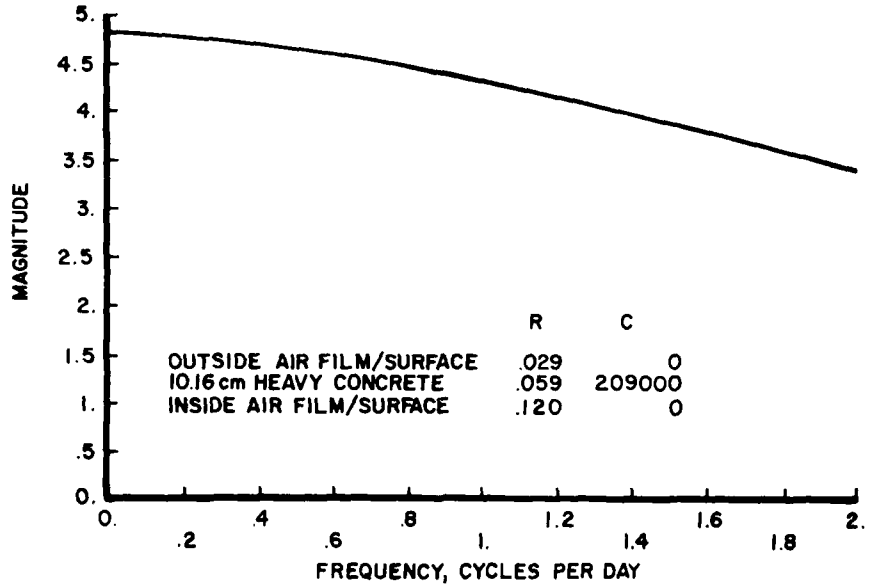

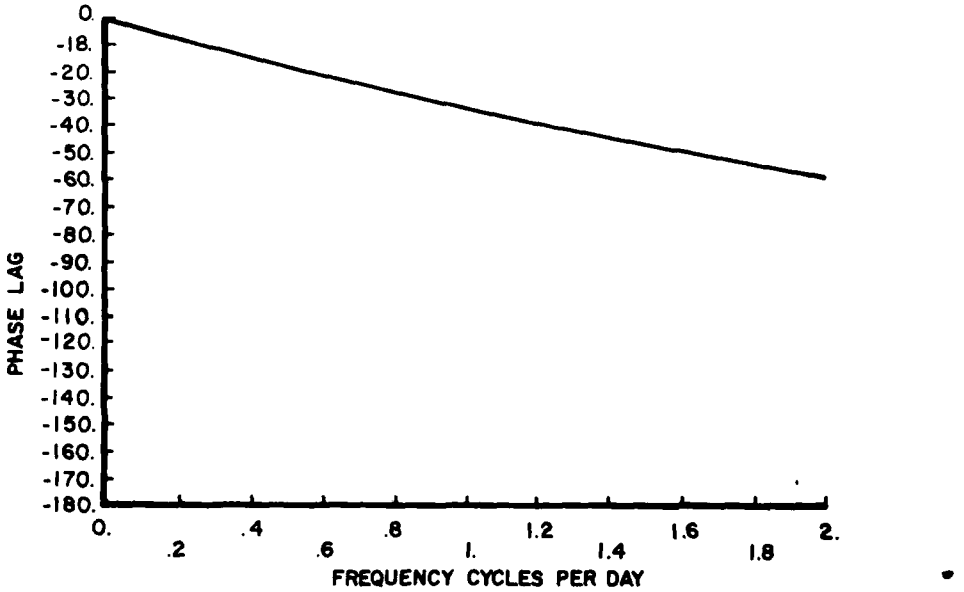

Figure 3-1. Exact frequency response of heavy concrete slab.

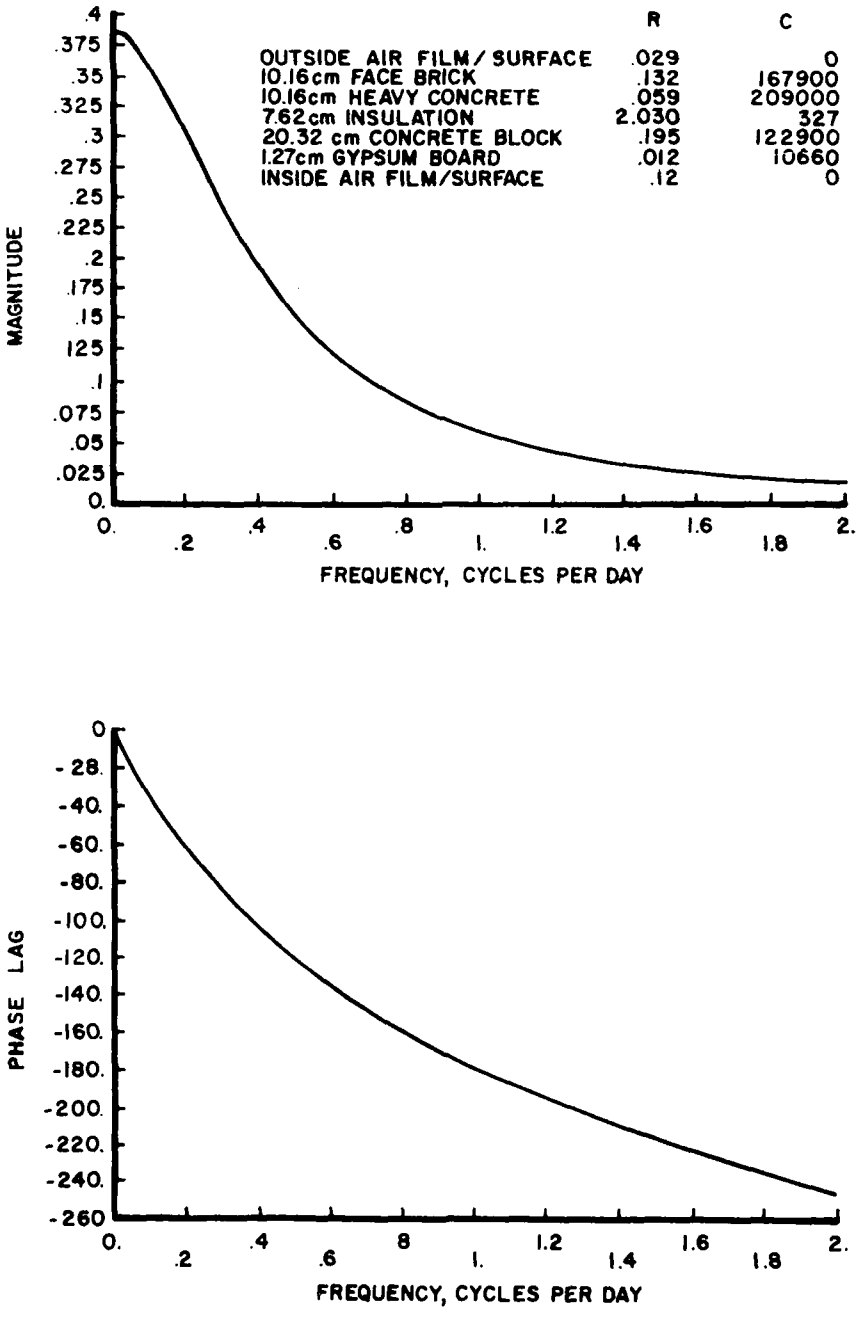

Figure 3-2. Frequency response for heavy multilayered slab.

Returning to the basic definition of the terms in the transmission matrix, we have for a single-layer slab:

$$B(s) = \frac{R_1}{\sqrt{sR_1C_1}} \sinh \sqrt{sR_1C_1} \qquad \text{[Eq 3-12]}$$

For a two-layered slab, we have:

$$\begin{aligned} B(s) &= A_1(s)B_2(s) + B_1(s)D_2(s) \\ &= \left(\cosh \sqrt{sR_1C_1}\right)\left(\frac{R_2}{\sqrt{sR_2C_2}} \sinh \sqrt{sR_2C_2}\right) \\ &\quad + \left(\frac{R_1}{\sqrt{sR_1C_1}} \sinh \sqrt{sR_1C_1}\right)\left(\cosh \sqrt{sR_2C_2}\right) \end{aligned} \qquad \text{[Eq 3-13]}$$

Now, if equivalent single-layer thermal properties, R_e and C_e, exist for a two-layered slab, then, from Equations 3-12 and 3-13, they clearly must satisfy the following condition:

$$\begin{aligned} \frac{R_e}{\sqrt{sR_eC_e}} \sinh \sqrt{sR_eC_e} &= \left(\cosh \sqrt{sR_1C_1}\right)\left(\frac{R_2}{\sqrt{sR_2C_2}} \sinh \sqrt{sR_2C_2}\right) \\ &\quad + \left(\frac{R_1}{\sqrt{sR_1C_1}} \sinh \sqrt{sR_1C_1}\right)\left(\cosh \sqrt{sR_2C_2}\right) \end{aligned} \qquad \text{[Eq 3-14]}$$

Unfortunately, while we can solve Equation 3-14 for R_e and C_e by equating real and imaginary parts to form two equations in two unknowns, we note that R_e and C_e are not independent of s. (This

implies, since $s = j\omega$ in our previous expression for $q(t)$ for the sinusoidal exterior boundary condition, that R_e and C_e are frequency-dependent.) The Taylor series expansion of Equation 3-14 will clarify this:

$$\text{Let } Z_i = \sqrt{sR_iC_i} \quad . \qquad \text{[Eq 3-15]}$$

The series expansion of sinh Z and cosh Z are as follows:

$$\sinh Z = Z + \frac{Z^3}{3!} + \frac{Z^5}{5!} + \frac{Z^7}{7!} \ldots\ldots \qquad \text{[Eq 3-16]}$$

$$\cosh Z = 1 + \frac{Z^2}{2!} + \frac{Z^4}{4!} + \frac{Z^6}{6!} \ldots\ldots \qquad \text{[Eq 3-17]}$$

Using Equations 3-15, 3-16 and 3-17 in Equation 3-14 provides:

$$\frac{R_e}{Z_e}\left[Z_e + \frac{Z_e^3}{3!} + \frac{Z_e^5}{5!}\ldots\right] = \frac{R_2}{Z_2}\left[Z_2 + \frac{Z_2^3}{3!} + \frac{Z_2^5}{5!}\ldots\right]\left[1 + \frac{Z_1^2}{2!} + \frac{Z_1^4}{4!}\ldots\right] + \frac{R_1}{Z_1}\left[Z_1 + \frac{Z_1^3}{3!} + \frac{Z_1^5}{5!}\ldots\right]\left[1 + \frac{Z_2^2}{2!} + \frac{Z_2^4}{4!}\ldots\right] \qquad \text{[Eq 3-18]}$$

Rearranging and simplifying produces:

$$R_e + \frac{R_e^2C_es}{3!} + \frac{R_e^3C_e^2s^2+\ldots}{5!} = (R_1+R_2) + \frac{\left(R_1^2C_1+3R_1R_2C_1+3R_1R_2C_2+R_2^2C_2\right)s}{3!} + \frac{\left(R_1^3C_1^2+5R_1R_2^2C_2^2+5R_2R_1^2C_1^2+R_2^3C_2^2\right)s^2+\ldots}{5!} \qquad \text{[Eq 3-19]}$$

We now see that if we approximate Equation 3-19 by using only the first two terms of both sides, we can define R_e and C_e independently

of s. Thus, we can define R_e and C_e as constant equivalent thermophysical properties only in this approximate sense.

We now consider whether, and under what circumstances, Equation 3-19 can be approximated by using only the first two terms. Under this approximation, R_e and C_e are defined as:

$$R_e = R_1 + R_2 \qquad \text{[Eq 3-20]}$$

$$C_e = \frac{R_1^2 C_1 + 3R_1 R_2 C_1 + 3R_1 R_2 C_2 + R_2^2 C_2}{R_e^2} \qquad \text{[Eq 3-21]}$$

We can apply Equations 3-20 and 3-21 recursively for slabs with more than two layers by first calculating R_e and C_e for the two outermost layers; then, treating the outer two layers as one equivalent layer, we substitute R_e for R_1, C_e for C_1, and R_3 and C_3 (properties of the third outermost layer) for R_2 and C_2 and calculate new values for R_e and C_e, etc. Since we can calculate R_e and C_e for any multilayered slab, we can compare the frequency response of a multilayered slab, calculated by the equivalent single-layer slab model, to the exact solution, obtained by evaluating the terms of the transmission matrix. To compare them, we set s equal to $j\omega$, and plot $\left|-\frac{1}{B(j\omega)}\right|$ and ϕ for various frequencies, using both models. These comparisons are shown for several multilayered slabs of practical interest in Figures 3-3 through 3-9.

Figure 3-3 shows results for a single 10.16-cm (4-in.) concrete slab with outside and inside air film/surface resistances of .029 $\frac{m^2 \cdot K}{\omega}$ and .12 $\frac{m^2 \cdot K}{\omega}$, respectively. (These air film resistances

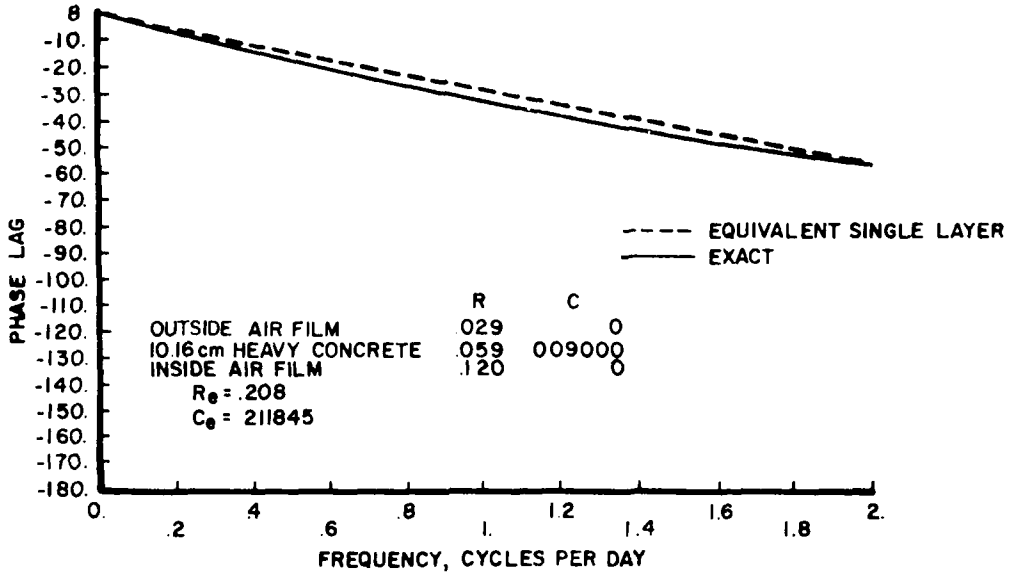

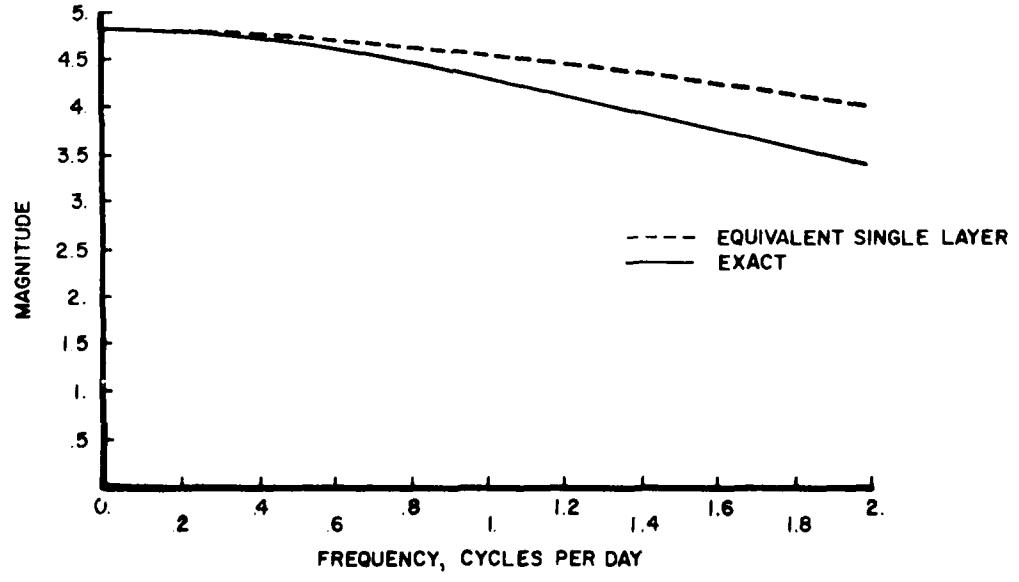

Figure 3-3. Frequency response of heavy concrete slab.

AD-A097 597 CONSTRUCTION ENGINEERING RESEARCH LAB (ARMY) CHAMPAIGN IL F/G 13/1
CALCULATING BUILDING HEATING AND COOLING LOADS USING THE FREQUE--ETC(
FEB 81 D C HITTLE
UNCLASSIFIED CERL-TM-E-169 NL

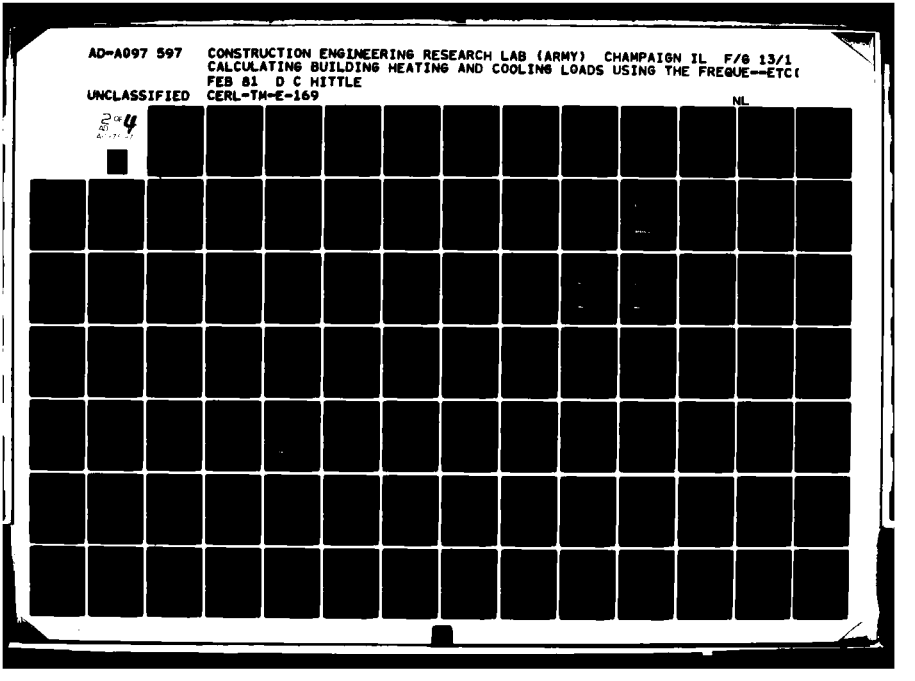

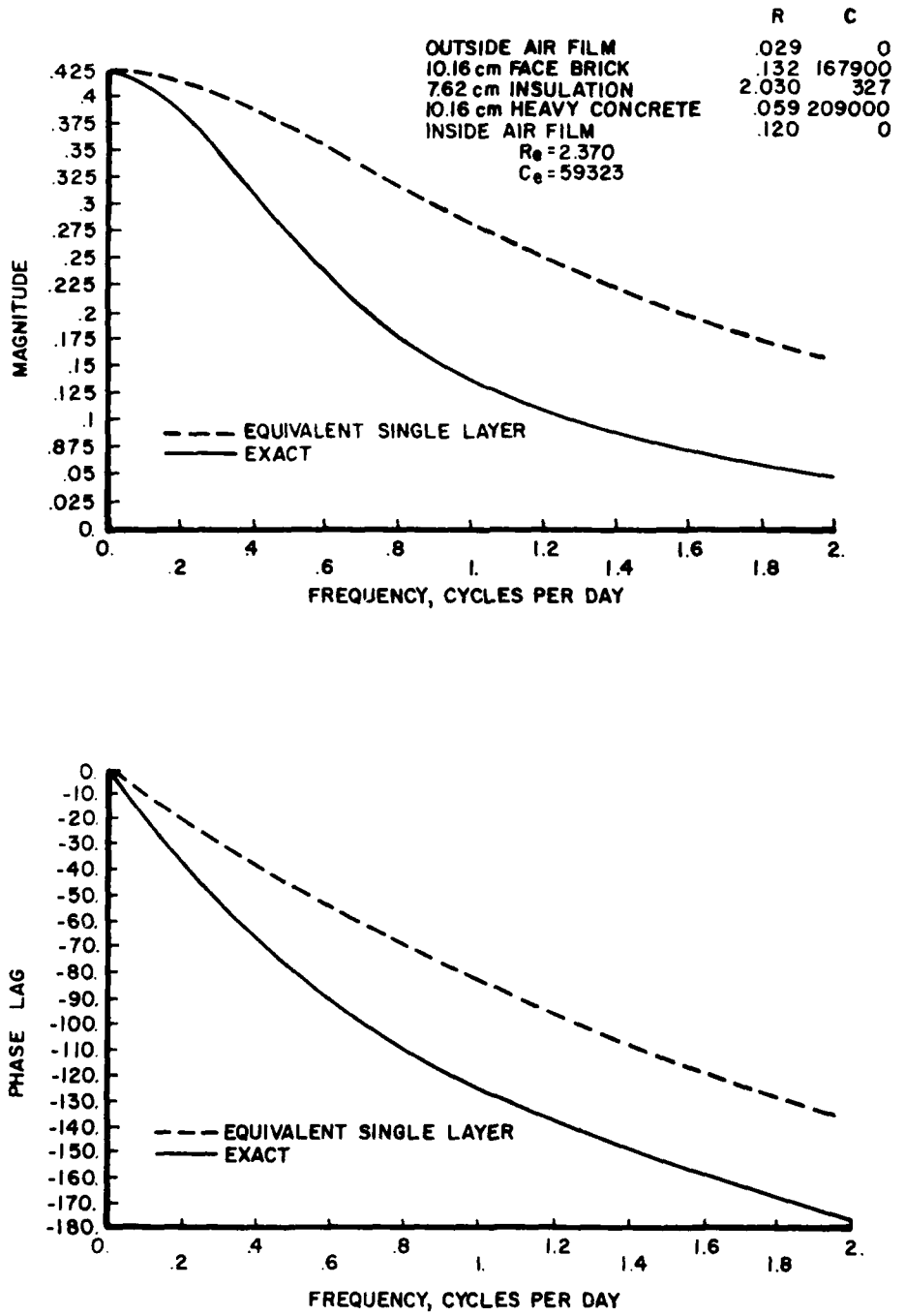

Figure 3-4. Frequency response of multilayered slab, two heavy layers separated by insulation.

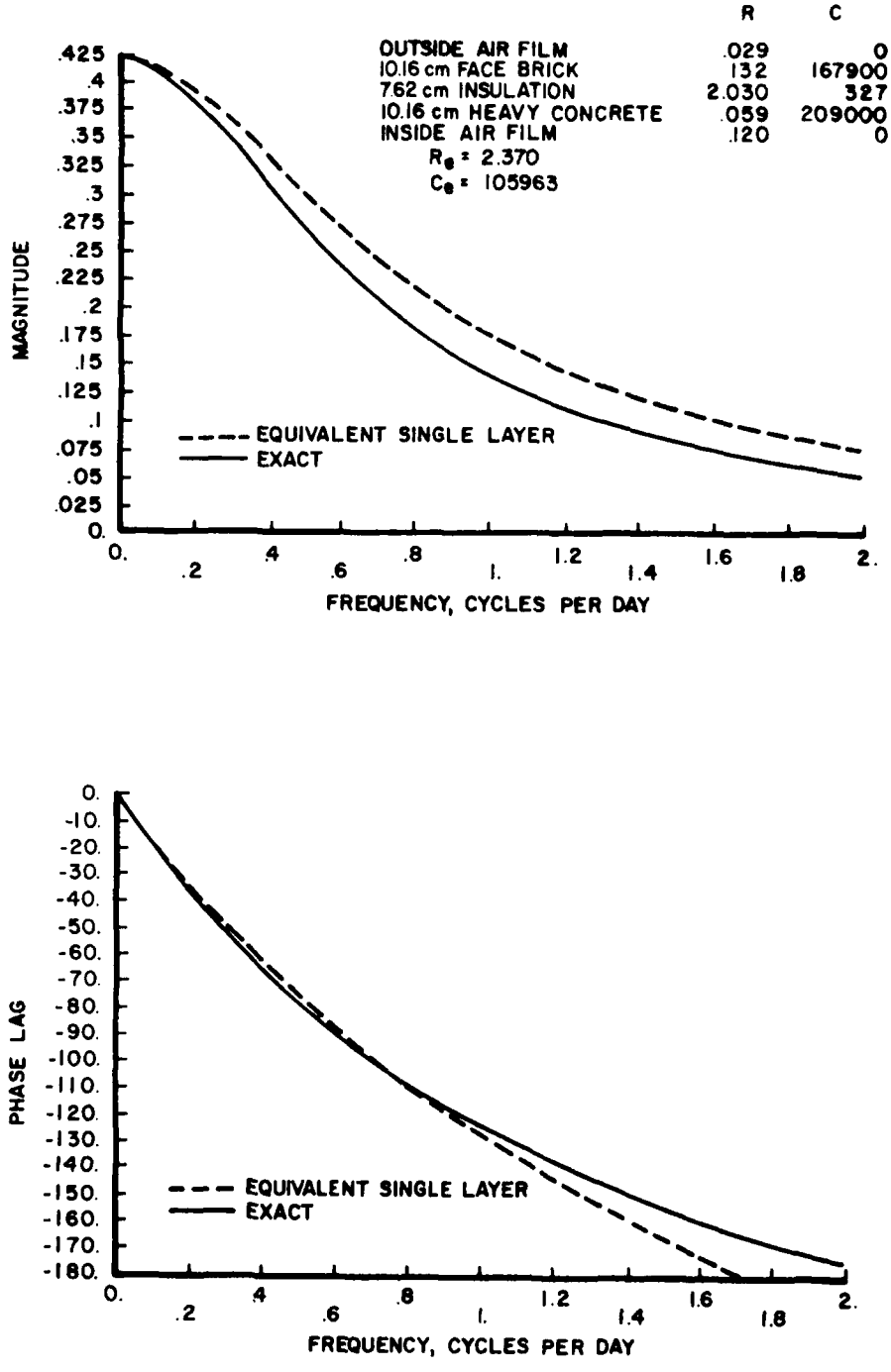

Figure 3-5. Frequency response of multilayered slab, two heavy layers separated by insulation, adjusted equivalent capacitance.

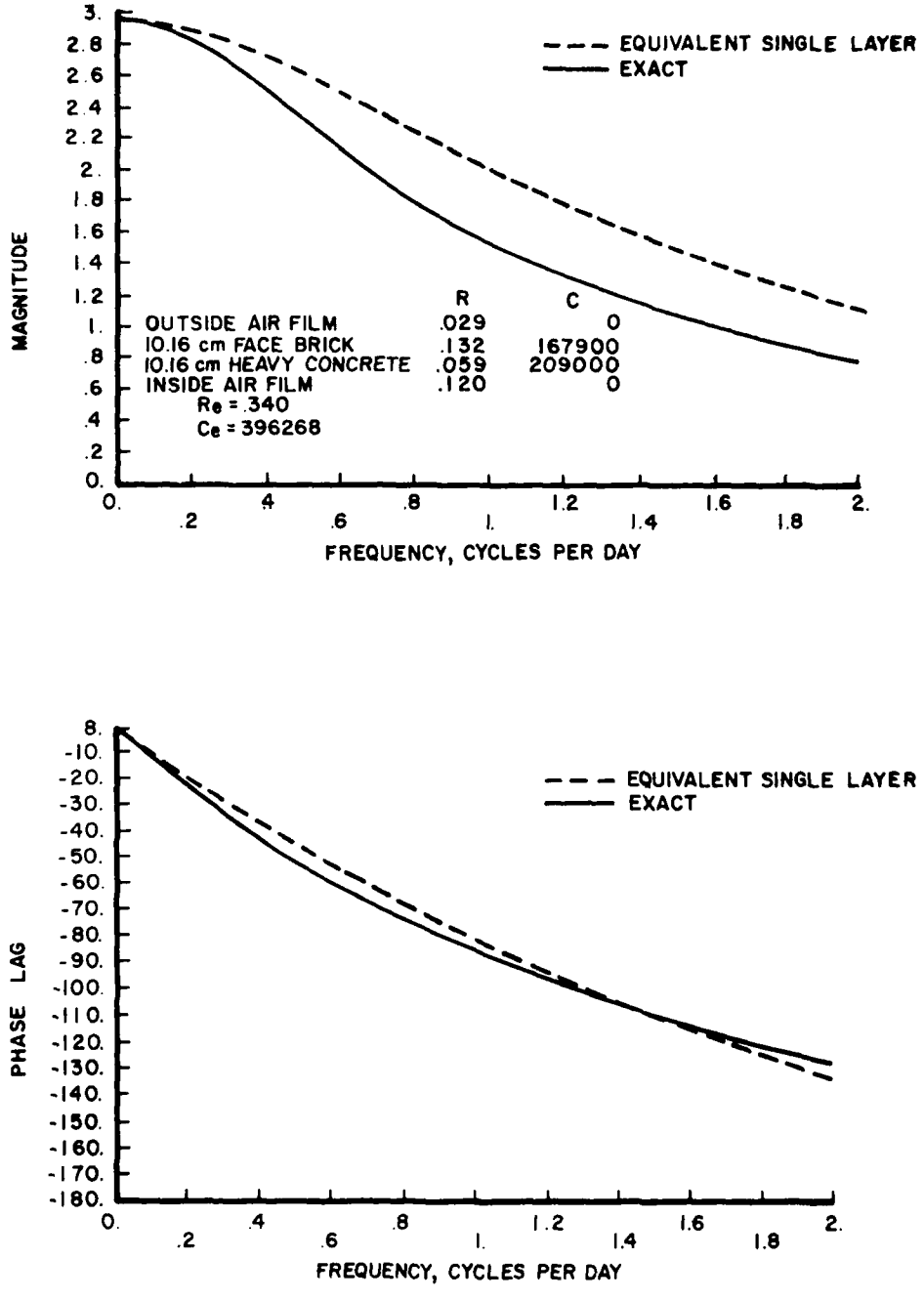

Figure 3-6. Frequency response of a multilayered slab, brick and heavy concrete.

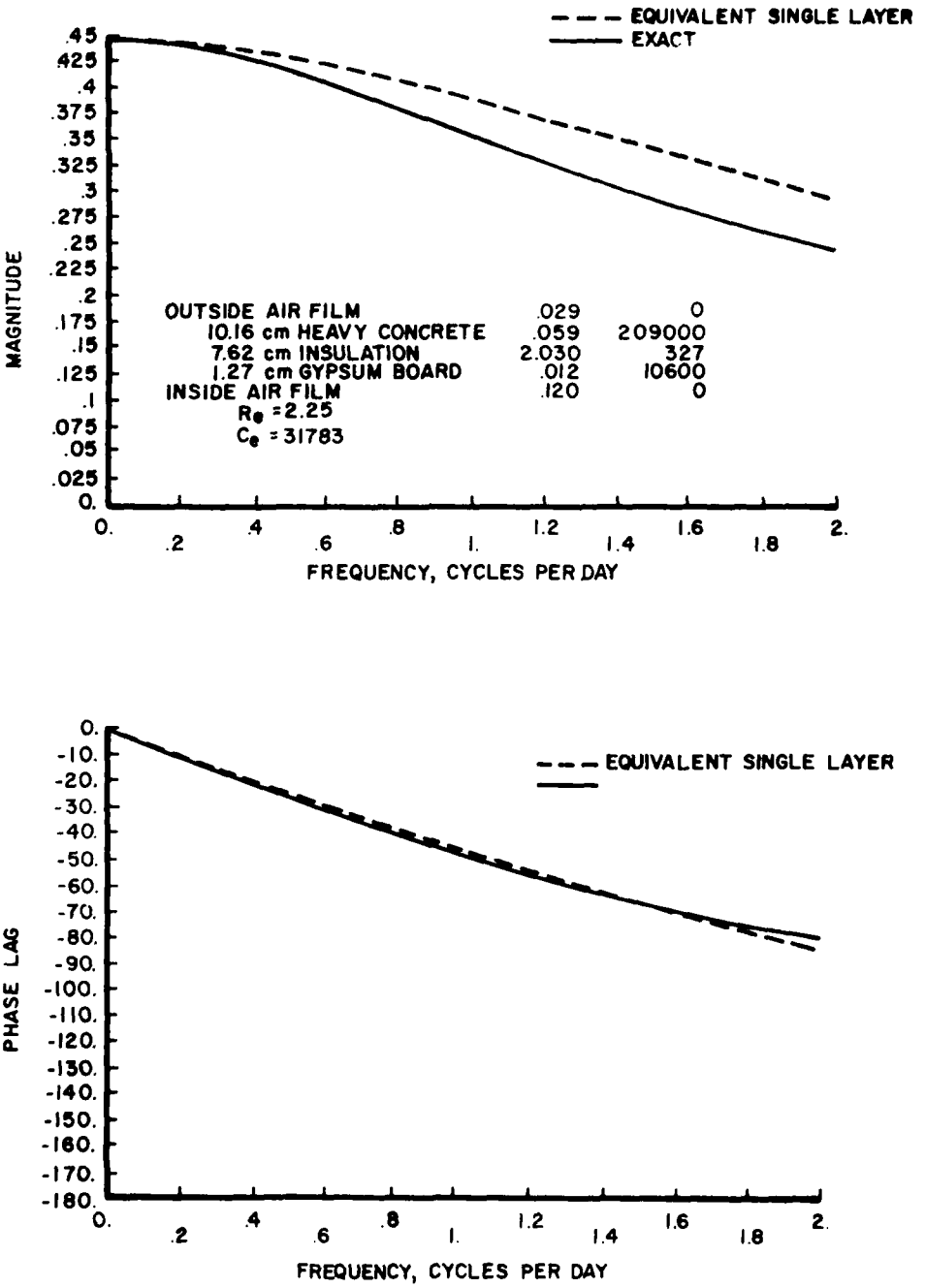

Figure 3-7. Frequency response of a multilayered slab, heavy concrete, insulation and gypsum board.

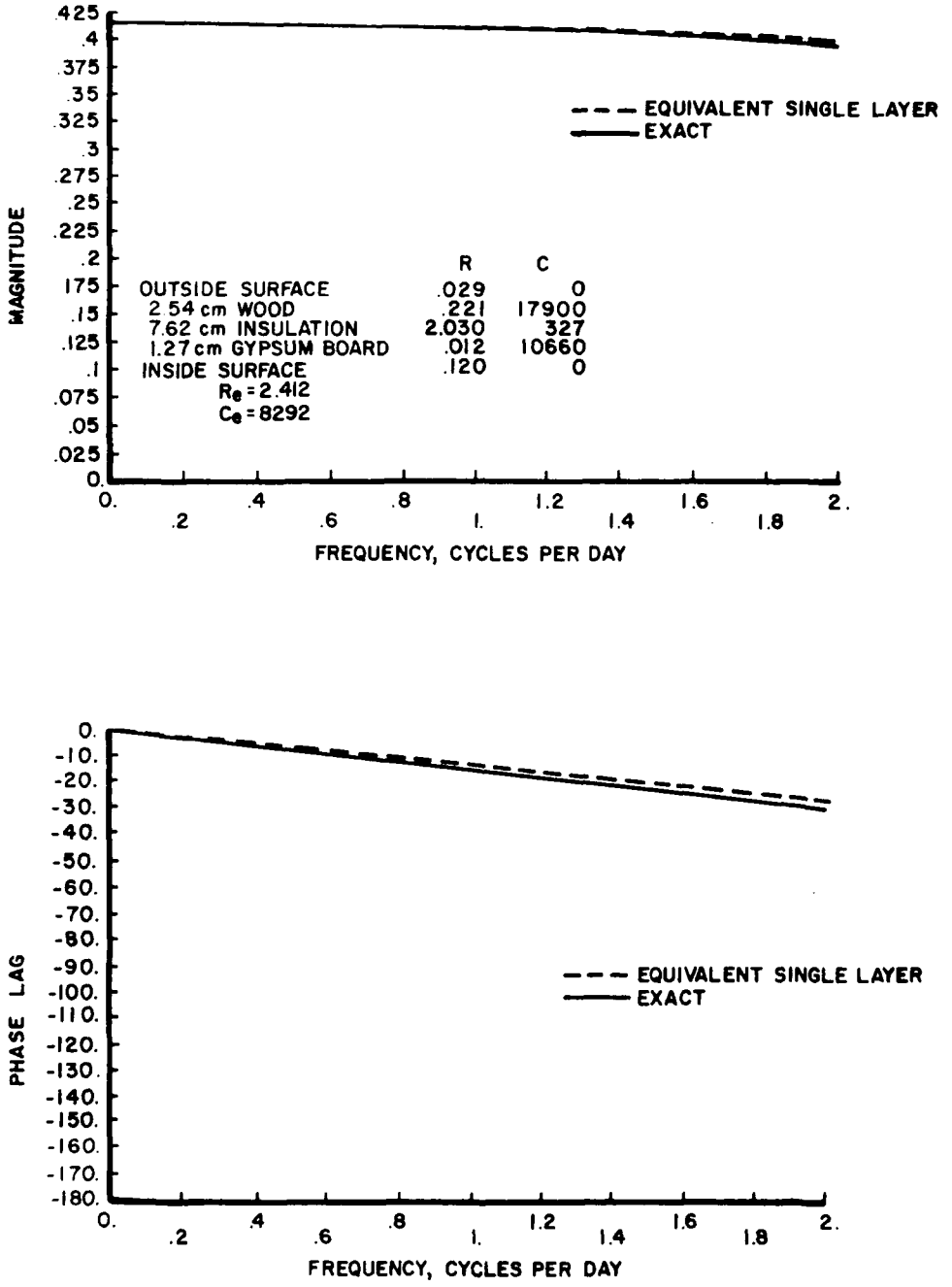

Figure 3-8. Frequency response of a lightweight multilayered slab.

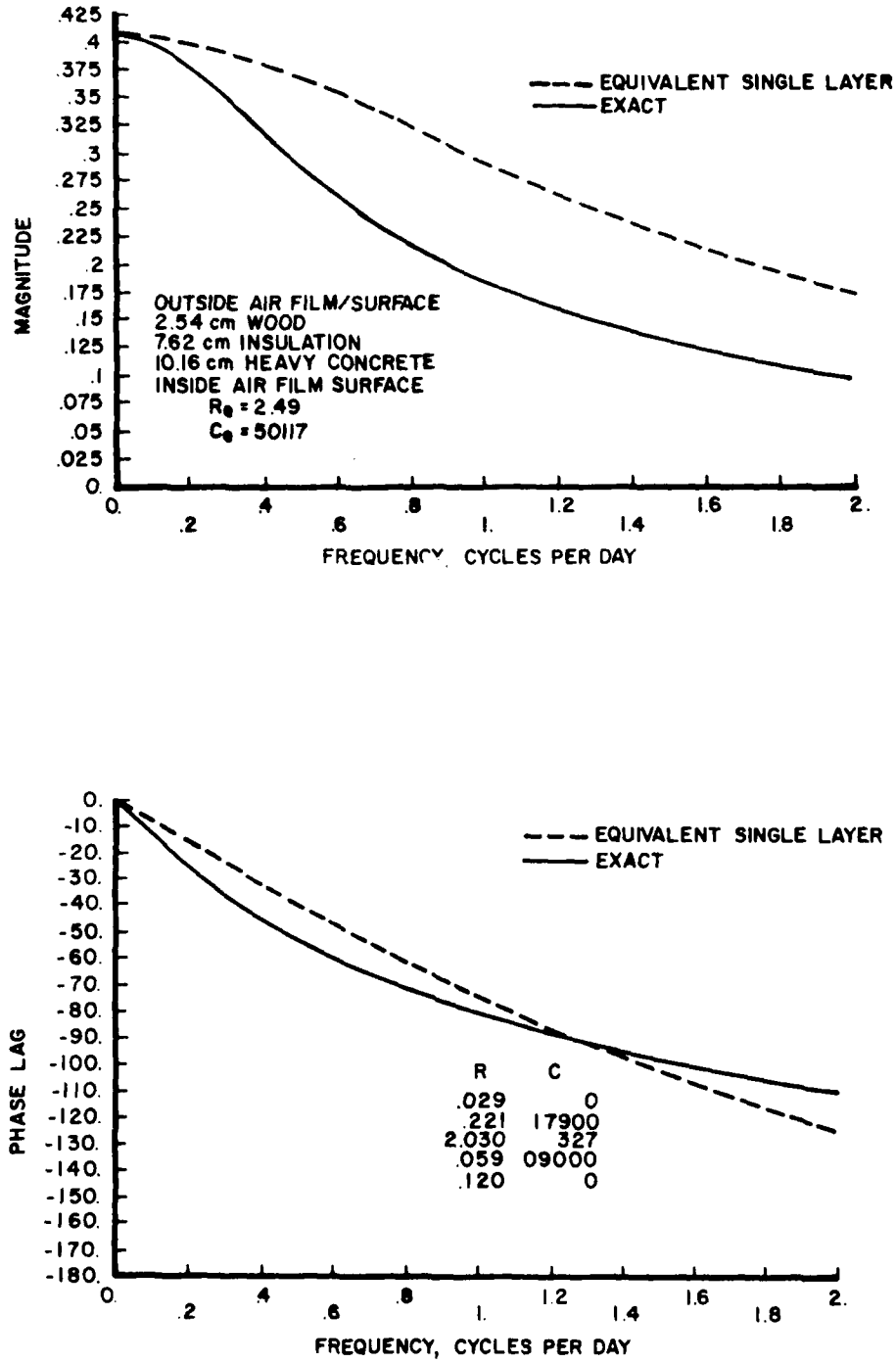

Figure 3-9. Frequency response of a heavy slab with insulation on the outside.

are combined radiative-convective resistances and are used for all wall sections studied.) We see that the single-layer equivalent slab model agrees reasonably well with the multilayered model. As expected, the agreement at low frequencies is nearly exact, since it is in this range (small $j\omega$) that the two-term approximations for sinh and cosh are very close to the actual values. However, we have little interest in this region, since it represents what is essentially steady-state heat transfer. As shown in Chapter 4, variation in climate is characterized by periodic variations at daily and twice-daily frequencies. Therefore, if we are to use the single-layer equivalent slab model, its agreement with the multilayered slab model must be usable at frequencies of one cycle per day and two cycles per day. For the slab in Figure 3-3, the single-layer model magnitude is in error by about 6 percent at one cycle per day, and about 18 percent at two cycles per day.

Much worse agreement is shown in Figure 3-4, which compares the single-layer slab model to the exact solution; this comparison is for a multilayered slab consisting of 10.6-cm face brick, 7.62-cm insulation, and 10.16-cm heavy concrete. In this case, the single-layer slab model predicts a magnitude which is nearly twice that of the exact solution at a frequency of one and two cycles per day. The phase lag is also in error by the equivalent of about 3 hours at one cycle per day and 1.5 hours at two cycles per day.

It was found that consistent, and often considerable, improvement in agreement between the equivalent single-layer model and the exact

model could be achieved by combining the inside air film/surface resistance with the resistance of the innermost wall layer. Calculating the equivalent capacitance in this way for the wall section of Figure 3-4 yields the much improved results shown in Figure 3-5.

Figures 3-6 through 3-8 compare several common wall sections for the modified equivalent single-layer slab model and the exact model. Figure 3-6 illustrates a wall section made of two different, but relatively heavy, masonry materials. Figure 3-7 shows a heavy wall layer that is exposed on the outside but insulated on the inside. Figure 3-8 shows a lightweight wall section (low on "thermal" mass), and confirms that heat flow through light walls can be analyzed using steady-state procedures; the magnitude of $B(j\omega)$ is nearly constant, and the phase lag is nearly zero.

Figure 3-9 shows that even with the modification used to calculate C_e, severe errors can occur when the equivalent single-layer model is used. This figure shows typical results obtained when a heavy, conductive layer is insulated on the outside. This type of wall construction, though not common in existing buildings, may prove important in future energy-conservative designs.

Figures 3-3 through 3-9 are but samples of the many comparisons made between the equivalent single-layer model and the exact model when calculating the frequency response of multilayered slabs. However, they provide enough information to evaluate the equivalent single-layer model.

It is therefore concluded that the equivalent single-layer model is a potentially dangerous means of quantitatively estimating the

dynamic behavior of multilayered slabs. For important frequencies and for realistic wall sections, the arguments of the hyperbolic functions making up the transmission matrix are simply too large to be approximated by a two-term expansion. For the same reason, the frequency response of multilayered slabs cannot be characterized with reasonable accuracy by any model simpler than the exact model used as the standard for comparison. Furthermore, the inclusion of more terms in the series expansions leading to the equivalent single-layer model forces us to acknowledge the true frequency dependence of the equivalent single-layer thermodynamic properties. Calculating frequency-dependent values for R_e and C_e involves the solution of simultaneous non-linear equations (like Equation 3-14) and is more laborious than calculating the exact solution itself.

The first section of this chapter showed how the frequency response of a multilayered slab can be calculated much more easily than response factors. In this second section we have shown that attempts to further simplify the dynamic heat conduction problem were only of limited value, and furthermore, given the simplicity with which frequency response can be calculated from the transmission matrix, further simplifications are probably unwarranted.

4 PERIODIC AND STOCHASTIC BEHAVIOR OF WEATHER DATA

Introduction

In Chapter 3, the calculation of heat conduction through multi-layered building walls and roofs was shown to be much less complicated if the outside surface temperature (or the sol-air temperature) is treated as the sum of pure sinusoids. This requires that the actual outside temperature and solar radiation be adequately approximated by a small set of sine and cosine functions of time. In this chapter, we analyze actual weather data to determine whether or not such an approximation is reasonable. The following sections describe: (1) the weather data chosen for analysis, (2) three analysis techniques applied to characterize weather behavior, and (3) the results of using these techniques.

Weather Data

Hourly weather data for four different locations in the United States were obtained from the Environmental Technical Applications Center (ETAC) Air Weather Service, United States Air Force. The tapes selected were of the so-called SOLMET format. These tapes contain about 20 years of measured hourly climate data. The four sites selected represented four distinctly different climates: Charleston, SC, represented a hot humid climate; Madison, WS, a cold northern

climate; Fort Worth, TX, a hot dry climate; and Santa Maria, CA, a marine climate.

From the 20 years of data available for each site, a 10-year period covering the years 1953 through 1962 for Charleston, Madison, and Fort Worth, and the years 1954 through 1963 for Santa Maria was chosen for analysis. Three types of data time series were analyzed to investigate short- and long-term data trends.

1. Thirty-day periods of hourly data and 40-day periods of data taken every other hour

2. Ten years of daily average data (3650 samples per weather data variable)

3. Ten years of 5-day average data (730 samples per weather data variable)

The two climate variables that affect building heat transfer most directly (contribute to the sol-air temperature) are dry-bulb temperature and beam solar radiation. Hence, both of these time series were analyzed.

Procedures

In order to characterize climate data, we must determine whether the data is the result of a deterministic process or a stochastic

process. If we can develop a model which enables us to calculate the value of a time-dependent variable (dry-bulb temperature, for example) nearly exactly at any instant of time, the model and the process are called deterministic. Box and Jenkins (ref 26) use the example of a projectile trajectory which can be calculated nearly exactly if the direction and velocity at launch are known. A stochastic process is one which cannot be modeled deterministically because there are unknown factors affecting the variable which prevent the exact calculation of its future behavior. We can develop stochastic models for these processes which allow us to calculate the expected future value of the process and the probability that a future value will be between two specified limits.

There are also certain time series which can be viewed as being the result of both deterministic and stochastic processes. A radio signal containing "static" is a familiar example. We expect that weather data can also be modeled as being the result of both deterministic and stochastic processes. Extraterrestrial (or "clear sky") radiation, for example, can be calculated from basic laws of astronomy (deterministically). The occasional passing of clouds cannot be exactly predicted, however; this must be viewed as a stochastic process.

In addition to our a priori expectation that both known and unknown factors contribute to climate variation, we must also recognize that we are searching for climate models which are to be used for the specific purpose of predicting energy use. If we are to take advantage of the results described in Chapter 3, we need a model which uses sines and cosines to describe climate variation. The three time series analysis techniques described below were chosen with this requirement in mind.

The first approach used to analyze the weather data time series was the discrete Fourier transform, which is one of the most direct methods of analyzing discrete, periodic data.* For a real data sequence, X_i of N equally spaced samples, the discrete Fourier transform of X_i consists of N coefficients a_r and b_r, r=0, 1,2...N/2 such that

$$X_i = a_0 + 2 \sum_{r=1}^{N/2-1} a_r \cdot \cos(2\pi ri/N) + 2 \sum_{r=1}^{N/2-1} b_r \sin(2\pi ri/N) + a_{N/2} \cos(2\pi iN/2N)$$

* The direct use of the Fourier transform would not be appropriate for a time series which exhibited only stochastic behavior (ref 27). We know, however, that the earth revolves about its axis and orbits the sun in a completely predictable way. We assume that this predictable behavior causes part of the variation in climate (the deterministic part). We can, therefore, expect to gain meaningful insight into the behavior of the weather data time series, particularly their deterministic components, by the direct use of the discrete Fourier transform.

where i denotes the ith sample beginning at 0. For a series sampled over time, X_i denotes the value of the series at time $i \cdot t$, where t is the sampling interval. The coefficients a_r and b_r are determined from the data as follows:

$$a_r = \frac{1}{N} \sum_{i=0}^{N-1} X_i \cos(2\pi ri/N) \qquad \text{[Eq 4-2]}$$

$$b_r = \frac{1}{N} \sum_{i=0}^{N-1} X_i \cos(2\pi ri/N) \qquad \text{[Eq 4-3]}$$

We see from Equation 4-1 that if many of the coefficients a_r and b_r turn out to be small for a given data set, then X_i can be approximated by taking the sum of a few sine and cosine terms.

To compare the importance of the various terms of the data sets under study, the discrete Fourier transform was calculated by using computer subroutines available in the International Mathematics and Statistics Library (IMSL), a subprogram library available at most computer centers. Computer software was developed to plot the magnitude of the contribution of a and b at each frequency. Specifically, a_0 (the mean of the data set) was plotted at zero frequency. The quantity $2\sqrt{a_r^2 + b_r^2}$ was plotted for discrete frequencies between one cycle per sampling period and (N/2-1) cycles per sampling period. $a_{N/2}$ was plotted for the Nyquist frequency of N/2.

Note that the so-called power spectrum in its discrete form would be plotted as $a_r^2 + b_r^2$. The decision not to use the power spectrum form stems from the physical interpretation which can be given to the quantities a_o and $2\sqrt{a_r^2 + b_r^2}$. a_o is the mean value of the variable (^oC for temperature, w/m^2 for radiation). The quantity $2\sqrt{a_r^2 + b_r^2}$ is the amplitude of the contribution to the variation about the mean due to a sinusoid of frequency r cycles per sampling period.

The second analysis approach used consisted of finding adequate autoregressive moving average (ARMA) models for the temperature and beam solar radiation time series. An ARMA model of order m,n (an ARMA (m,n) model) has the form

$$X_t = \phi_1 X_{t-1} + \phi_2 X_{t-2} + \phi_3 X_{t-3} + \cdots + \phi_m X_{t-m} + a_t - \theta_1 a_{t-1} - \theta_2 a_{t-2} - \cdots - \theta_n a_{t-n} \qquad \text{[Eq 4-4]}$$

where X_t is the value of the discrete time series variable at time t, and X_{t-1} is the value of the time series at time t- Δt, where Δt is the sampling interval. X_{t-2} is the value of the time series variable at t-2 Δt, and so on. The phi's and theta's are constants. a_t is the value at time t of a sequence of independent random impulses, normally distributed with variance σ_a^2 (white noise). a_{t-1} is the impulse occurring at t- Δt, and so on.

Comparing Equations 4-1 and 4-4, we see that if we use discrete Fourier coefficients to estimate a weather variable, the estimate is deterministic; it is a function only of time. (The right-hand side of Equation 4-1 contains only constants and the variable i, where t = i•t.) If we use an ARMA model to estimate the weather variable, the estimate is stochastic; it is a function only of past values of the variable and the current and past random impulses (the estimate is independent of time).

A third analysis technique used was a combined deterministic plus stochastic model. For this approach, sinusoids were used to account for the deterministic periodic component in the data, and autoregressive moving average terms were used to account for the stochastic component.

We will show that the results of the application of these three techniques, taken together, allows the deterministic periodic behavior of the weather data to be identified.

We will now develop a few of the ARMA modeling properties that are particularly useful for weather data time series applications. More complete discussions can be found in the works of Kapoor (ref 28) and Box and Jenkins (ref 26). Pandit (ref 29) presents a detailed mathematical and historical treatment of ARMA modeling theory, and Kuo (ref 30), Franklin and Powell (ref 31),

and Kline (ref 32) discuss ARMA modeling in the context of digital control theory.

We can view an ARMA model as a discrete linear filter (see Figure 4-1), which produces a time series, X_t, as output when subjected to an input of random impulses (white noise). This filter has various forward paths and feedback loops, depending on the order of the ARMA model. This visualization helps define the procedures used to find an adequate ARMA model for a given time series. We invert the ARMA filter as part of the model identification process. By viewing X_t as input, we can construct a time series, a_t, for any candidate ARMA model (see Figure 4-2). This procedure is made obvious by rearranging Equation 4-4:

$$a_t = \Theta_1 a_{t-1} + \Theta_2 a_{t-2} + \cdots + \Theta_n a_{t-n} + X_t - \Phi_1 X_{t-1} - \Phi_2 X_{t-2} - \cdots - \Phi_m X_{t-m} \qquad \text{[Eq 4-5]}$$

Given that we can calculate a_t, there are two steps to the model identification process:

1. For a model of a given order, e.g., ARMA (4,3), we must find the best values for the model parameters (the phi's and theta's). This is accomplished by repeatedly calculating the complete a_t time series while systematically adjusting model parameters until the sum of squares of a_t is minimized.

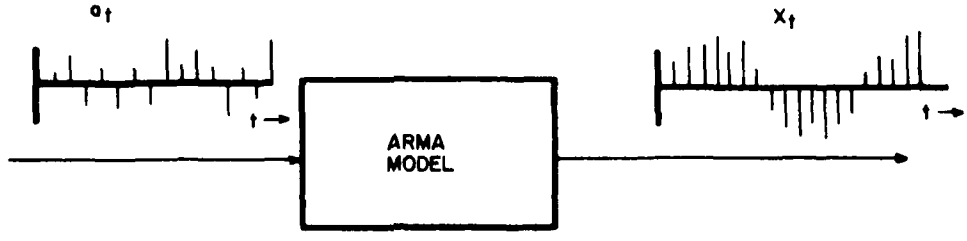

Figure 4-1. ARMA model viewed as a digital filter.

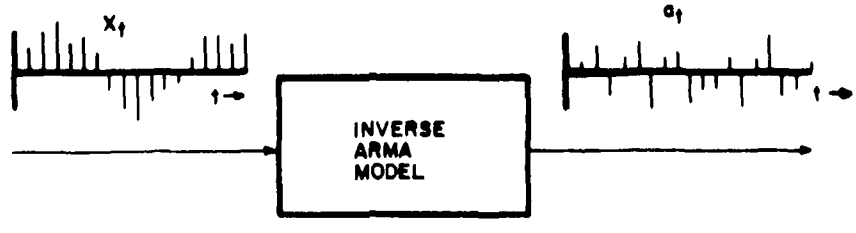

Figure 4-2. Digital filter used for ARMA model identification.

2. Given that we can find the best parameters for a given ARMA model, we further require that the a_t time series produced by the "inverse" ARMA filter be random, normally distributed impulses (white noise). Thus, we must repeat step 1 above for candidate ARMA models of increasing order until this criterion is met.

The computer software system entitled, "University of Illinois Dynamic Data System (UIDDS)," developed by W. A. Kline and R. E. DeVor (ref 33), provided the tool needed to identify adequate ARMA models for the weather data time series under study. The first step in the model identification process is largely automatic in UIDDS through the use of optimization algorithms which usually yield the best values for the parameters of a given ARMA model. Part 2 of the model identification process is not automatic; however, selection of an adequate model from candidate ARMA models is made possible by the wide range of information that UIDDS provides for each candidate ARMA model.

The procedure for selecting candidate ARMA models recommended by Pandit (ref 29) was used to analyze the weather data time series with UIDDS. First, parameters for an ARMA (2,1) model were determined. Next, model order was increased according to ARMA (2n,2n-1), n = 2, 3, 4... until an adequate model was obtained.

Model adequacy was assessed using a variety of statistics designed to establish (1) the degree to which the a_t time series approximates white noise, and (2) whether increasing the model order yields statistically "better" models. The autocorrelation function and the Q-statistic were used as a measure of the randomness of the a_t series. The autocorrelation function is a series which measures the correlation of a_t on itself. For example, the value of the autocorrelation function at lag one, ρ_1, is simply the correlation between values of the residual series at time t and values of the series at t-1; it is the correlation between a_t and a_{t-1}. Similarly, ρ_2, the autocorrelation at lag two, is the correlation between a_t and a_{t-2}, and so on, for ρ_k, k = 1,2,3,4,5... If the a_t series produced by a given "inverted" ARMA model approaches white noise, then the series will be uncorrelated; that is, values of the autocorrelation function at all lags will be nearly zero. UIDDS produces plots of the autocorrelation function which were inspected for each candidate ARMA model to determine whether the values of the function were all nearly zero. The Q-statistic is a cumulative measure of autocorrelation; it is simply the sum of squares of the autocorrelation function times N, the number of points in the time series. The Q-statistic has been shown to vary like the chi-squared statistic and can be compared to chi-squared for a given confidence limit and degrees of freedom of the model.

The F-test and Akaike Information Criteria (AIC) were used as a measure of model "goodness." (They were used to distinguish between models whose autocorrelation functions and Q-statistics were roughly the same.) The F-test is a comparative test between two models, one of which contains more terms than the other. It is a test of the hypothesis that the extra parameters in the higher-order model are zero. If the F-test is large, the parameters are probably significant. The F-test is not a test of model adequacy, but rather an indicator of the benefit of increasing the order of ARMA models. AIC, unlike the F-test, is a measure of a model's absolute merit. It is a measure of the model's information content and has its origins in information theory. The lower the AIC, the better the model; however, a model may be judged to be adequate even if other models have slightly lower AICs.

Results

The first sets of weather data analyzed were hourly measured dry-bulb temperature and measured solar beam radiation for Charleston, SC, for the year 1953. The first 40 days of the data were used for this study; for most of this first modeling effort, every other hour of the data set was removed because of the difficulty in applying ARMA modeling techniques to data having an important period every 24 sampling intervals. This period of 24 sampling intervals--the

diurnal cycle for hourly weather data--was too long to be successfully modeled by ARMA methods.

The data are obviously periodic (12 samples per 24-hour day). However, because solar radiation is zero at night (never negative), beam radiation is square-wave-like when compared to the more sinusoidal temperature data. One way of approximating a square wave with a sinusoid is to use several harmonics of the fundamental frequency. Therefore, we anticipate that several harmonics of the diurnal frequency may be needed to model beam radiation.

We begin with the discrete Fourier spectrum of the temperature and the beam radiation time series shown in Figures 4-3 and 4-4, respectively. The very clear peaks at 40 cycles per sample, or one cycle per day, and at the first few harmonics of the daily cycle are evident for both temperature and radiation. As expected, the first harmonic is more pronounced for the beam radiation than for temperature, due to the square wave nature of the radiation time series. Higher harmonics are present in both time series but are comparatively insignificant.

We now turn to results of the ARMA modeling techniques application. These results are summarized in Tables 4-1 and 4-2, which show the residual sum of squares, AIC, the Q test, the various F tests, and the coefficient of determination, R^2, for various ARMA models for both time series. An ARMA (10,9) model proved to be the best model

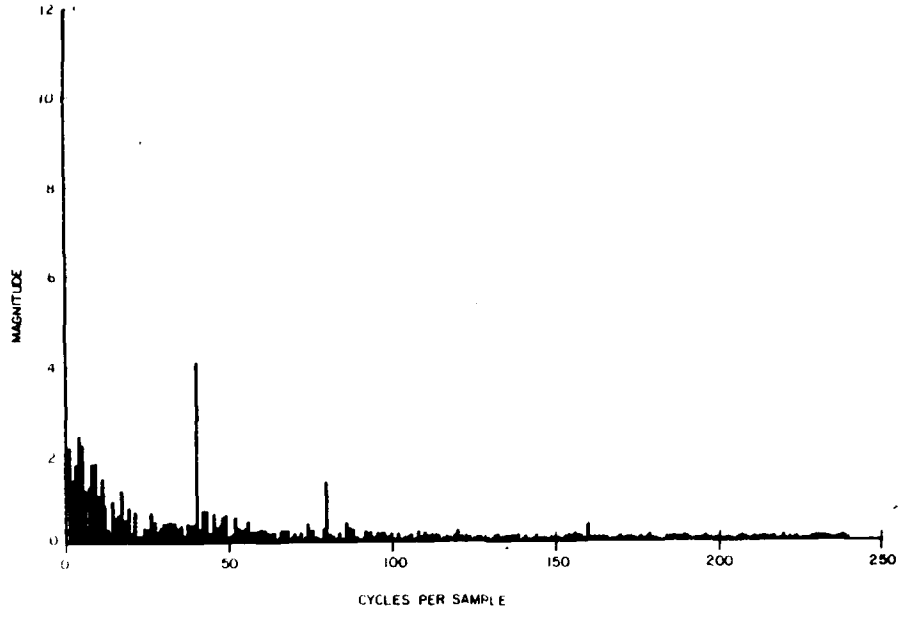

Figure 4-3. Spectrum for temperature, Charleston, SC.

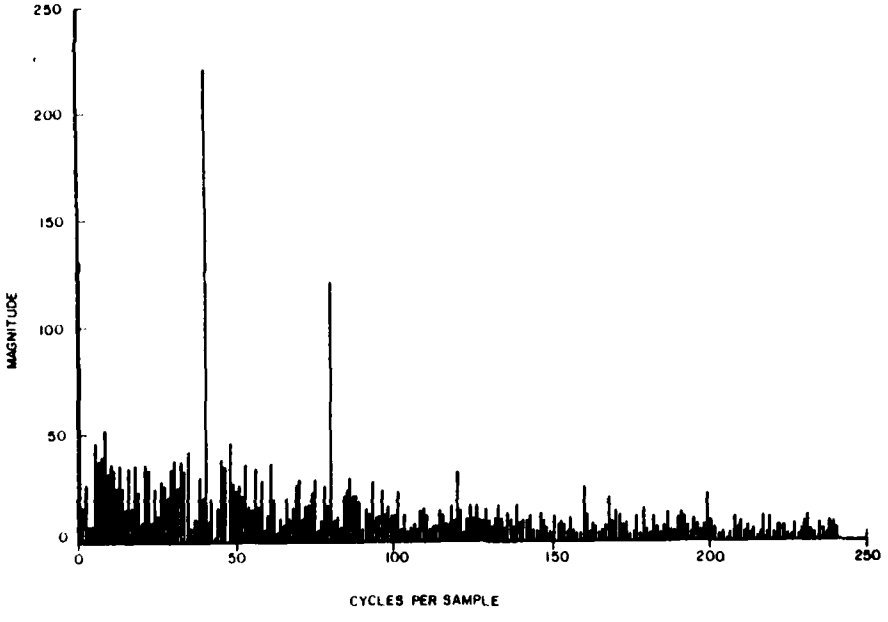

Figure 4-4. Spectrum for beam solar radiation, Charleston, SC.

Table 4-1

Statistics for Dry-Bulb Temperature ARMA Models

		RSS	AIC	Q/Q(95)	F Test to Model - #	R^2
1	ARMA(4,3)	1623	600	202/38		.89
2	ARMA(6,5)	1507	573	170/38	9-1	.90
3	ARMA(8,7)	1238	487	63/38	25-2	.92
4	ARMA(10,9)	1149	459	34/38	9-3	.92
5	ARMA(12,11)	1142	465	34/38	.6-4	.92
6	ARMA(10,8)	1179	469	45/38	3-5	.92
7	ARMA(8,6)	1195	468	38/38	-16-3	.92

Table 4-2

Statistics for Solar Beam Radiation ARMA Models

		RSS	AIC	Q/Q(95)	F Test to Model - #	R^2
1	ARMA(4,3)	12.8E6	4910	135/38		.59
2	ARMA(6,5)	11.2E6	4850	53/38	18-1	.65
3	ARMA(8,7)	10.3E6	4819	25/38	9.8-2	.67
4	ARMA(10,9)	9.58E6	4793	22/38	8.5-3	.70
5	ARMA(12,11)	9.72E6	4808	33/38	-1.6-4	.69
6	ARMA(10,8)	9.77E6	4801	23/38		.69
7	ARMA(8,6)	10.1E6	4806	20/38		.68
8	ARMA(6,4)	10.4E6	4816	19/25		.67

for both temperature and solar beam radiation. However, in both cases, the (10,9) model had a small θ_9, and the (10,8) model was nearly as good, particularly for solar beam radiation.

Recall that we have visualized an ARMA model as a discrete filter which transforms white noise into the requisite time series. By applying the Z transform to an ARMA (m,n) model of Equation 4-4, a discrete transfer function, G(Z), can be written relating X(Z) to a(Z), where X(Z) is the Z transform of X_t, and a(Z) is the Z transform of a_t:

$$G(Z) = \frac{X(Z)}{a(Z)} = \frac{(1 - \theta_1 Z^{-1} - \theta_2 Z^{-2} - \theta_3 Z^{-3} - \cdots - \theta_n Z^{-n})}{(1 - \Phi_1 Z^{-1} - \Phi_2 Z^{-2} - \Phi_3 Z^{-3} \cdots - \Phi_3 Z^{-m})} \quad \text{[Eq 4-6]}$$

Like the transfer function for a digital filter or digital controller, this transfer function has real and/or complex poles and zeros. Also, since a_t is assumed to be white noise, the theoretical spectrum for the model can be calculated in the same way that frequency response is calculated for a digital filter or controller--by finding the magnitude of G(Z) for various frequencies ω, with Z set equal to $e^{j\omega}$ ($j = \sqrt{-1}$). Viewed in this way, an autoregressive moving average model can be analyzed using pole placement and frequency response techniques common to digital control theory.

For example, in the case of both time series analyzed, pairs of complex conjugate poles and zeros began to appear near the unit

circle in the complex Z-plain for ARMA models of order as low as (4,3), as shown in the sample pole-zero plots of Figure 4-5. These pole zero pairs were of nearly equal value. Near, but not exact, complex conjugate pole zero cancellation near the unit circle is characteristic of periodic time series. However, for both series, two poles remained well within the unit circle as the order of the models was increased. One zero tended to appear near the origin in the higher-order ARMA (2n, 2n-1) models. The conclusion which can be drawn from this behavior is that the time series are characterized by periodic behavior (indicated by the pole zero pairs near the unit circle) and by stochastic AR(2) behavior (indicated by the remaining poles which are non-zero but well inside the unit circle).

We can also compare the spectrum of the autoregressive moving average model for temperature and solar radiation to the Fourier spectrum computed previously. Figures 4-6 and 4-7 show the spectrum of the ARMA (10,9) models for temperature and radiation, respectively. We immediately see one difficulty which arises when strongly periodic functions are modeled using stochastic ARMA methods. The spectral peaks for the ARMA transfer functions are at the same frequencies as those of the discrete Fourier transform (see Figures 4-3 and 4-4). However, the ARMA spectrum is a <u>continuous</u> spectrum, and we must integrate the square of the spectrum shown in Figures 4-6 or 4-7 from $\omega-\pi/N$ to $\omega+\pi/N$ in order to compare the "power" at frequency ω with the "power" represented by the square of the discrete line

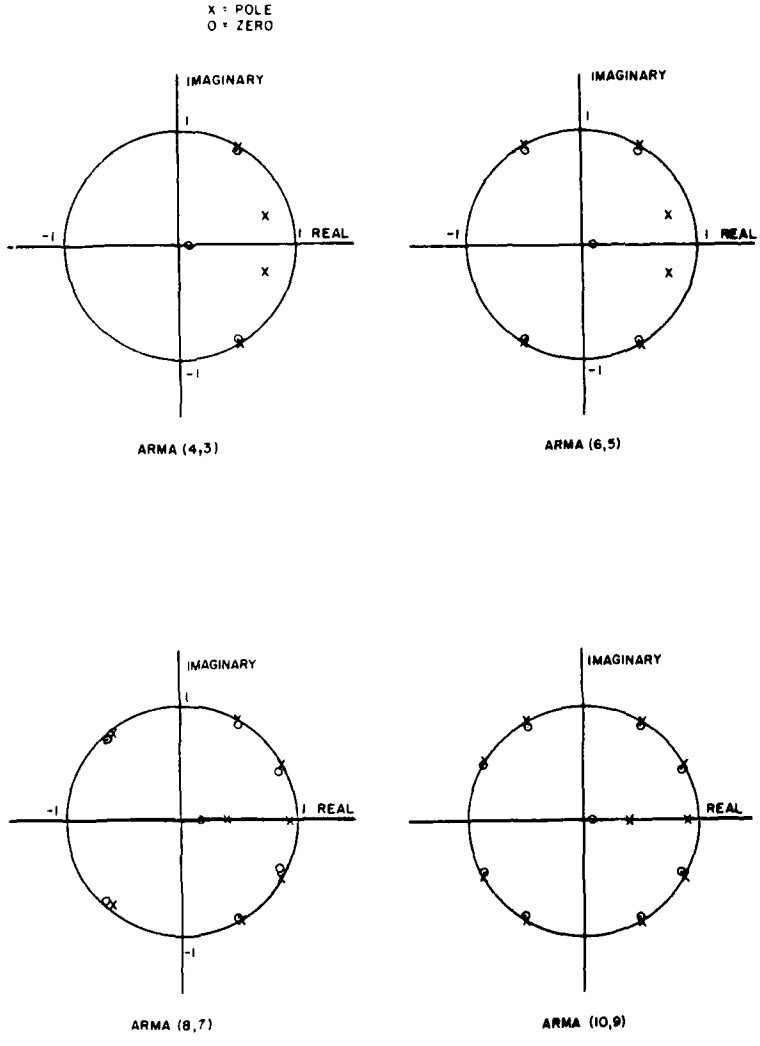

Figure 4-5. Pole-zero plots for successive ARMA models for dry-bulb temperature, Charleston, SC.

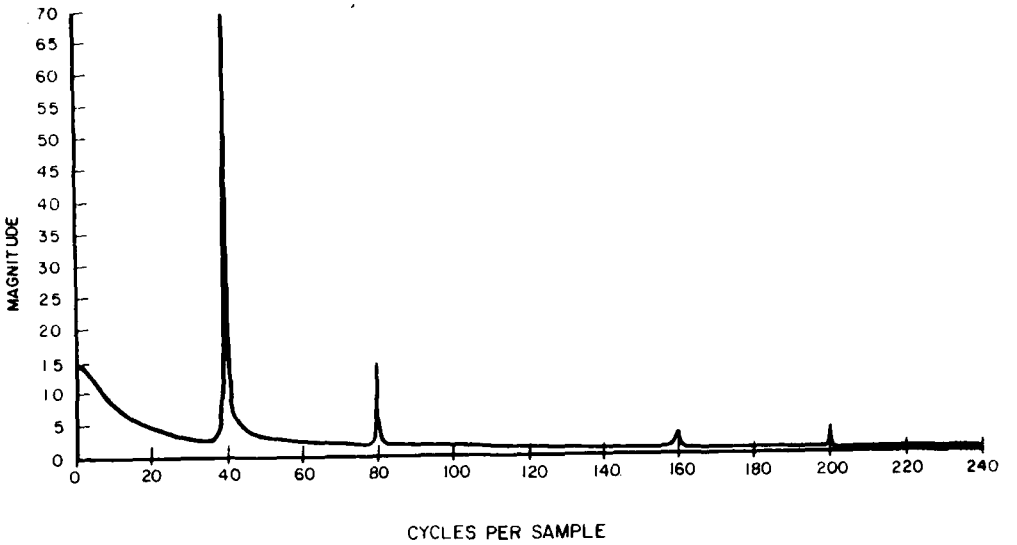

Figure 4-6. Model spectrum--temperature, Charleston, SC.

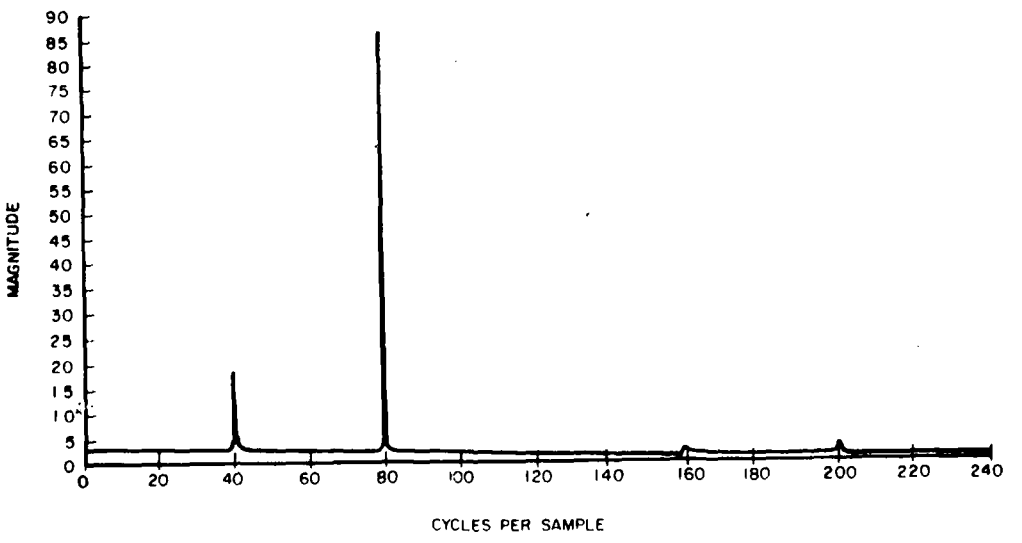

Figure 4-7. Model spectrum--beam solar radiation, Charleston, SC.

spectrum at ω. While we can carry out this integration, it is tedious. There are also other mathematical difficulties. If, as physical reasoning and the discrete Fourier spectrum suggest, the weather data contain deterministic sinusoidal components, then the continuous spectrum of a climate model containing these sinusoids would be discontinuous at the frequencies corresponding to the principal sinusoids. In order for the ARMA spectrum to have such discontinuities, pairs of conjugate poles would have to appear on the unit circle, not just near it. Such a model would not be stable and would be of little utility. If we are careful to choose our sampling interval so that the periods of the sinusoids in the data are exact integer multiples of the sampling interval, then the discrete Fourier transform provides the best estimate of the amplitude of the sinusoids. The sharp spikes at exactly the diurnal frequency and its first harmonic in the ARMA spectrum confirm that periodicity exists at exactly these frequencies which are integer multiples of the sampling interval.

We must be satisfied that ARMA modeling alone confirms the need for combined deterministic plus stochastic models.*

We deal briefly now with the reason for removing every other hourly sample from this original weather data set. If we consider a simple sinusoid with 24 samples per period, we see that much of the

* We use the phrase "deterministic plus stochastic model" to identify a single model with deterministic and stochastic components.

sine wave is like a straight line from the microscopic view of one sample looking at its nearest four or five neighbors (from the perspective of an ARMA model). Thus, we can estimate the value of the time series at time t with reasonable accuracy by looking only at a few past values of the time series and one or two values of the past a_t time series. For such a finely sampled time series, the residual sum of squares can be reduced substantially with a model that does not portray the periodic behavior of the data at all.

The results of the spectral analysis and ARMA modeling both suggest the need for a deterministic (i.e., time-dependent sinusoids) plus stochastic (i.e., low-order ARMA) model. The UIDDS software system also allows the parameters of combined deterministic plus stochastic models to be estimated using nonlinear regression.

To begin this modeling step, the form of a combined model and the initial estimates of the model parameters must be established by first finding an adequate deterministic only model and then finding an adequate ARMA model for the residuals left after the deterministic behavior is removed. Thus, for both the temperature and beam radiation time series, sinusoidal deterministic models were tested by first including just the diurnal frequency, then the first harmonic, then another harmonic, and so on, until there was no substantial improvement in the residual sum of squares between successive models. Tables 4-3 and 4-4 show the results of these tests. In both cases,

Table 4-3

Deterministic Model Statistics, Dry-Bulb Temperature, Charleston, SC

Model	Periods	Amplitudes	RSS	R2	Standard Deviation
1	12	4.07	11.43E3	.26	4.88
2	12	4.07	11.00E3	.29	4.79
	6	1.33			
3	12	4.07	10.98E3	.29	4.78
	6	1.33			
	3	.32			

Standard deviation of the data = 5.66

Table 4-4

Deterministic Model Statistics, Solar Beam Radiation, Charleston, SC

Model	Periods	Amplitudes	RSS	R2	Standard Deviation
1	12	219.6	20.10E6	.36	204
2	12	219.6	16.58E6	.48	185
	6	120.6			
3	12	219.6	16.47E6	.48	185
	6	120.6			
	2.4	20.8			

Standard deviation of the data = 257

the fundamental diurnal frequency and its first harmonic were needed, but use of additional terms did not significantly improve the deterministic models. Notice that the addition of the first harmonic produced a much larger change in the residual sum of squares for the solar beam radiation series than for the temperature series; this confirms our earlier expectation that the first harmonic would play a more important part in the characterization of the square-wave-like solar data.

Next, adequate ARMA models were developed for the residuals from two-term deterministic models. For each of the two series, an AR(2) model was found to be adequate.

Finally, the model parameters were estimated for combined sinusoidal/AR(2) models for both series. Tables 4-5 and 4-6 show the final results. Note that even though two sinusoidal terms were found to be significant in the deterministic phase of the model development, in the combined phase, three sinusoids plus AR(2) models proved best for both weather data sequences, although the third sinusoid has a very small amplitude. The residual sum of squares and the AIC for these best combined models is lower than their counterparts for the best ARMA models.

We now compare the results of the three analysis techniques applied to the two Charleston weather data time series.

Table 4-5

Deterministic Plus Stochastic Models for Every Other Hour Dry-Bulb Temperature, Charleston, SC, 1953

Model	Period	Amplitude	Residual Sum of Squares	AIC	R2	Standard Deviation	Standard Deviation of the Data
1	12	4.07	1229	455	.92	1.60	5.66
	6	1.33					
	PHI(1) = 1.183						
	PHI(2) = -.259						
2	12	4.06	1128	414	.93	1.53	5.66
	6	1.33					
	3	.33					
	PHI(1) = 1.230						
	PHI(2) = -.303						

Table 4-6

Deterministic Plus Stochastic Models for Every Other Hour Solar Beam Radiation

Model	Period	Amplitude	Residual Sum of Squares	AIC	R2	Standard Deviation	Standard Deviation of the Data
1	12	220.1	9.612 x 106	4758	.70	141	257
	6	120.4					
	PHI(1) = .746						
	PHI(2) = -.178						
2	12	220.4	9.261 x 106	4740	.71	139	257
	6	120.2					
	2.4	20.8					
	PHI(1) = .774						
	PHI(2) = -.205						

Both the discrete Fourier transform spectrum and the ARMA modeling procedure allow identification of deterministic periodic behavior in the weather data time series studied. However, even though adequate ARMA models can be found for the strongly periodic time series, the ARMA model spectra are not adequate indicators of spectral peak heights in the data; consequently, they do not provide good estimates of the amplitudes of the principal sinusoids in the data. Notice, however, that the amplitudes of the sinusoidal terms of the combined deterministic plus stochastic models are very nearly equal to the height of the spectral peaks of the discrete Fourier transform (see Figures 4-1 and 4-2). For the time series studied, and for other deterministic periodic time series, the discrete Fourier transform can provide good amplitude estimates.

Generally, the combined model is more satisfactory than ARMA-only models for characterizing weather data time series, since the deterministic periodic behavior of the data is separated from the stochastic autoregressive behavior.

The development of pure ARMA models is unnecessary for these weather data time series, since their discrete Fourier spectral peaks are extremely pronounced. A combined model can be developed directly from amplitude and period information obtained from the Fourier spectrum and from ARMA modeling of the residuals. We can carry out this procedure on a sequence of hourly data rather than on data from every

other hour, since the problems associated with ARMA-only modeling of a timely sampled data sequence described earlier will no longer be relevant.

We must ensure that we correctly interpret the discrete Fourier spectrum and the spectra of the ARMA models at points away from the spikes in the spectrum. The small "hill" beginning at zero frequency and tailing off rapidly in the temperature data spectrum is characteristic of an AR(2) model; it does not represent the presence of low-frequency components in the weather data series. From the frequency perspective, only the diurnal frequency and its harmonics exist in the weather data time series. These are the only frequencies which are physically justifiable. (Longer periods may exist in longer data records.)

To verify that our conclusion from the Charleston data analysis can be generalized, Fourier spectra were plotted for a number of samples from different sites during different times of the year. These spectra, shown in Figures 4-8 through 4-13, are for records of hourly samples (720 hours per sample) rather than samples taken every other hour. In addition, deterministic plus stochastic models were developed, using the diurnal and the first harmonic of the diurnal as the frequency components of the deterministic model. In each case, the autoregressive component was AR(2). Notice that the AR(2) behavior persists, even though we have changed the sampling interval.

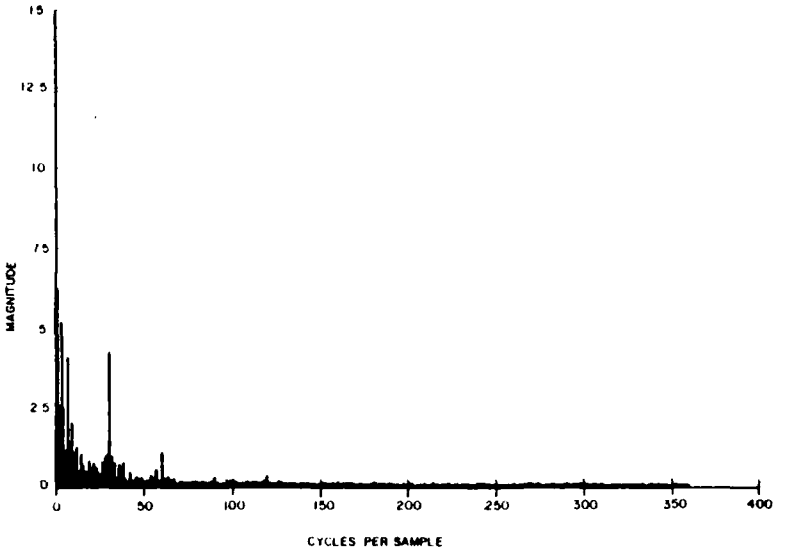

Figure 4-8. Spectrum for temperature, Fort Worth, TX (1 February through March 1955).

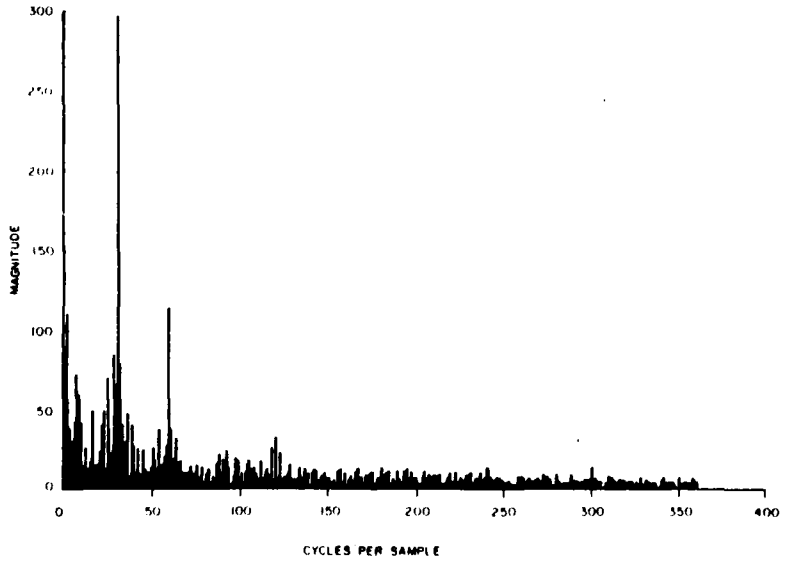

Figure 4-9. Spectrum for beam solar radiation, Fort Worth, TX (1 February through 22 March 1955).

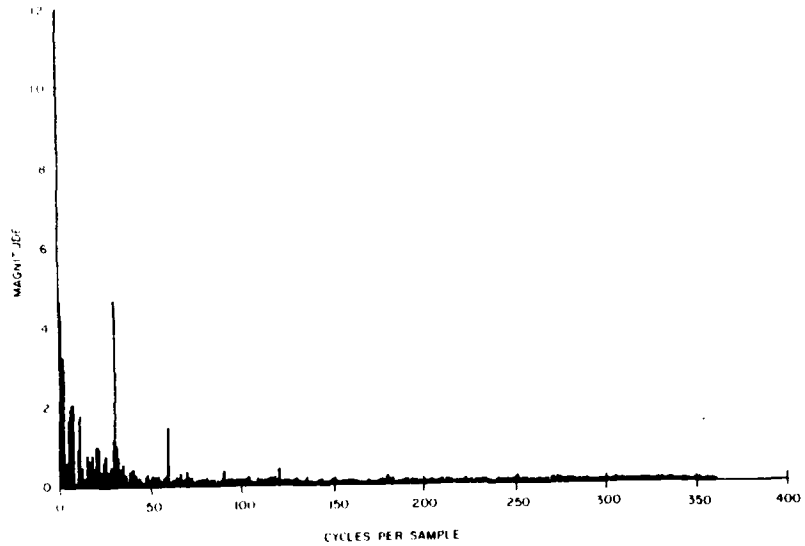

Figure 4-10. Spectrum for temperature, Madison, WI (25 September through 25 October 1955).

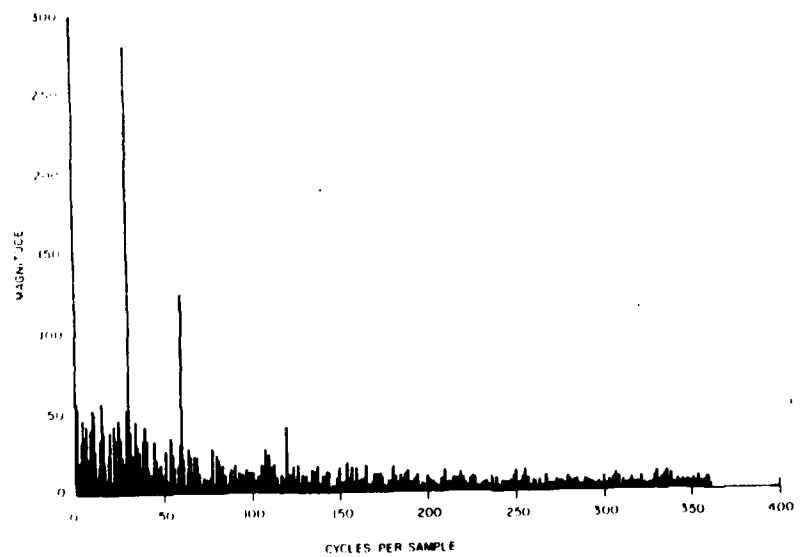

Figure 4-11. Spectrum for beam solar radiation, Madison, WI (25 September through 25 October 1960).

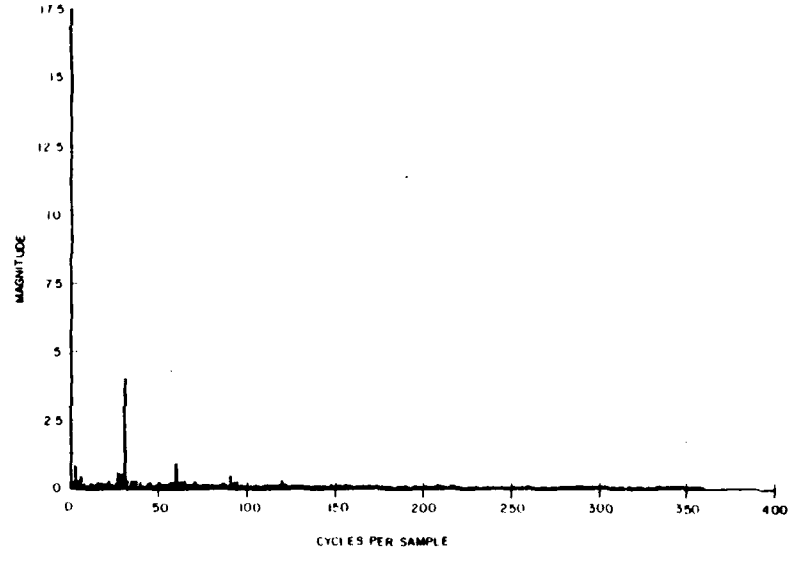

Figure 4-12. Spectrum for temperature, Santa Maria, CA (29 June through 28 July 1963).

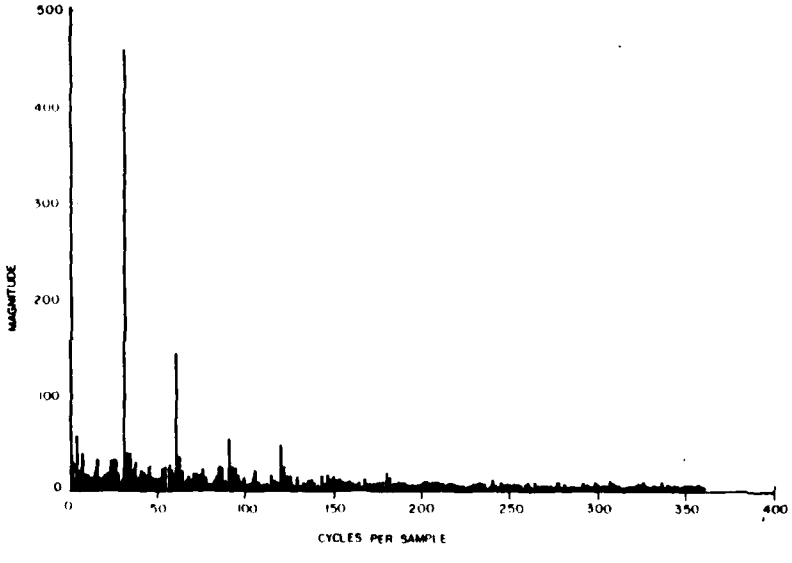

Figure 4-13. Spectrum for beam solar radiation, Santa Maria, CA (29 June through 28 July 1963).

Table 4-7 shows the coefficients of deterministic plus stochastic models for Madison, WI, Fort Worth, TX, and Santa Maria, CA.

Having characterized the short-term behavior of weather data, we must determine the extent of the annual weather cycle (which we know exists on physical grounds) and determine if there is any other periodic behavior in the data between the diurnal and the annual cycles. We can also look for stochastic behavior in longer data records. To examine long-term weather data trends, two time series were constructed for both temperature and beam radiation; one consisted of the daily averages of the hourly data for a 10-year period (3650 points); the other consisted of 5-day averages of the hourly data for a 10-year period (730 points). Data from Charleston, SC, Madison, WI, and Santa Maria, CA, were used for this part of the study.

As before, we first examine the Fourier spectra of each time series. The time series of daily averages is used to ensure that any cyclical behavior with a period between 2 and 10 days will show up clearly. Any regular behavior with periods longer than 10 days will be revealed by the spectra of the time series of 5-day averages; these time series are also short enough to be analyzed using the deterministic plus stochastic modeling techniques.

Table 4-7

Deterministic Plus Stochastic Models for Various Weather Data Time Series

Location	Weather Data	Period	Amplitude	Stochastic Parameters	Residual Sum of Squares	R^2	Standard Deviation	Standard Deviation of Data
Fort Worth, TX 1 Feb - 2 Mar 55	Temperature	24 12	4.04 1.05	PHI(1) = 1.363 PHI(2) = -.377	743	.98	1.01	8.41
	Solar Beam Radiation	24 12	296 114	PHI(1) = .927 PHI(2) = -.088	1.070×10^7	.86	122	324
Madison, WI 25 Sep - 25 Oct 60	Temperature	24 12	4.49 1.49	PHI(1) = 1.178 PHI(2) = -.206	1004	.97	1.18	6.62
	Solar Beam Radiation	24 12	279 124	PHI(1) = .863 PHI(2) = -.096	$.984 \times 10^7$	.84	117	288
Santa Maria, CA 29 Jun - 28 Jul 63	Temperature	24 12	4.04 1.18	PHI(1) = 1.075 PHI(2) = -.283	385	.95	.73	3.23
	Solar Beam Radiation	24 12	458 144	PHI(1) = .945 PHI(2) = -.291	$.725 \times 10^7$	.93	100	373

Figure 4-14 shows the spectrum for the daily average temperature time series for Madison, WI. There is quite clearly only one spectral peak, which occurs at 10 cycles per sample or one cycle per year. Everywhere else, the spectrum resembles a "white noise" spectrum (at least by comparison to the annual cycle peak). We cannot yet conclude that all that will remain after the annual cycle is removed will be random noise, but Figure 4-14 clearly allows us to eliminate short-term (2- to 10-day) periodicity from further consideration. This was confirmed by the spectra for the other five time series of daily averages (not shown) which had exactly the same spectral character.

We now examine the spectra for the time series of 5-day averages (Figures 4-15 through 4-20). Again, the annual cycle (10 cycles per sample) is the only obvious characteristic of these data. The first harmonic of the annual cycle appears only for beam radiation for Charleston, SC; in this case, both the annual cycle and its first harmonic are relatively small when compared to the mean. On the basis of these spectra, we conclude that a combined deterministic plus stochastic model for the 5-day average time series should include only the annual sinusoid as its deterministic component.

To determine whether stochastic behavior (other than random variance) existed in the weather data time series, ARMA modeling techniques were applied to the residuals from a deterministic model

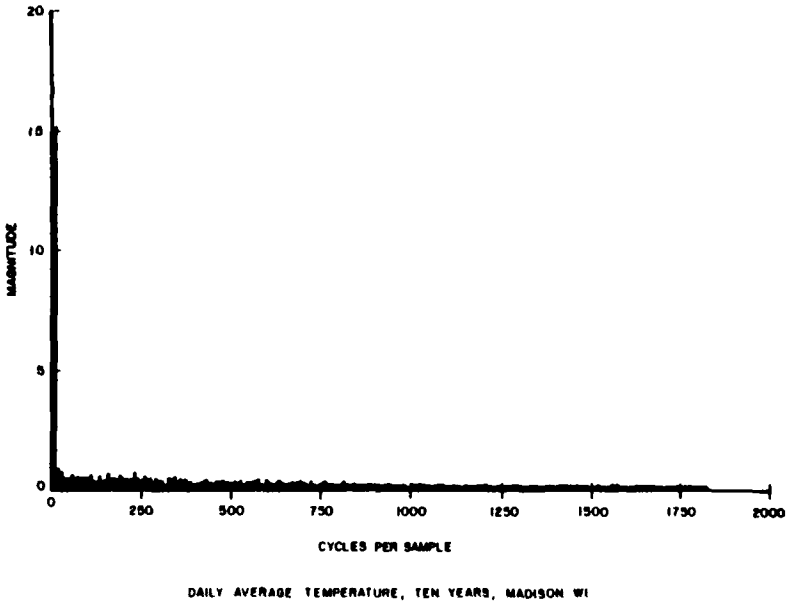

Figure 4-14. Spectrum for daily average temperature, Madison, WI (1953-1962).

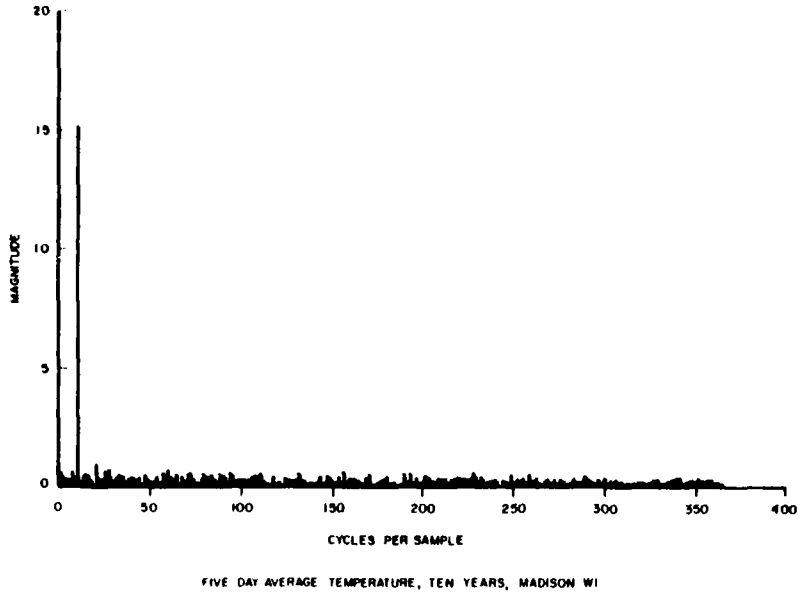

Figure 4-15. Spectrum for 5-day average temperature, Madison, WI (1953-1962).

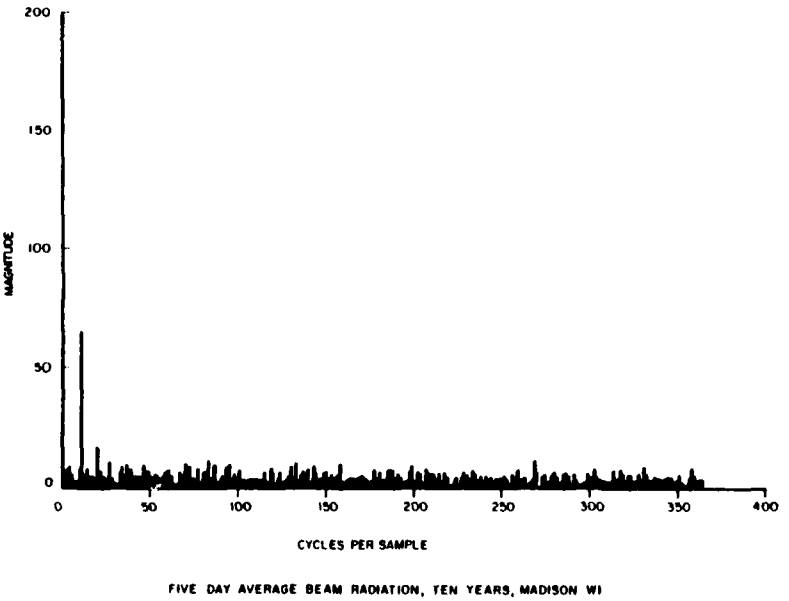

Figure 4-16. Spectrum for 5-day average beam solar radiation, Madison, WI (1953-1962).

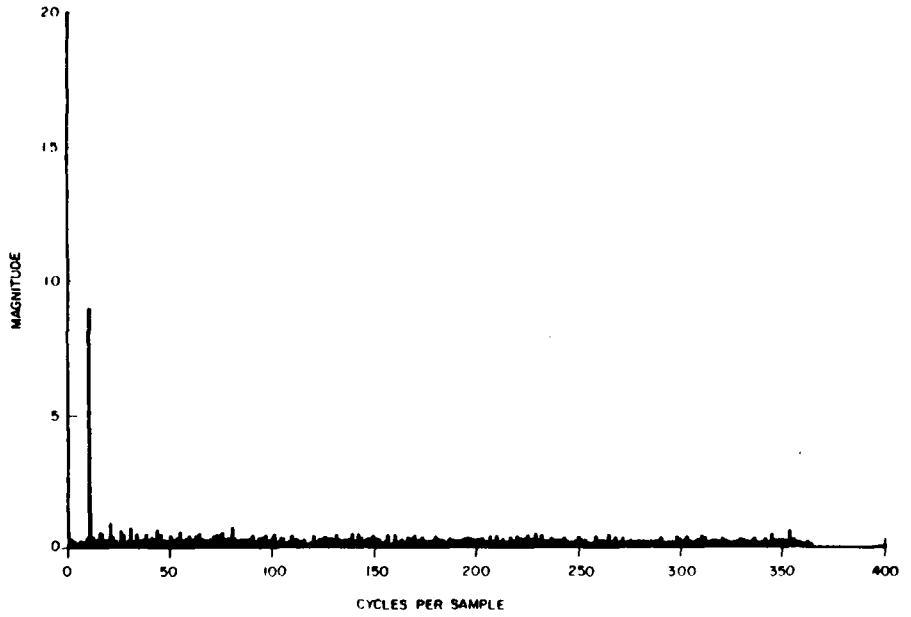

Figure 4-17. Spectrum for 5-day average temperature, Charleston, SC (1953-1962).

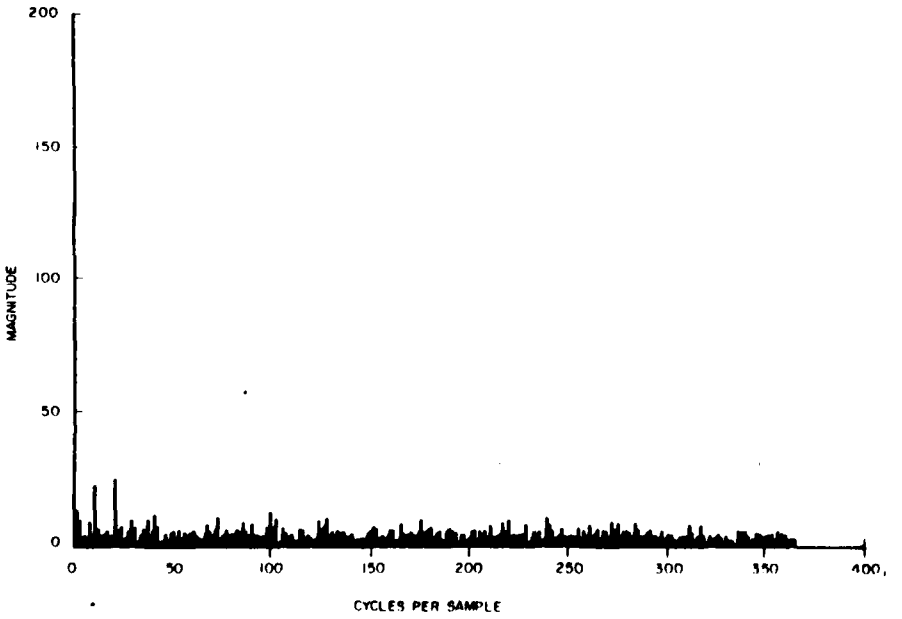

Figure 4-18. Spectrum for 5-day average beam solar radiation, Charleston, SC (1953-1962).

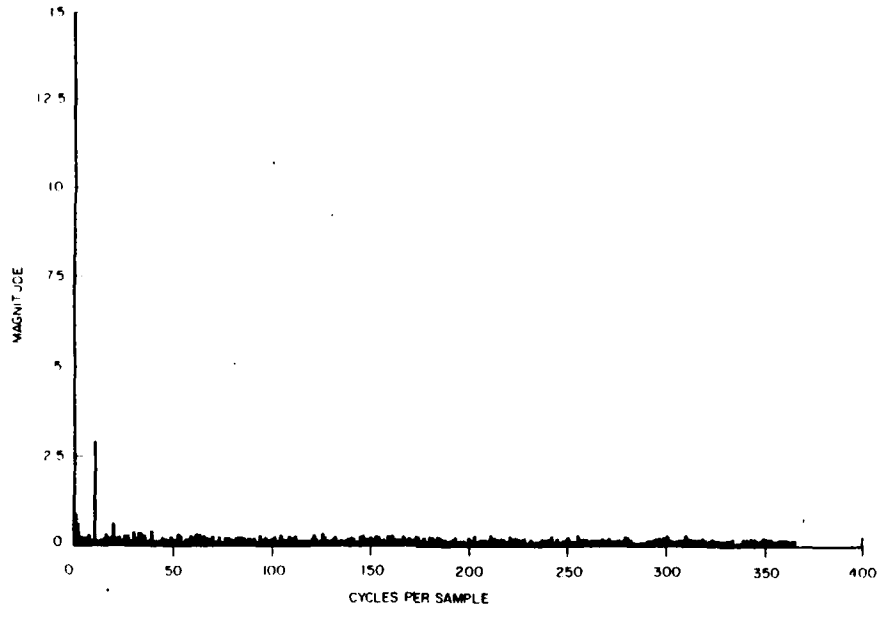

Figure 4-19. Spectrum for 5-day average temperature, Santa Maria, CA (1954-1963).

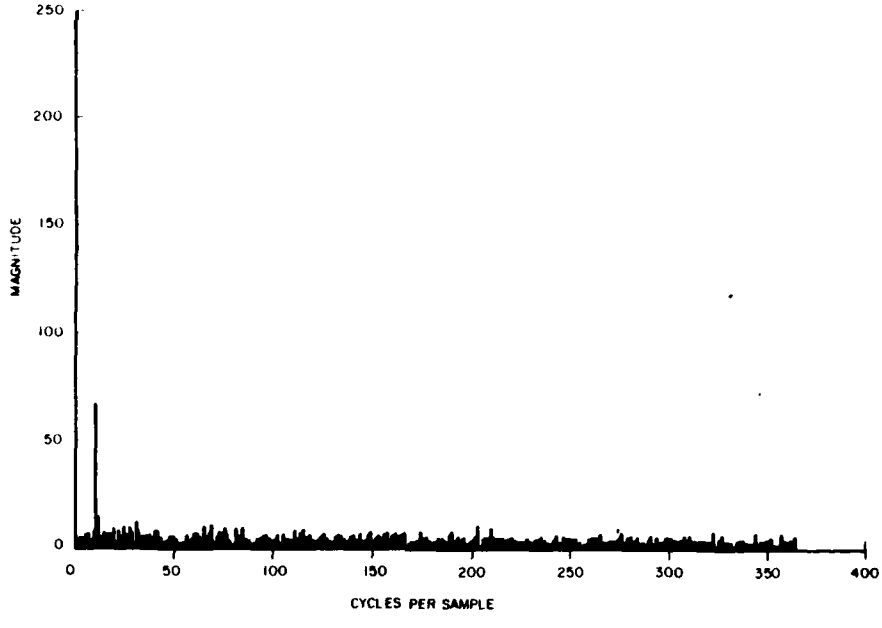

Figure 4-20. Spectrum for 5-day average beam solar radiation, Santa Maria, CA (1954-1963).

for each time series (the deterministic model included only the annual sinusoid). An AR(1) model was found to be adequate in each case. Finally, combined deterministic plus stochastic models were found for each time series.

Table 4-8 shows the results for the deterministic only models and for the deterministic plus stochastic models. We see that for climates like Madison and Charleston, which have pronounced annual temperature variations, the annual sinusoid accounts for a large fraction of the variance in the temperature data. For Santa Maria, annual temperature swings are small, and the annual temperature cycle is less important than daily temperature cycles (see Tables 4-6 and 4-7 for comparison).

Comparing the annual cycles for solar beam radiation with the daily cycles of Tables 4-6 and 4-7, we see, as expected, that annual variations are much less pronounced than daily variations. This is particularly true for Charleston with its southern latitude.

We can assess the importance of the AR components in the models shown in Table 4-8 by comparing the standard deviation of the deterministic only models with its counterpart for the deterministic plus stochastic models. At each site, we see that the AR(1) component produces only a nominal reduction in the standard deviation for the 5-day average temperature data (less than $.2^{o}$ C) and almost no reduction for the 5-day average solar data. The very small improvement in

Table 4-8

Deterministic and Deterministic Plus Stochastic Models for 5-Day Averaged Weather Data Time Series

Location	Data	Frequency (Cycles/Year)	Amplitude	PHI(1)	Sum of Squares	R^2	Standard Deviation
Madison, WI	Temperature (Deterministic)	1	15.24	---	9690	.90	3.64
	Temperature (Deterministic Plus Stochastic)	1	15.24	.315	8728	.91	3.46
	Solar Beam Radiation (Deterministic)	1	65.52	---	2.898×10^6	.35	62.00
	Solar Beam (Deterministic Plus Stochastic)	1	65.52	.167	2.817×10^6	.37	62.11
Santa Maria, CA	Temperature (Deterministic)	1	2.89	---	2455	.55	1.65
	Temperature (Deterministic Plus Stochastic)	1	2.89	.452	1953	.64	1.64
	Solar Beam Radiation (Deterministic)	1	66.06	---	2.391×10^6	.40	55.38
	Solar Beam Radiation (Deterministic Plus Stochastic)	1	65.95	.272	2.215×10^6	.44	55.68

the models due to the AR(1) component does not justify the additional model complexity that including this term would cause.

Having analyzed both the short-term (hourly) and long-term (5-day averages) character of weather data time series, we can now write the general form for a deterministic plus stochastic model with a 1-hour time step for both temperature and beam solar radiation (models for both temperature and radiation have the same form):

$$X_t = a_o + 2(a_1 \cos(2\pi t/8760) + b_1 \sin(2\ t/8760))$$
$$+ 2(a_{365} \cos(2\pi 365t/8760) + b_{365} \sin(2\pi 365t/8760))$$
$$+ 2(a_{730} \cos(2\pi 730/8760) + b_{730} \sin(2\pi 730t/8760))$$
$$+ \text{(other frequency components; see discussion)}$$
$$+ \Phi_1 X_{t-1} + \Phi_2 X_{t-2} + a_t \qquad \text{[Eq 4-7]}$$

where: X_t is the value of the weather data variable at time t

a_o is the mean of the weather data variable

a_1 and b_1 are the annual cycle Fourier coefficients

a_{365} and b_{365} are the daily cycle Fourier coefficients

a_{730} and b_{730} are the Fourier coefficients of the first harmonic of the daily cycle

Φ_1 and Φ_2 are constant autoregressive model parameters

X_{t-1} and X_{t-2} are the values of the weather data variable at t-1 and t-2, respectively

a_t is the random impulse at time t.

Notice that we have used the Fourier coefficients as the deterministic model components rather than coefficients derived from nonlinear regressions. This is because the amplitudes of the sinusoids, which result from the nonlinear regression used to find deterministic plus stochastic models, are almost exactly equal to the corresponding Fourier spectrum peak heights for all the cases we have studied. Thus, we may as well use the more efficient fast Fourier transform technique to find the deterministic model parameters.

The "other frequency components" of Equation 4-7 allow for the inclusion of other harmonics if they are determined to be significant for a particular site or climate variable and for the inclusion of any significant side bands. Side bands were shown to be important in the work described in ref 2 and by the Fourier transforms of 1 year of hourly data described below and in Chapter 5.

Side bands are spectral peaks which occur on either side of a fundamental frequency or its harmonics. For example, spectral peaks at 364 and 366 cycles per year are side bands of the diurnal cycle (365 cycles per year is the diurnal cycle). Side bands are properly interpreted as indicating the presence of amplitude modulation. For example, side bands at 364 and 366 indicate that the amplitude of the diurnal cycle varies sinusoidally about its mean value (as indicated by the height of the spectral peak at 365 cycles per year). The fact that the side bands occur at 365 ± 1 indicates that the amplitude of the diurnal cycle modulates at 1 cycle per year.

Side bands around the diurnal cycle and its harmonics are most pronounced for solar radiation in northern climates (e.g., Madison). This simply indicates that there is substantial seasonal variation in the amplitude of the diurnal variation in solar radiation, a fact well known from astronomy.

Equation 4-7 represents the culmination of the analysis which has accomplished the following: separation of the deterministic periodic behavior from the stochastic behavior in the weather data time series; demonstration that there are only a few statistically significant frequencies in the climate data (the annual cycle, the diurnal cycle, and the first harmonic of the diurnal are the most important; other harmonics and side bands may be important, depending on the site and the climate variable); and discovery that the weather data time series has a significant stochastic component.

As a final step in the weather data analysis, we need to determine sample statistics for an hourly model which includes the mean, the annual cycle, the diurnal cycle, and the diurnal cycle's first harmonic, but does not include the stochastic component. To achieve this, fast Fourier transform coefficients were determined for 1 year of hourly data for 1955 from Fort Worth, Santa Maria, Charleston, and Madison. Hourly temperature and solar beam radiation were modeled

for each site for a 1-year period, using only the mean, the annual cycle, the diurnal cycle, and the first harmonic of the diurnal cycle; results were then compared to the actual data (see Table 4-9). We can see from the table that the larger deterministic components in the weather data account for a substantial portion of the variance in the data--more of the variance than is indicated in the results shown in Table 4-3.

Conclusion

As demonstrated in Chapter 3, the use of the sinusoidal components of the weather data model without the use of the stochastic component greatly simplifies the calculation of loads for building energy analysis. The analysis presented in this chapter shows that true periodicity in the data exists only at the annual cycle and at the diurnal cycle plus its harmonics. We have also shown that the fast Fourier transform is an adequate procedure for determining the amplitude of the periodic components. Using the fast Fourier transform, we can also analyze much longer periods of hourly data than we have shown in the preceding analysis or than could be analyzed by other methods, such as nonlinear regression.

These weather data models also have other significant applications. One of the most obvious is the potential use of deterministic plus stochastic models in lieu of weather data tapes as input to

Table 4-9

Deterministic Sinusoidal Models for Hourly Weather Data for 1 Year

Location	Weather Data	R2	Standard Deviation	Standard Deviation of the Data
Fort Worth, TX	Temperature	.73	5.61	9.86
	Solar Beam Radiation	.60	204	322
Charleston, SC	Temperature	.72	4.40	8.32
	Solar Beam Radiation	.50	190	269
Madison, WI	Temperature	.83	5.36	13.04
	Solar Beam Radiation	.47	203	280
Santa Maria, CA	Temperature	.59	3.15	5.94
	Solar Beam Radiation	.66	194	335

energy analysis programs. Equations like Equation 4-7 could simply be included in the energy analysis programs themselves, and the model coefficients would be part of the input to the program. The hourly value for a_t could be produced by a seeded random-number generator with the variance of a_t supplied as input. This approach could completely eliminate the need to routinely access weather data tapes or files (simultaneously eliminating controversy over data formats and weather data file/energy analysis program interfaces). The coefficients for a combined deterministic plus stochastic model need to be generated and tabulated only once for any given site, and they could be based on very long periods of hourly recorded data. The generation of the coefficients would be quite straightforward. The sinusoidal terms can be derived using fast Fourier transform techniques (available on most computer systems) which are very efficient and can accommodate very large data sets (several years or even tens of years of hourly data). The stochastic model component has only AR behavior, which means that the model parameter can be determined using linear regression, again allowing the analysis of very large data sets.

The weather data models which would result from the above data analysis would be truly "typical" in a statistical sense, thereby perhaps laying to rest much of the controversy over what weather data to use for energy analysis purposes.

Another possible application of the deterministic plus stochastic climate models is short-term weather forecasts for use in microprocessor-based building energy system controls. The control of chilled water storage, for example, might be based on an algorithm which included forecasts of outdoor temperatures and/or solar radiation for the next several hours or days. The forecasts would be updated with measured data each hour. The availability of a good short-term forecast (perhaps 10 to 20 hours ahead) could be useful in controlling a variety of HVAC system parameters, such as morning startup time, chilled and hot water temperatures, length of duty cycling used to avoid peak loads, and staging or load sharing in large boiler or chiller plants. The use of climate forecasts, combined with the calculated or measured dynamics of the building and its energy systems (room and system "response factors"), would allow the control system to anticipate heating and cooling requirements. The potential for reducing building energy consumption by applying control systems which use climate forecasts remains to be explored.

5 EFFECTS OF DETERMINISTIC CLIMATE MODELS ON ENERGY CALCULATIONS

Problem Definition

In Chapter 3, we showed that calculating heat flow through multi-layered slabs is greatly simplified if the temperature boundary condition on one side of the slab is assumed to be sinusoidal rather than a discrete temperature time series. In particular, calculating the frequency-dependent U-value of a multi-layered slab is much easier than calculating conduction transfer functions. We expected to be able to use frequency response methods as part of a simplified procedure for calculating hourly heating and cooling loads in buildings.

We then sought to determine how many terms of a Fourier series would be required to provide an "adequate" approximation of an actual weather data time series. The results of the application of time series analysis techniques to weather data, summarized in Chapter 4, led us to conclude that truly sinusoidal behavior is exhibited only at very few frequencies (one cycle per year and one cycle per day plus harmonics of one cycle per day). The rest of the variation in weather data is stochastic in nature. We could account for more variance in a weather data time series by using greater numbers of Fourier coefficients to approximate the series; however, using

coefficients whose frequencies did not correspond to the annual cycle or the diurnal cycle and its harmonics or to their side bands would be an artificial means of accounting for the portion of climate variation that is really stochastic rather than deterministic.

In this chapter, we examine results of a study to determine how much error will be introduced in calculating expected energy use in a building if we use only the mean, the annual cycle, and the diurnal cycle and its first harmonic to characterize weather variation.

The procedure used to carry out this investigation consisted of the following steps:

1. For each of four representative locations, a fast Fourier transform was performed on 1 year of hourly weather data for each climate variable affecting building energy use calculations.

2. The mean of each climate variable and the Fourier coefficients corresponding to the annual cycle, the diurnal cycle, and the first harmonic of the diurnal cycle were used to synthesize 1 year of hourly weather data.

3. The energy use of typical buildings served by several different heating and cooling systems was calculated using both actual and synthesized hourly weather data. The Building Loads Analysis and System Thermodynamics (BLAST) program, a detailed energy analysis computer program, was used to calculate expected energy use.

4. Results of Step 3 were compared and analyzed.

Weather Data

The same weather data tapes used for the analysis described in Chapter 4 were used for this part of the study. Recall that the four sites selected were Charleston, SC, a hot humid climate; Madison, WI, a cold northern climate; Fort Worth, TX, a hot dry climate; and Santa Maria, CA, a marine climate. The year 1955 was selected from the available data records as being reasonably representative.

The BLAST program used the following climate variables to calculate expected building energy:

1. Outdoor dry-bulb temperature

2. Outdoor wet-bulb temperature

3. Barometric pressure

4. Humidity ratio (derived from dry-bulb, wet-bulb, and barometric pressure data)

5. Wind speed

6. Beam radiation

7. Diffuse radiation

8. Ground-reflected radiation (calculated from beam and diffuse radiation, ground reflectivity, and a snow cover indicator).

A fast Fourier transform was performed on 1 year of hourly data for each climate variable. Figure 5-1 shows sample results of the Fourier transform for beam radiation at Santa Monica, CA. Once the fast Fourier transform was completed, coefficients representing the mean, the annual cycle, the diurnal cycle, and the first harmonic of the diurnal cycle, were obtained.

A complete 1-year record of hourly weather data was then synthesized, using the mean for each weather variable and the pair of Fourier coefficients corresponding to the annual, the diurnal, and the first harmonic of the diurnal for each variable. Thus, at the end of this phase of the analysis, a 1-year record of actual weather data for 1955 and a 1-year record of synthesized weather data existed for each of the four sites selected.

Building Energy Analysis Test Cases

To compare the effects of using synthesized and actual weather data, a hypothetical building was designed that would be reasonably (but not overly) sensitive to climatic variations. Also, since the performance of different building fan systems is influenced by climate, even when satisfying the same building loads, several candidate building fan systems were designed and simulated. Finally, for the

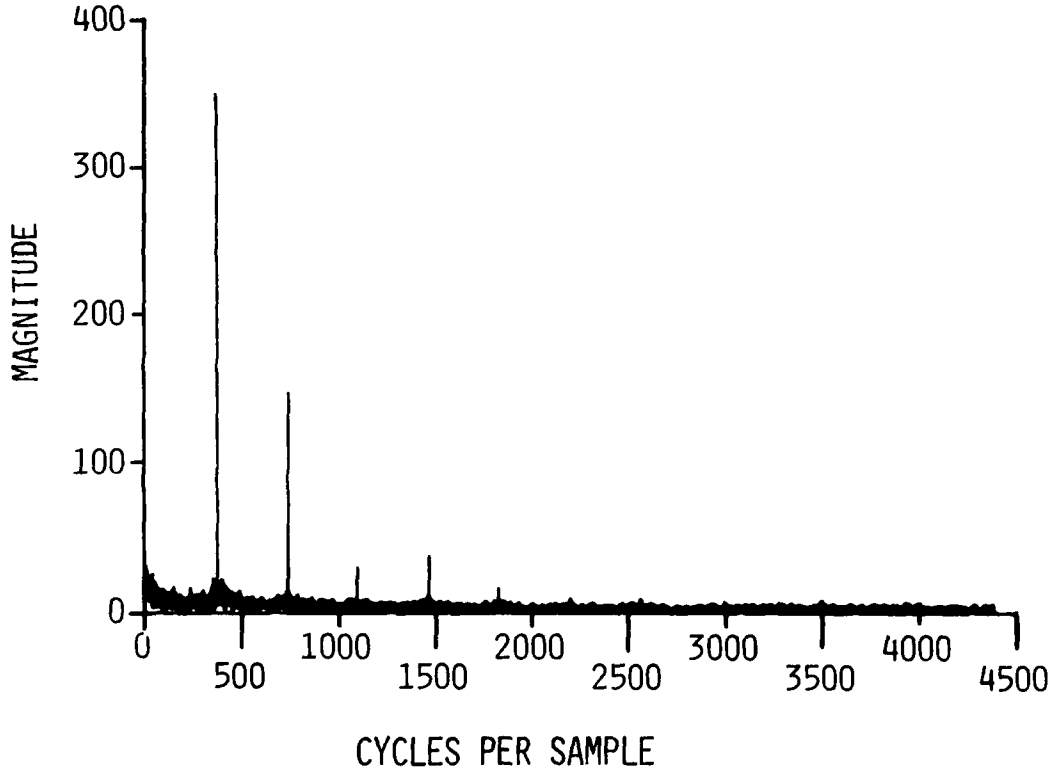

Figure 5-1. Spectrum for solar beam radiation, Santa Maria, CA, 1955.

sake of completeness, and because changes in hourly demand profiles can cause performance to vary, a boiler/chiller plant was designed to serve the building fan systems.

The hypothetical building consisted of 24 exterior office modules, an interior computer room, and three interior office modules. The exterior modules were assumed to be bounded on three sides by interior building partitions and were assumed to have an exterior roof, a slab floor heavily insulated from below, and an exterior wall of various constructions and with varying amounts of glass. Six modules were assumed to be on each of the north, south, east, and west sides of the building. Figure 5-2 illustrates an office module. During the course of this study, three different exterior wall constructions were considered: one was all-glass, another had a heavy conductive exterior wall with about 16 percent glass, and the third had a heavily insulated exterior wall with 16 percent glass. Table 5-1 gives details of these exterior wall constructions. The interior office module was assumed to be 72 m^2 in area, square in shape, and in contact with the environment only through its roof. Three identical interior office modules were simulated. The remaining module represented a computer room and was dominated by interior electric load.

Appropriate occupancy lighting and equipment schedule were selected for all spaces, and a control strategy designed to maintain

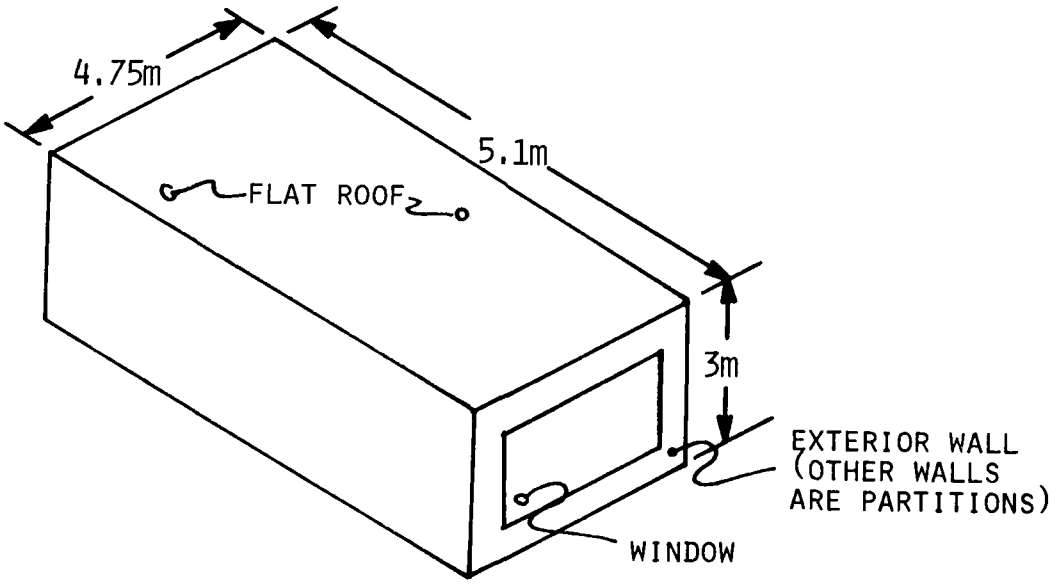

Figure 5-2. Typical exterior office module.

Table 5-1

Properties of Exterior Walls, Partitions, Roofs, and Floors

	Layers	Thickness (m)	Density (kg/m3)	Conductivity (W/m oK)	Specific Heat (kJ/kg oK)	Solar Absorptivity
Heavy Conductive Wall	Face Brick	.1020	2082	1.298	.794	.60
	Heavy Concrete	.1020	2242	1.731	.919	---
	Gypsum Board	.0173	801	.640	1.087	---
Heavy Insulated Wall	Wood	.0254	512	1.379	.115	.5
	Loose Fill	.0762	5.4	.038	.794	---
	Heavy Concrete	.1020	2242	1.731	.919	---
Glass Wall	Single-Pane Heavy Glass	.0063		---(R = .008 m^2 oK/W)---		
Partitions	Concrete Block	.2030	689	1.04	.878	---
Floor	Insulation	------(R = 5 m^2 - oK/W)-------				
	Heavy Concrete	.1020	2242	1.731	.919	
Roof	Stone	.0127	881	1.436	1.674	.55
	Membrane	.0095	1121	.190	1.674	---
	Insulation,	.0509	91	.043	.837	---
	Steel-Deck,	.0015	7688	44.469	.418	--
	Air-Space,	---(R = .176 m^2 - oK/W)---				
	Acoustic Tile	.0191	480	.061	.837	---

the space temperature between 22.8 and 25°C was assigned. Heating and cooling were assumed to be available, as required, throughout the year.

Five separate fan systems were simulated, with each designed to serve all zones in the building. The first was a reheat fan system of conventional design. The second was a reheat fan system with (1) cold-deck reset (i.e., the cold deck was reset to deliver air no colder than was necessary for the zone requiring the most cooling), and (2) an enthalpy economy cycle (any time the enthalpy of the outdoor air was less than the enthalpy of the return air for the system, outdoor air was used to offset all or part of the cooling requirements). The third system was a conventional, single-duct variable air-volume system with reheat. The fourth system was a variable air-volume system with reheat, cold-deck reset, and an enthalpy economy cycle, and the fifth was a conventional, four-pipe fan-coil system. Figures 5-3 through 5-5 are schematics of these systems. Each system was simulated for each of the three different exterior building treatments previously described. Thus, fifteen 1-year fan system simulations were performed for each site and for both actual and synthesized data. Finally, identical modular boiler/chiller plants (three chillers, two boilers) were simulated for each simulated fan system.

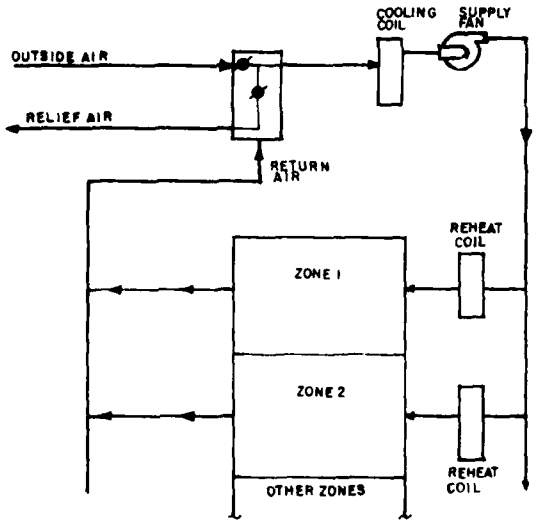

Figure 5-3. Terminal reheat system.

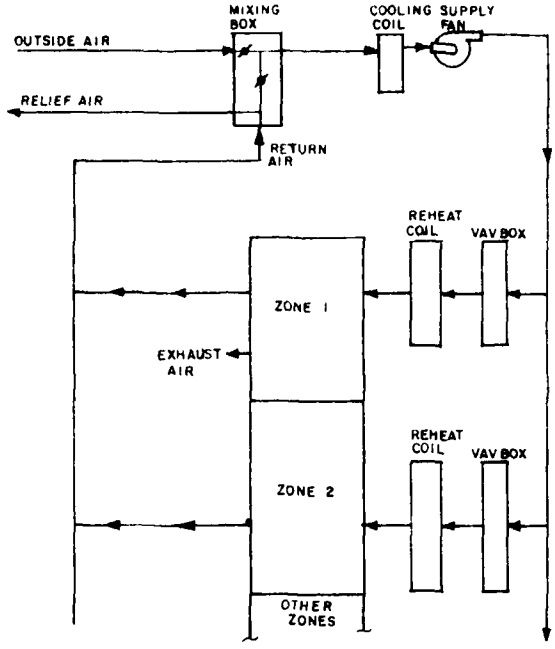

Figure 5-4. Variable volume system.

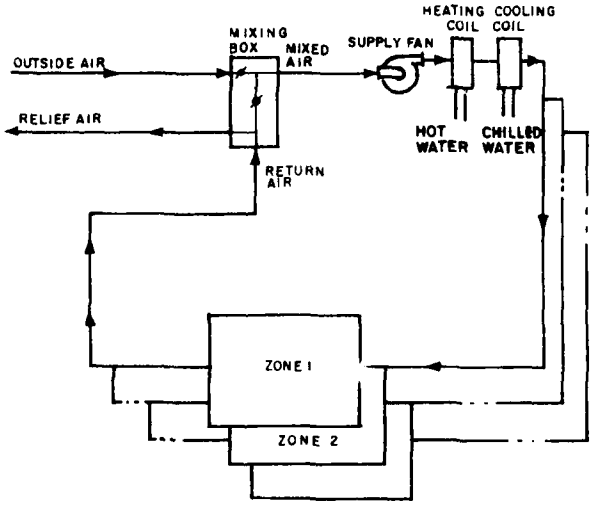

Figure 5-5. Four-pipe fan-coil system (one fan-coil system per zone).

Analysis of Results

We now assess the calculation errors in expected energy use resulting from the use of sinusoidal weather data approximations. The procedure described in the previous section provided the necessary quantitative data. We must now examine this data to determine whether or not the errors are acceptable. To do this, we will review how results of energy analysis calculations are used (or should be used) to design or redesign buildings and their energy systems and determine if errors resulting from the use of synthesized weather data affect the usefulness of the results.

Building architecture and space utilization affect building heating and cooling loads. Heating and cooling loads are the amount of energy which must be added to or removed from a space to maintain it within the specified comfort temperature range. A design objective is to minimize these loads by properly selecting the building envelope elements. For example, we might expect that an all-glass building will have a considerably higher cooling load on a hot summer day due to the solar transmission through the glass than a building with a modest glass area. Similarly, because glass is not a good insulating medium, the same building might have an extremely high heating requirement on a cloudy winter day. As designers, we are interested in both the heating and cooling loads within a building's zones as a measure of the building envelope performance. If we are

to use a sinusoidal approximation for climate, simulation results from the synthesized data should conform to results obtained by simulating the zones using the actual weather data; in particular, the differences between different building architectural and construction options should be the same, whether we use synthesized or actual weather data. Figures 5-6 through 5-13 show the calculated annual cooling load and annual heating load for the exterior zones for each of the four climates and each of the three different building wall constructions considered. Results of the use of actual and synthesized weather data are compared. These figures provide the first evidence that we are on relatively firm ground when we treat climate as a sum of sinusoidal components. Notice in particular that, except in cases where the differences in loads are very small, the rank order of the loads for each option remains unchanged, whether we use actual or synthesized data. For example, when we use the actual data, the annual cooling load is substantially higher for an all-glass wall option than for a well-insulated wall; the same is true when we use the synthesized data. Thus, for both types of weather data, the difference in load between the two options is very nearly the same. Even more subtle differences, like the slight increase in calculated annual cooling load between the heavy-conductive and heavy-insulated wall options, are generally preserved when synthesized weather data is used. It is quite clear that the utility of the results in terms of assessing the performance of the building

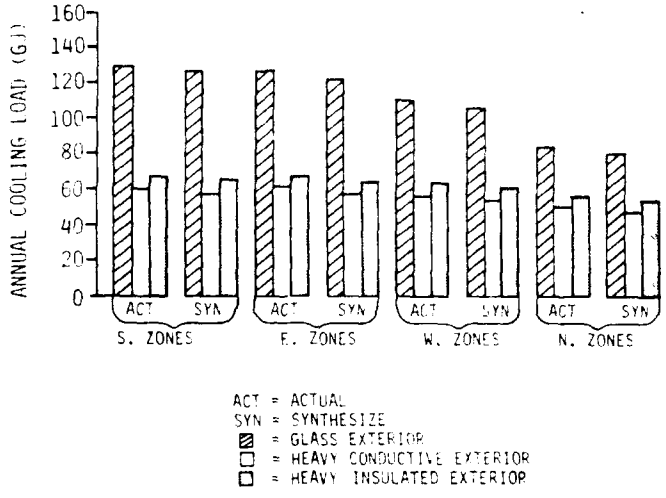

Figure 5-6. Annual cooling load for exterior zones, Charleston, SC.

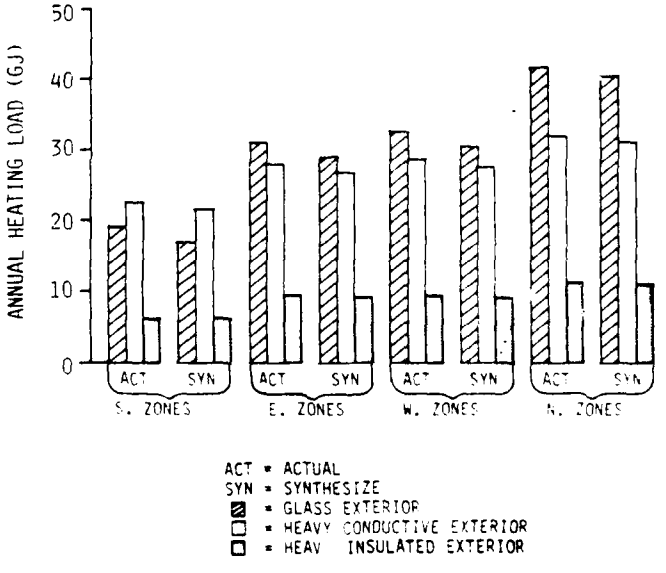

Figure 5-7. Annual heating load for exterior zones, Charleston, SC.

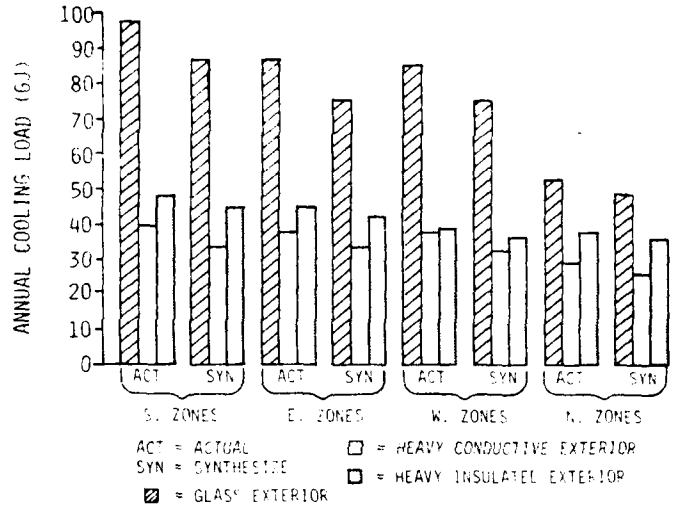

Figure 5-8. Annual cooling load for exterior zones, Madison, WI.

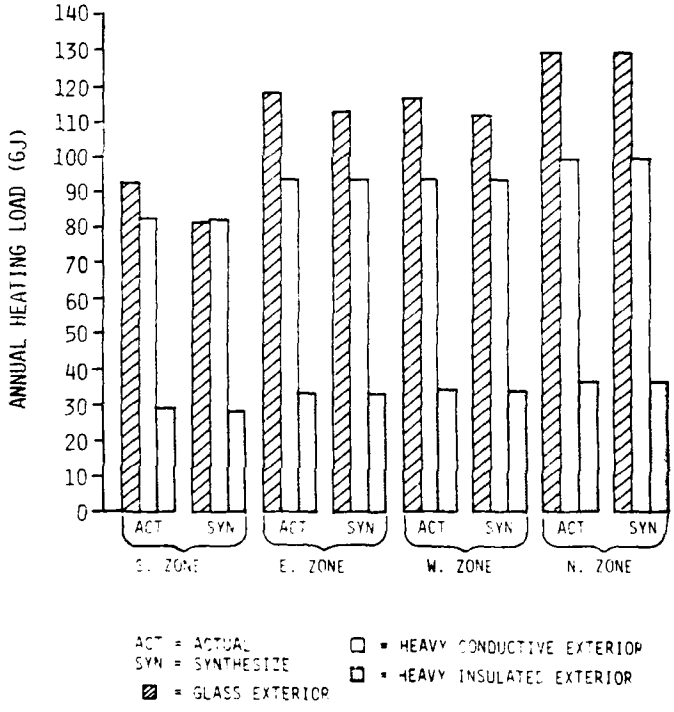

Figure 5-9. Annual heating load for exterior zones, Madison, WI.

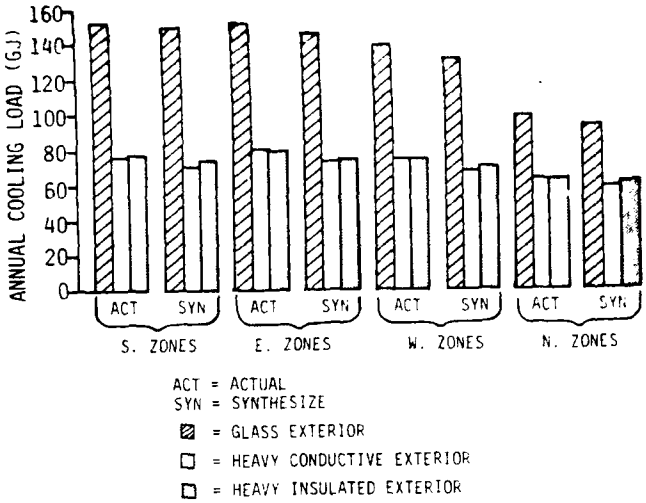

Figure 5-10. Annual cooling load for exterior zones, Fort Worth, TX.

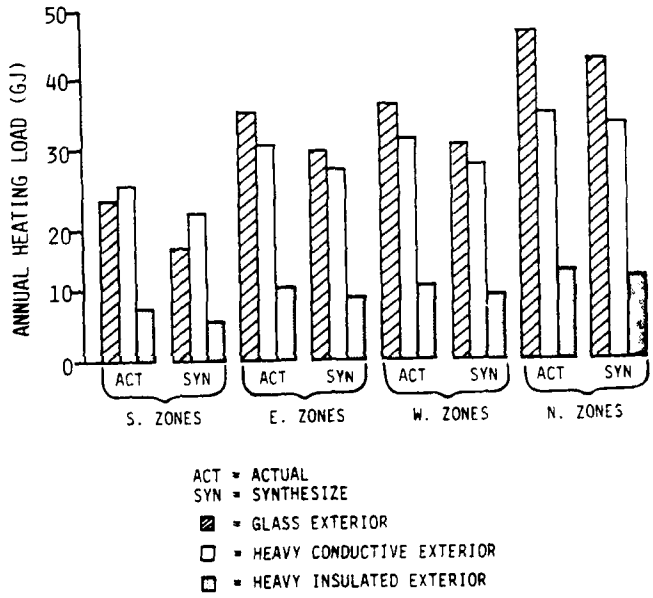

Figure 5-11. Annual heating load for exterior zones, Fort Worth, TX.

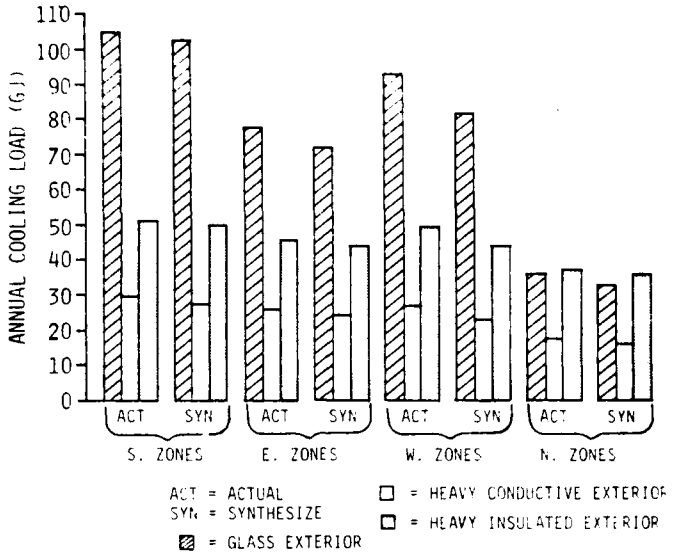

Figure 5-12. Annual cooling load for exterior zones, Santa Maria, CA.

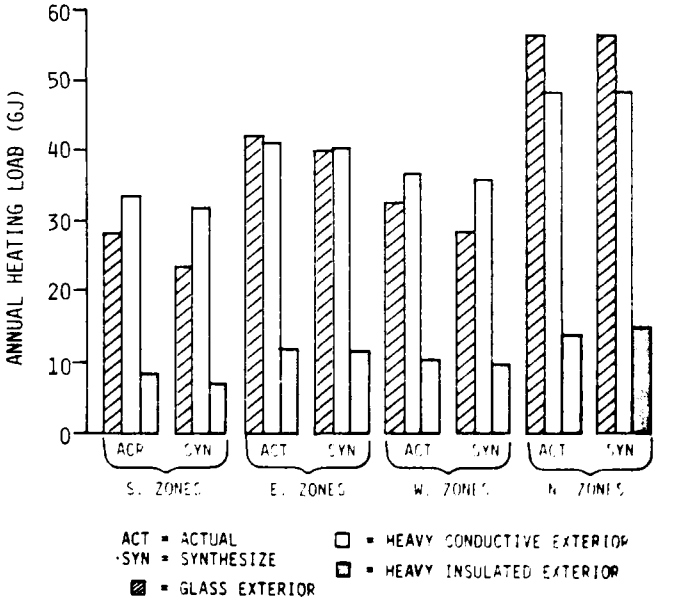

Figure 5-13. Annual heating load for exterior zones, Santa Maria, CA.

envelope is the same, whether we use synthesized or actual data; there is only a small error in absolute value if we use the synthesized data.

We next examine the fan systems meeting heating and cooling loads in the buildings and assess whether using synthesized weather data will cause any error in the demand that the fan system places on the central plant (i.e, hot and chilled water demands). Five separate types of fan systems were examined for each architectural option. Figures 5-14 through 5-21 summarize the results. In these figures, system 1 is the conventional reheat system, system 2 is the reheat system with cold-deck reset and an enthalpy economy cycle, system 3 is the conventional variable air volume system, system 4 is the variable air-volume system with cold-deck reset and an enthalpy economy cycle, and system 5 is the four-pipe fan-coil system.

We must now assess, for a given building envelope, how the use of actual vs. synthesized weather data will affect the rank order of the calculated energy consumption for each fan system type. An examination of Figures 5-14 through 5-21 clearly indicates that there is no effect. In every case where different fan systems exhibit substantially different hot and chilled water demands, the variations are roughly the same, whether we use synthesized or actual data; in fact, we see better agreement in the absolute values for annual hot and chilled waste demands than we did for the annual heating and

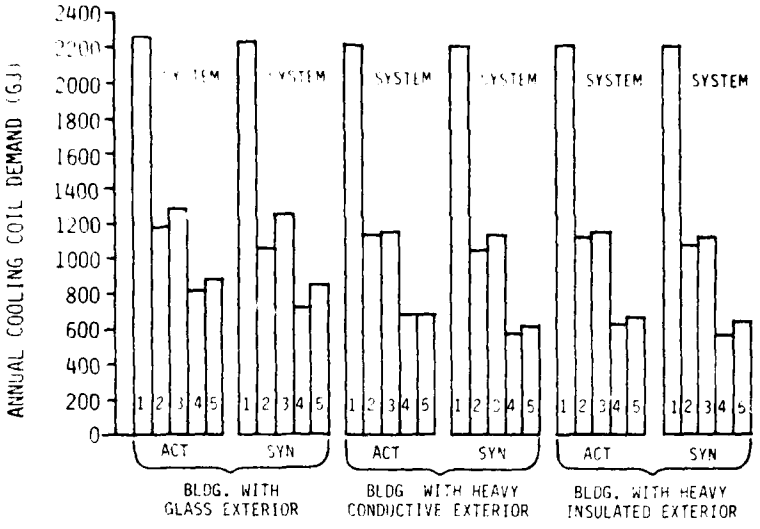

Figure 5-14. Annual cooling coil demand, Charleston, SC.

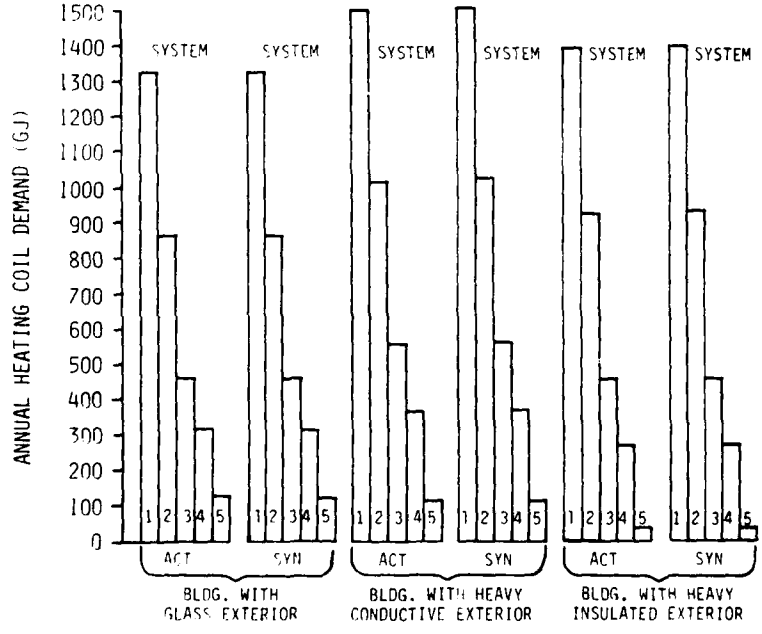

Figure 5-15. Annual heating coil energy demand, Charleston, SC.

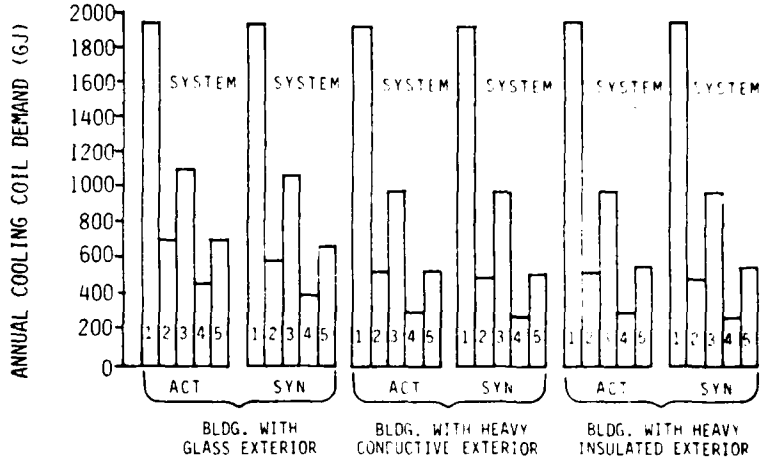

Figure 5-16. Annual cooling coil demand, Madison, WI.

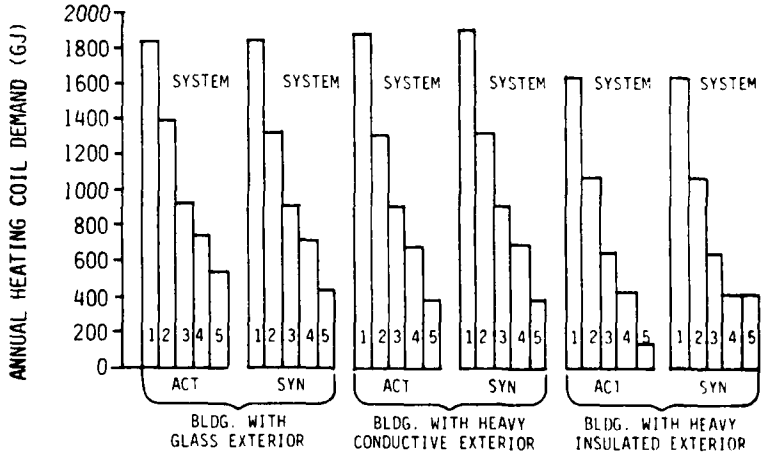

Figure 5-17. Annual heating coil demand, Madison, WI.

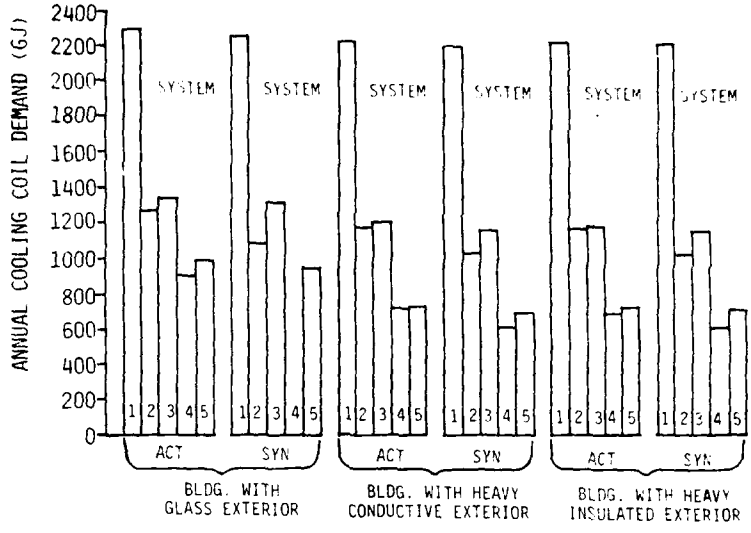

Figure 5-18. Annual cooling coil demand, Fort Worth, TX.

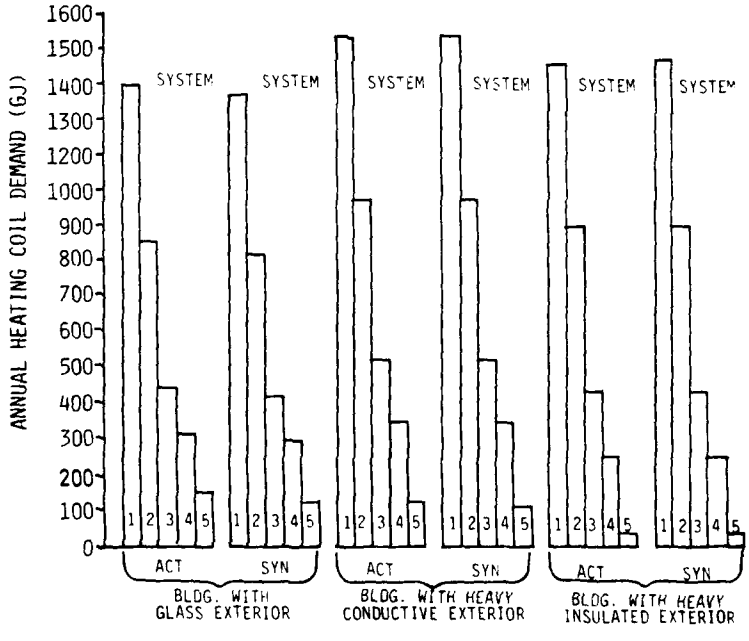

Figure 5-19. Annual heating coil demand, Santa Maria, CA.

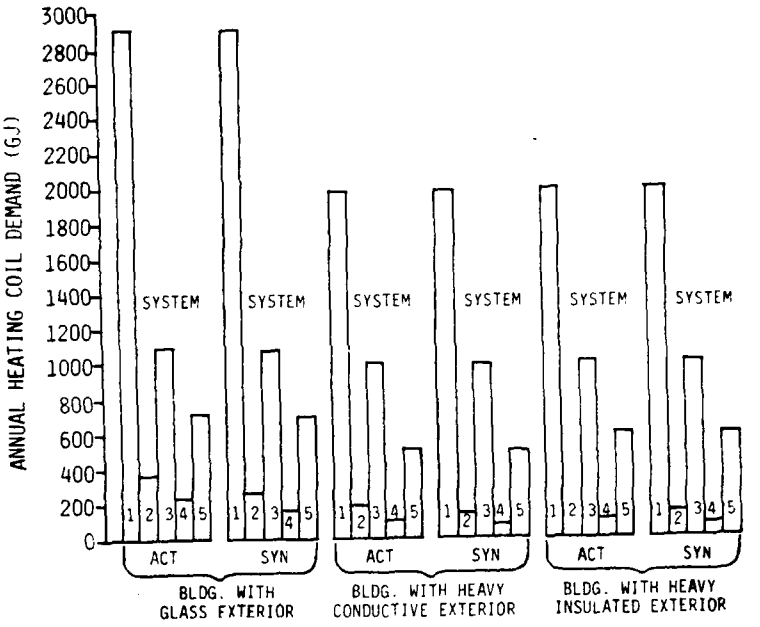

Figure 5-20. Annual cooling coil demand, Santa Maria, CA.

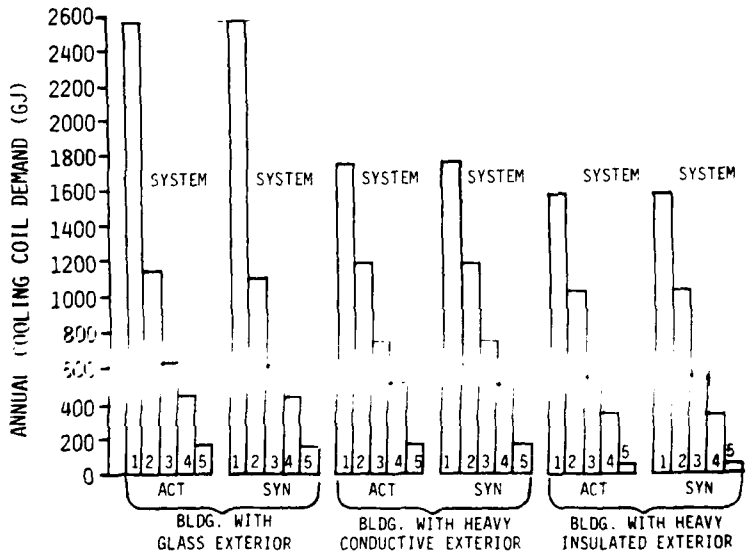

Figure 5-21. Annual heating coil demand, Santa Maria, CA.

cooling loads. Thus, using either synthesized weather data or actual weather data, building designers would make the same decision in terms of the design of the building fan system.

Finally, we examine the performance of the boiler/chiller plant. In the context of this simulation, this central plant is the final consumer of fuel and electric power and is the point where we can determine the cost/benefit of various building and energy system design options. Tables 5-2 through 5-5 present overwhelming evidence that for all the cases studied, use of either actual or synthesized data produces the same rank order result. After the synergistic effects of climate on the building loads, fan system performance, and central plant performance have all had an opportunity to affect the results, the absolute value for energy consumption obtained using either actual or synthesized data are nearly identical. Of the 120 comparisons reported under the "% of Actual" heading in Tables 5-2 through 5-5 (two comparisons per plant per building option per site), 97 percent of the synthesized weather data results are within 5 percent of the actual weather data results. Eighty-seven percent of the results agree to within 3 percent. Notice also that the greatest percentage disagreement is for consumption of heating fuel at sites like Fort Worth and Charleston, where very little fuel is required when efficient fan systems are used. In these instances, a relatively small error in absolute value is a relatively large fractional error.

Table 5-2

Estimated Total Annual Building Energy Consumption, Charleston, SC

Building With Glass Exterior

Plant No.	Total Electric Actual	Total Electric Synthesized	Total Electric % of Actual	Fuel Actual	Fuel Synthesized	Fuel % of Actual
1	1311	1311	100.0	1901	1903	100.1
2	1070	1047	97.8	1284	1277	99.5
3	1067	1067	100.0	700	690	98.6
4	956	940	98.3	495	487	98.4
5	939	937	99.8	211	203	96.2

Building With Heavy Conductive Exterior

Plant No.	Total Electric Actual	Total Electric Synthesized	Total Electric % of Actual	Fuel Actual	Fuel Synthesized	Fuel % of Actual
1	1304	1305	100.0	2117	2136	100.9
2	1062	1040	97.9	1471	1478	100.4
3	1041	1042	100.0	910	857	94.1
4	919	905	98.5	586	594	101.3
5	895	894	99.9	196	193	98.5

Building With Heavy Insulated Exterior

Plant No.	Total Electric Actual	Total Electric Synthesized	Total Electric % of Actual	Fuel Actual	Fuel Synthesized	Fuel % of Actual
1	1305	1307	100.1	1990	2005	100.7
2	1062	1040	97.9	1342	1347	100.4
3	1042	1042	100.0	721	727	100.8
4	918	904	98.5	464	467	100.5
5	899	899	100.0	78	77	98.3

Note:
Plant 1 is serving the conventional reheat fan system.
Plant 2 is serving the reheat fan system with cold-deck reset and enthalpy economy cycle.
Plant 3 is serving the conventional variable air volume system.
Plant 4 is serving the variable air volume system with cold-deck reset and enthalpy economy cycle.
Plant 5 is serving the conventional four-pipe, fan-coil system.

Table 5-3

Estimated Total Annual Building Energy Consumption
Madison, WI

Building With Glass Exterior

Plant No.	Total Electric Actual	Total Electric Synthesized	% of Actual	Fuel Actual	Fuel Synthesized	% of Actual
1	1269	1266	99.8	2560	2578	100.7
2	956	940	98.3	1991	1909	95.9
3	1044	1032	98.9	1350	1335	98.8
4	869	855	98.3	1089	1060	97.3
5	917	911	99.4	704	676	96.1

Building With Heavy Conductive Exterior

Plant No.	Total Electric Actual	Total Electric Synthesized	% of Actual	Fuel Actual	Fuel Synthesized	% of Actual
1	1266	1264	99.8	2655	2684	101.1
2	932	924	99.1	1888	1913	101.3
3	1016	1014	99.8	1340	1357	101.2
4	838	829	99.0	1018	1032	101.3
5	885	882	99.6	586	586	100.0

Building With Heavy Insulated Exterior

Plant No.	Total Electric Actual	Total Electric Synthesized	% of Actual	Fuel Actual	Fuel Synthesized	% of Actual
1	1271	1268	99.8	2340	2350	100.4
2	931	924	99.3	1542	1548	100.4
3	1018	1016	99.8	979	984	100.5
4	837	830	99.1	686	689	100.4
5	889	887	99.7	256	253	98.7

Table 5-4

Estimated Total Annual Building Energy Consumption
Fort Worth, TX

Building With Glass Exterior

Plant No.	Total Electric Actual	Total Electric Synthesized	Total Electric % of Actual	Fuel Actual	Fuel Synthesized	Fuel % of Actual
1	1316	1313	99.8	1856	1826	98.4
2	1086	1053	97.0	1267	1217	96.1
3	1079	1078	99.9	658	632	96.1
4	975	956	98.1	478	455	95.1
5	959	958	99.8	235	204	86.8

Building With Heavy Conductive Exterior

Plant No.	Total Electric Actual	Total Electric Synthesized	Total Electric % of Actual	Fuel Actual	Fuel Synthesized	Fuel % of Actual
1	1302	1304	100.1	2037	2060	101.1
2	1069	1041	97.4	1411	1413	100.1
3	1046	1046	100.0	784	789	100.7
4	933	914	98.0	542	541	99.8
5	909	906	99.7	212	194	91.4

Building With Heavy Insulated Exterior

Plant No.	Total Electric Actual	Total Electric Synthesized	Total Electric % of Actual	Fuel Actual	Fuel Synthesized	Fuel % of Actual
1	1303	1305	100.1	1935	1953	100.9
2	1068	1041	97.5	1300	1306	100.5
3	1044	1044	100.0	680	683	100.5
4	927	909	98.1	429	428	99.7
5	907	908	100.1	87	76	87.3

Table 5-5

Estimated Total Annual Building Energy Consumption,
Santa Maria, CA

Building With Glass Exterior

Plant No.	Total Electric Actual	Total Electric Synthesized	Total Electric % of Actual	Fuel Actual	Fuel Synthesized	Fuel % of Actual
1	1540	1542	100.1	3503	3523	100.6
2	899	868	96.5	1625	1564	96.3
3	1049	1045	99.6	913	900	98.6
4	820	809	98.6	696	673	96.7
5	924	921	99.7	285	271	95.0

Building With Heavy Conductive Exterior

Plant No.	Total Electric Actual	Total Electric Synthesized	Total Electric % of Actual	Fuel Actual	Fuel Synthesized	Fuel % of Actual
1	1287	1287	100.0	2209	2217	100.3
2	861	855	99.3	1424	1427	100.2
3	1033	1032	99.9	841	844	100.3
4	792	788	99.5	557	559	100.4
5	898	897	99.4	102	98	96.4

Building With Heavy, Insulated Exterior

Plant No.	Total Electric Actual	Total Electric Synthesized	Total Electric % of Actual	Fuel Actual	Fuel Synthesized	Fuel % of Actual
1	1287	1287	100.0	2209	2217	100.3
2	861	855	99.3	1424	1427	100.2
3	1033	1032	99.9	841	844	100.3
4	792	788	99.5	557	559	100.4
5	898	897	99.9	102	98	96.4

Use of synthesized data typically produces somewhat smaller annual heating and cooling load estimates than the use of actual data; however, the use of synthesized data never affects the rank order of choices, has a minimal effect on the difference in energy consumption between choices, and, in the final analysis, has a very small effect on the absolute value of the energy use calculated using the BLAST energy analysis program. In fact, the use of synthesized data need not produce any larger differences when compared to actual data than the use of two different years of actual data. Figures 5-22 and 5-23 show the results for Madison, WI, for the case with heavy insulated walls using synthesized data from 1955 and 1960. In many cases, the difference in annual load estimates made with the synthesized data compared to those made with 1955 data are less than the differences between the 1960 and 1955 weather data.

We therefore conclude that the use of synthesized climate data composed of the mean, the annual sinusoidal cycle, the diurnal sinusoidal cycle, and the first harmonic of the diurnal cycle for each weather parameter provides completely adequate weather data for input to energy analysis tools. Note that we have not emphasized the absolute value of the error caused by using synthesized data because it is only in very specialized applications that precise absolute values are important (i.e., establishing conformance with building energy performance standards -- a legal requirement). Instead, we have focused on the utility of the results for comparing system

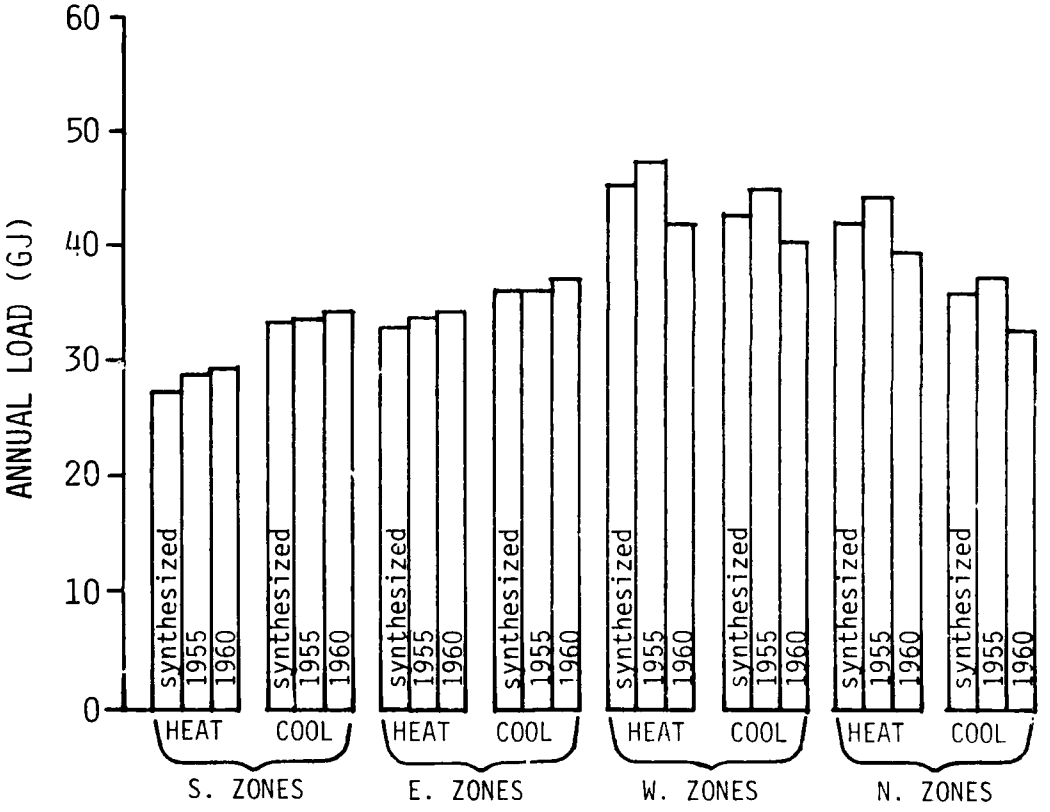

Figure 5-22. Loads calculated with synthesized weather data and with weather data from 1955 and 1960 for Madison, WI.

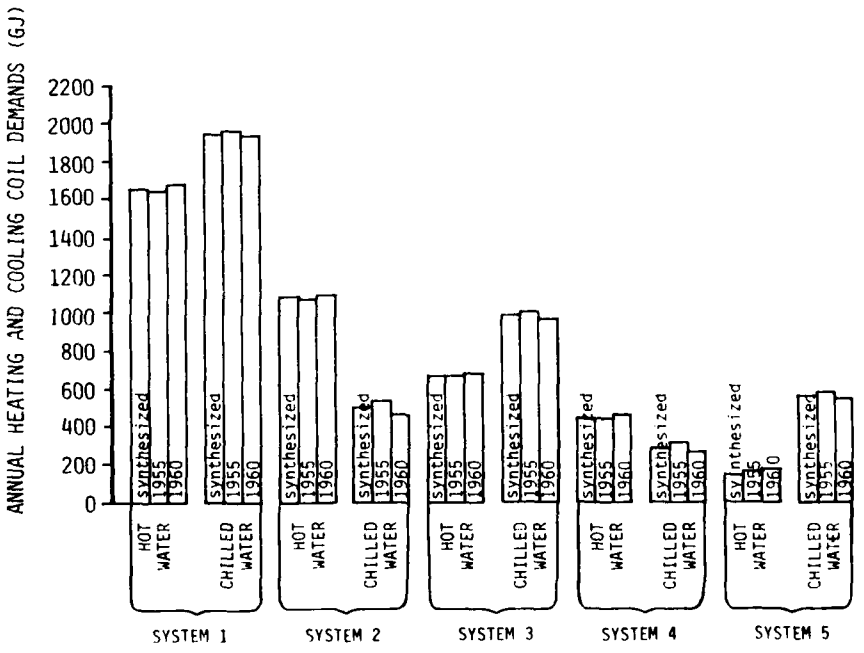

Figure 5-23. Annual heating and cooling coil demands calculated with synthesized weather data and with weather data from 1955 and 1960.

alternatives -- the principal utility of energy analysis calculations. Surprisingly, however, there are only small errors in absolute value, as illustrated by Tables 5-2 through 5-5 and by the extensive tabulations in Appendix A, which show the percentage errors associated with all the options illustrated in Figures 5-6 through 5-21. These errors are small, even though we have not included higher-order harmonics or side bands in the weather data model.

Having concluded that the use of a sinusoidal climate approximation is appropriate, we now describe the load-calculating scheme which takes full advantage of such an approximation.

6 CALCULATING HOURLY LOADS USING FREQUENCY RESPONSE

Introduction

We showed in Chapter 5 that sinusoidal weather data approximation produced results which agreed very closely with those of actual data. We now show that the results obtained when the frequency response approach to calculating heat conduction through multilayered slabs is used agree with those obtained when using response factors and hourly room heat balance techniques.

The BLAST program was used to calculate the hourly loads for several typical rooms for selected days. These results were compared, hour by hour, with results calculated using a sinusoidal sol-air temperature as the outside surface temperature, and using the frequency response conduction model described in Chapter 3. Only heat transfer through opaque surfaces was considered, since in the proposed method, solar heat gain, and internal heat gain were to be accounted for using existing weighting factor techniques.

Procedure

The BLAST computer program calculates room heating and cooling loads by performing a detailed heat balance on both the inside and outside of each room surface and on the room air volume. For a room

at fixed-air temperature, the heating or cooling load is the amount of heat which must be added or removed from the room air to offset convective heat losses or gains. While convection is the only mechanism by which heat can be transferred to the room air, radiation and conduction must also be considered when performing the heat balance on each surface. Radiation and conduction affect the equilibrium temperature of each surface and thereby affect the amount of energy transferred by convection into the room air.

In the proposed simplified model, heat flux through opaque walls and roofs is calculated using an approach which combines the effects of radiation, conduction, and convection. For each exterior wall or roof, we assume that heat transfer takes place between an outside sol-air temperature and a fixed inside room temperature. The sol-air temperature is the equilibrium temperature of a perfectly insulated surface of specified orientation and absorptivity and is due to the combined effects of incident solar radiation, radiation to or from the surroundings, and convection to or from the ambient air. By using the sol-air temperature as one boundary condition, we can use a combined radiative-convective outside surface heat transfer coefficient to account for the heat transfer by both mechanisms. Similarly, we use the room air temperature and a combined inside surface heat transfer coefficient to account for radiation and convection occurring on the inside surface. We first calculate the thermal resistances corresponding to these inside and outside heat transfer

coefficients; these are used with the thermal resistance and capacitance of each layer in the wall or roof to calculate the frequency-dependent transmittance of the wall, as described in Chapter 3. Using the notation of Chapter 3, the real part of the frequency-dependent transmittance at frequency ω is $U_{\omega S}$ and the imaginary part is $U_{\omega C}$.

We now show by simple example how the flux is calculated. Suppose the sol-air temperature for a given wall or roof contains a mean, an annual sinusoidal cycle, a diurnal cycle, and the first harmonic of the diurnal cycle (as suggested in Chapter 4). The sol-air temperature at time t is (use Equation 4-1 for comparison):

$$T_{SOL\text{-}AIR}(t) = a_o + 2a_1 \cos(\omega_1 t) + 2b_1 \sin(\omega_1 t) + 2a_{365} \cos(\omega_{365} t) + 2b_{365} \sin(\omega_{365} t) + 2a_{730} \cos(\omega_{730} t) + 2b_{730} \sin(\omega_{730} t) \qquad \text{[Eq 6-1]}$$

where:

a_o is the mean annual sol-air temperature

a_1 and b_1 are the Fourier coefficients corresponding to annual sol-air temperature variation

a_{365} and b_{365} are the Fourier coefficients corresponding to the diurnal sol-air temperature variation

a_{730} and b_{730} are the Fourier coefficients corresponding to the first harmonic of the diurnal sol-air temperature variation

ω_1, ω_{365}, and ω_{730} are the frequencies corresponding to the annual cycle, the diurnal cycle, and the first harmonic of the diurnal cycle, respectively.

Since even the heaviest multilayered walls or roofs respond in steady state to the annual cycle, we can lump the annual mean and the annual cycle variation into a local mean sol-air temperature, $T_m(t)$, which is:

$$T_m(t) = a_0 + 2a_1 \cos(\omega_1 t) + 2b_1 \sin(\omega_1 t) \qquad \text{[Eq 6-2]}$$

The flux through the wall is:

$$\begin{aligned} q(t) = {} & U_{ss}(T_m(t) - T_R) + (U_{365c}\ 2b_{365} + U_{365s}\ 2a_{365})\cos(\omega_{365}t) \\ & + (U_{365s}\ 2b_{365} - U_{365c}\ 2a_{365})\sin(\omega_{365}t) \\ & + (U_{730c}\ 2b_{730} + U_{730s}\ 2d_{730})\cos(\omega_{730}t) \\ & + (U_{730s}\ 2b_{730} - U_{730c}\ 2a_{730})\sin(\omega_{730}t) \end{aligned} \qquad \text{[Eq 6-3]}$$

where:

U_{365s} and U_{365c} are the real and imaginary parts, respectively, of the transmittance of the wall at the diurnal frequency

U_{730s} and U_{730c} are the real and imaginary parts, respectively, of the transmittance of the wall at the first harmonic of the diurnal frequency

U_{ss} is the steady-state transmittance (U-value) of the wall.

Other variables are as defined for Equation 6-2.

The total flux through the wall is:

$$Q(t) = A\ q(t) \qquad \text{[Eq 6-4]}$$

where A is the area of the wall.

We can determine the total flux, $Q_T(t)$, due to heat flow through all opaque walls and roofs by applying Equations 6-3 and 6-4 to each wall or roof and summing the results. Note that the steady-state transmittance and the components of transmittance at each frequency are different for each different wall or roof construction and that the Fourier coefficients for sol-air temperature are different for each different surface orientation and absorptivity.

To determine the room heating or cooling load due to heat flow through the opaque walls and roofs, we must recognize that radiant heat gain, which is accounted for in the combined inside surface heat-transfer coefficient, is really a delayed room load, since it must be absorbed by other room surfaces before it can be convected into the room air. We use the weighting factor approach detailed in the ASHRAE Handbook of Fundamentals (ref 21) to account for this

delay. Using this procedure, the room load at time t caused by heat flow through opaque walls and roofs (or by conduction but not by transmission through non-opaque surfaces) is:

$$L(t) = V_0\, Q_T(t) + V_1\, Q_T(t-\Delta t) - W_0\, L(t-\Delta t) \qquad \text{[Eq 6-5]}$$

where:

$L(t)$ is the room load due to heat flow through opaque surfaces at time t

$L(t-\Delta t)$ is the room load due to heat flow through opaque surfaces at time $t-\Delta t$ (the previous hour if Δt is 1 hour)

$Q_T(t)$ is the total heat flux through opaque surfaces at time t

$Q_T(t-\Delta t)$ is the total flux through opaque surfaces at time $t-\Delta t$

V_0, V_1, and W_0 are constants which depend on room geometry and construction. Note that $V_1 = 1 + W_0 - V_0$.

To determine if any substantial error results from using Equations 6-3 through 6-5 instead of the detailed heat balance embodied in BLAST, BLAST was executed using weather data which yielded sol-air temperatures containing only a mean, a diurnal component, and the first harmonic of the diurnal. The room loads calculated in this way were compared to results obtained by using Equations 6-3 through 6-5. In all cases, the rooms for which loads were calculated were at fixed inside temperature and had no internal or solar transmission energy inputs. The same room geometry and wall types described for the

exterior zones in Chapter 5 were studied, except that no windows were included and a single wood sheet was used in lieu of the all-glass exterior as representative of a light, conductive exterior wall.

Results

Two days were simulated: one was a cold sunny day with sol-air temperatures on a south vertical exposure (absorptivity of .6) ranging from -14.5°C to 15.5°C; the other was a hot sunny day with south vertical sol-air temperatures ranging from 24°C to 44.7°C. Table 6-1 provides the Fourier coefficients for sol-air temperature for these days. These sol-air temperature coefficients were used along with the transmittances shown in Table 6-2 to calculate the heat flow through the exterior wall and roof of the typical exterior zone described in Chapter 5. Results were compared to BLAST calculations made with appropriate sinusoidally varying hourly sol-air temperature for each of the 2 days studied.

Figures 6-1 through 6-7 compare the results. For cold sunny days, the fluxes and loads represent outward heat flow and heating loads. For hot sunny days, the fluxes are heat gains and the loads are cooling loads. In each figure, the curve labeled "Total Flux" is the flux calculated using Equations 6-3 and 6-4. The curve labeled "Load, Simplified Model" results from the use of Equation 6-5. The

Table 6-1

Fourier Coefficients for Sol-Air Temperature,
South Wall, Absorptivity = .6

	Mean	a_{365}	b_{365}	a_{730}	b_{730}
Cold Sunny Day	1.3875	-5.7417	-4.4375	1.0787	.8237
Hot Sunny Day	33.0417	-3.9583	-3.0592	.7433	.5650

Table 6-2

Frequency-Dependent Transmittance for Exterior Walls
and Roof

Section	Steady-State U-Value ($w/m^2{}^0k$)	Diurnal		1st Harmonic Diurnal	
		Real	Imaginary	Real	Imaginary
Heavy Conductive Wall	2.9201	.2065	-1.5233	-.4168	-.6898
Heavy Insulated Wall	.4049	.0110	-.1551	-.0339	-.0715
Wood Sheet Wall	2.4646	2.4420	-.2684	2.3760	-.5264
Roof	.4674	.3455	-.2594	.1273	-.3330

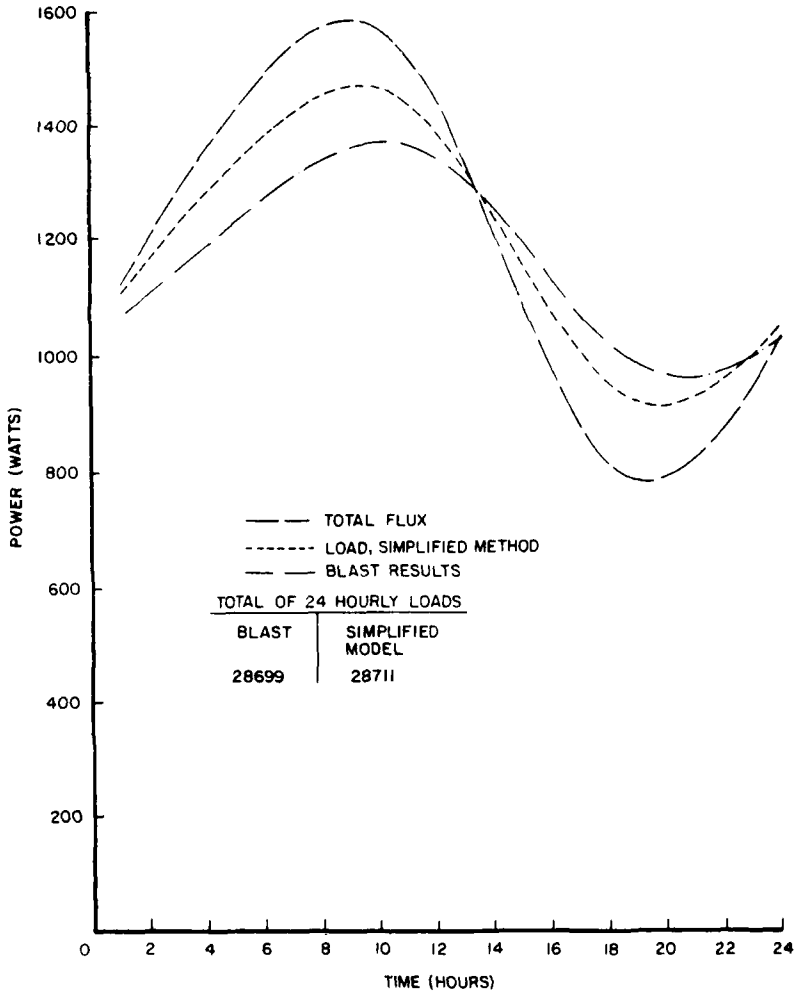

Figure 6-1. Flux and loads for cold sunny day and a heavy conductive exterior wall using precalculated weighting factors.

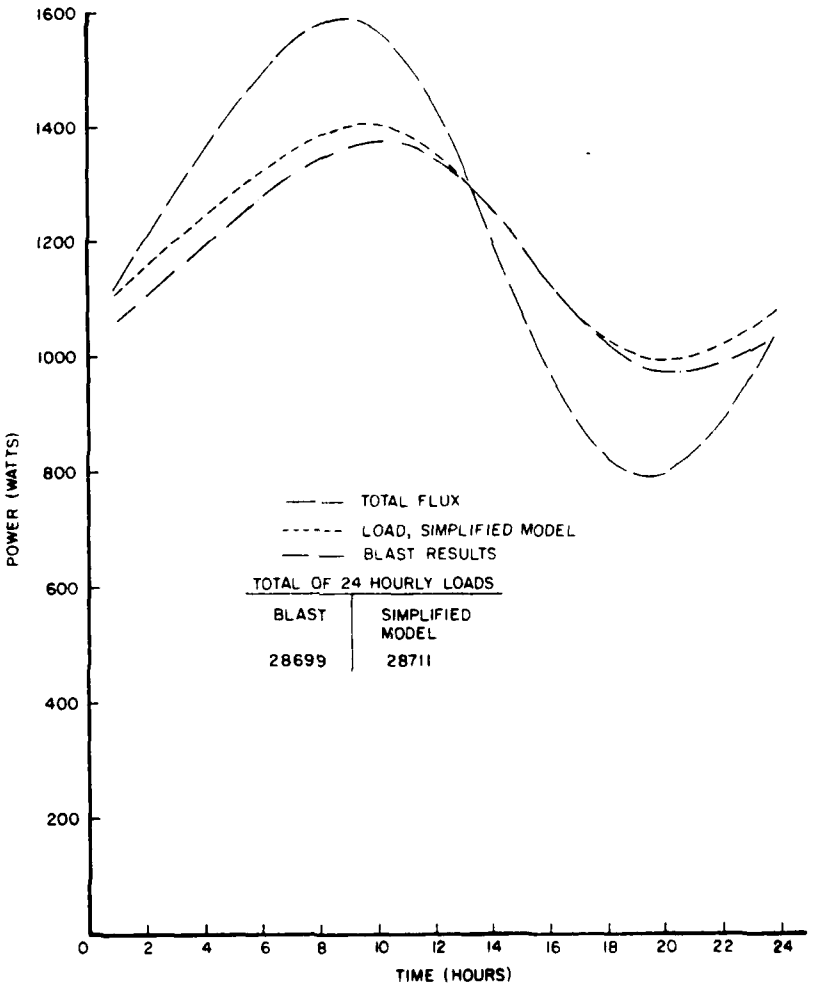

Figure 6-2. Flux and loads for cold sunny day and a heavy conductive exterior wall.

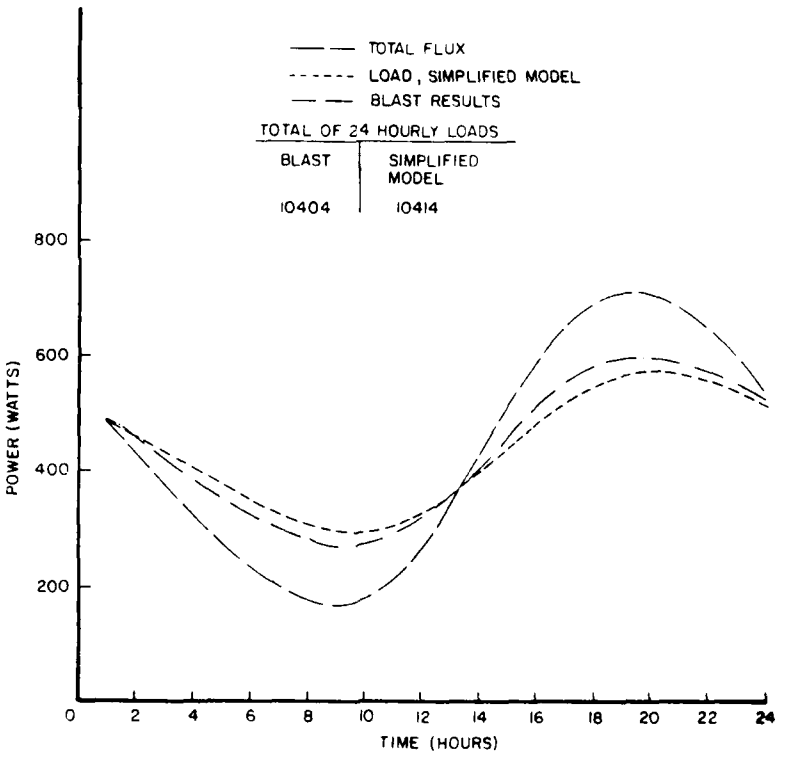

Figure 6-3. Flux and loads for hot sunny day and a heavy conductive exterior wall.

AD-A097 597 CONSTRUCTION ENGINEERING RESEARCH LAB (ARMY) CHAMPAIGN IL F/G 13/1
CALCULATING BUILDING HEATING AND COOLING LOADS USING THE FREQUE--ETC(
FEB 81 D C HITTLE
UNCLASSIFIED CERL-TM-E-169 NL

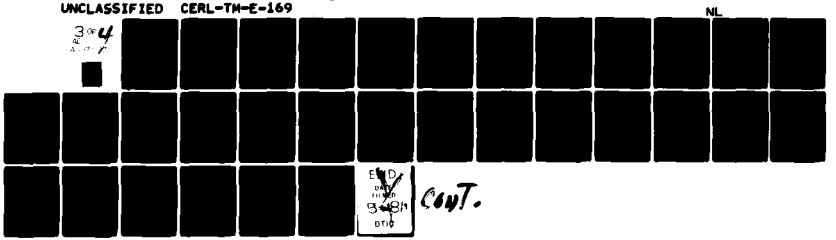

Cont.

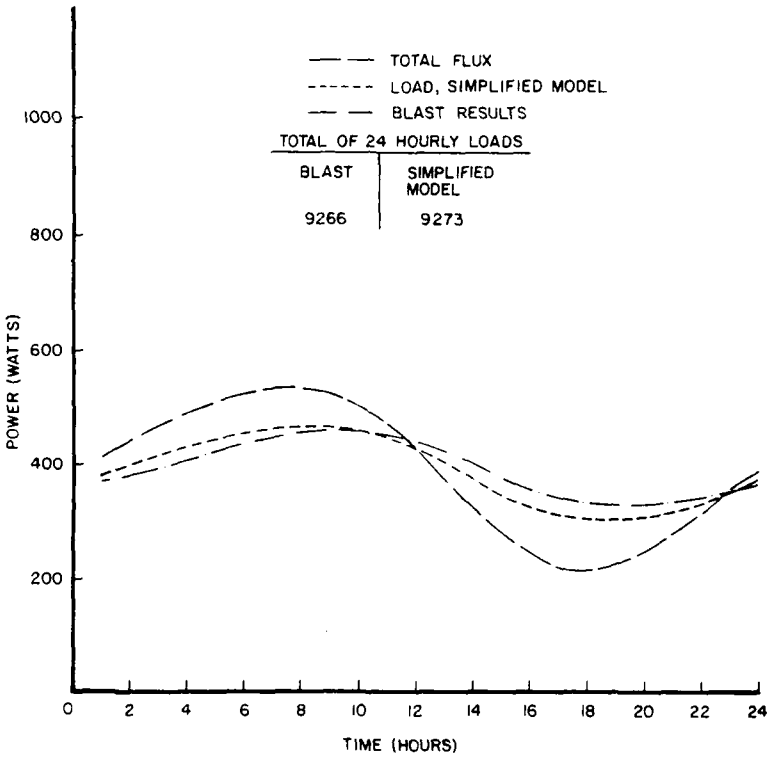

Figure 6-4. Flux and loads for cold sunny day and heavy insulated exterior.

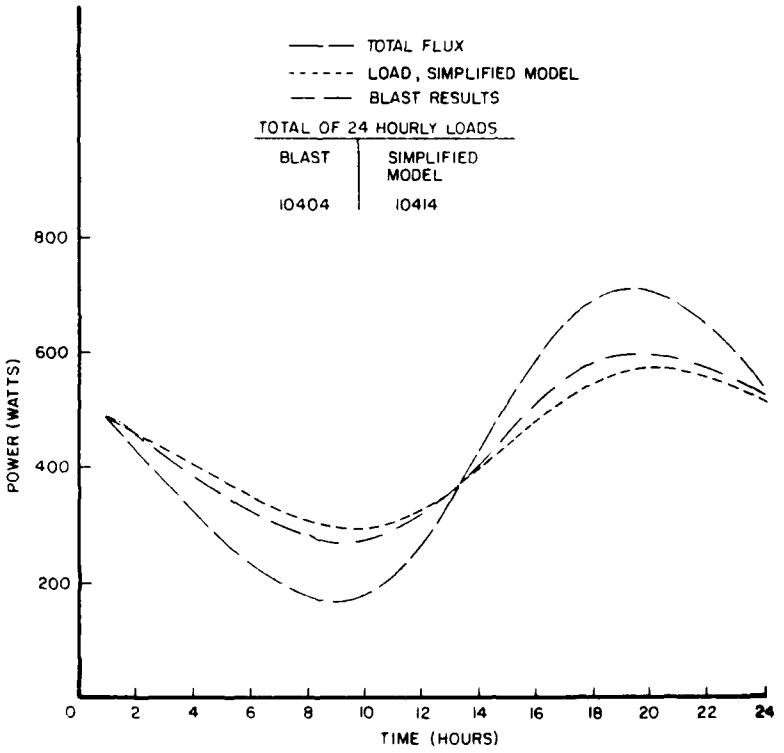

Figure 6-3. Flux and loads for hot sunny day and a heavy conductive exterior wall.

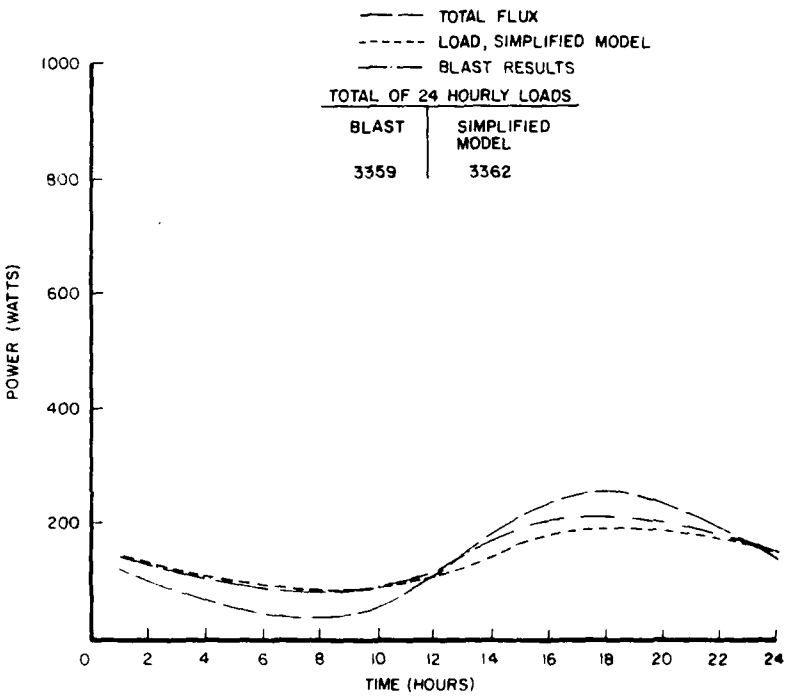

Figure 6-5. Flux and loads for hot sunny day and heavy insulated exterior walls.

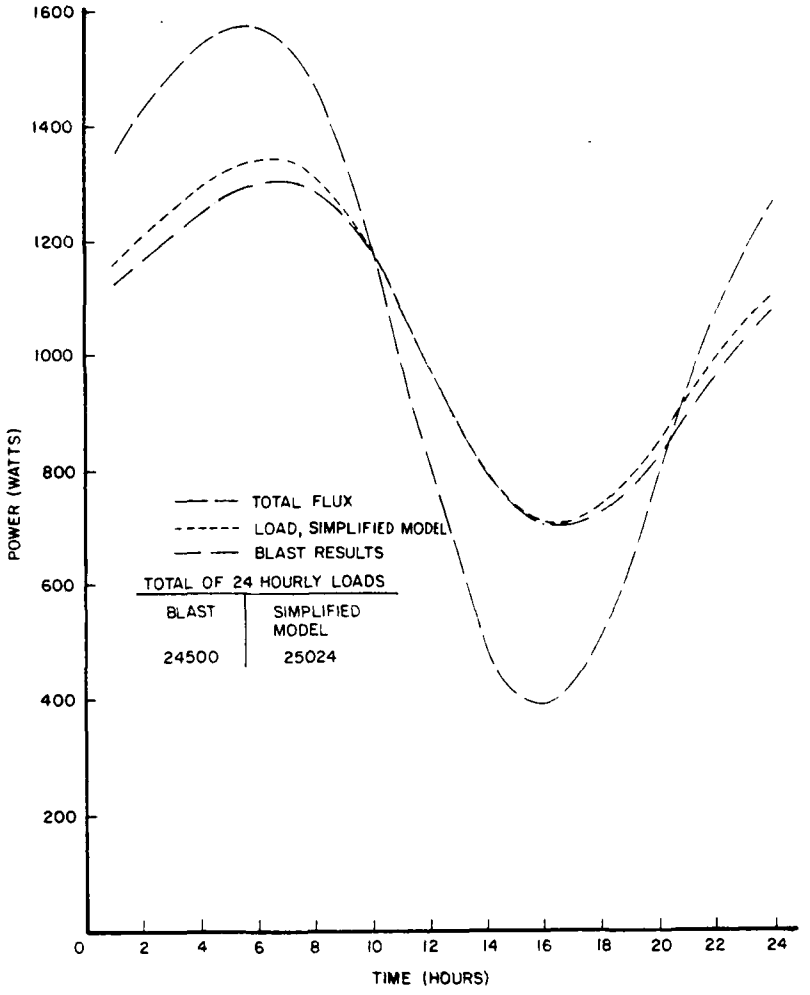

Figure 6-6. Flux and heating loads for a cold sunny day and a wood exterior wall.

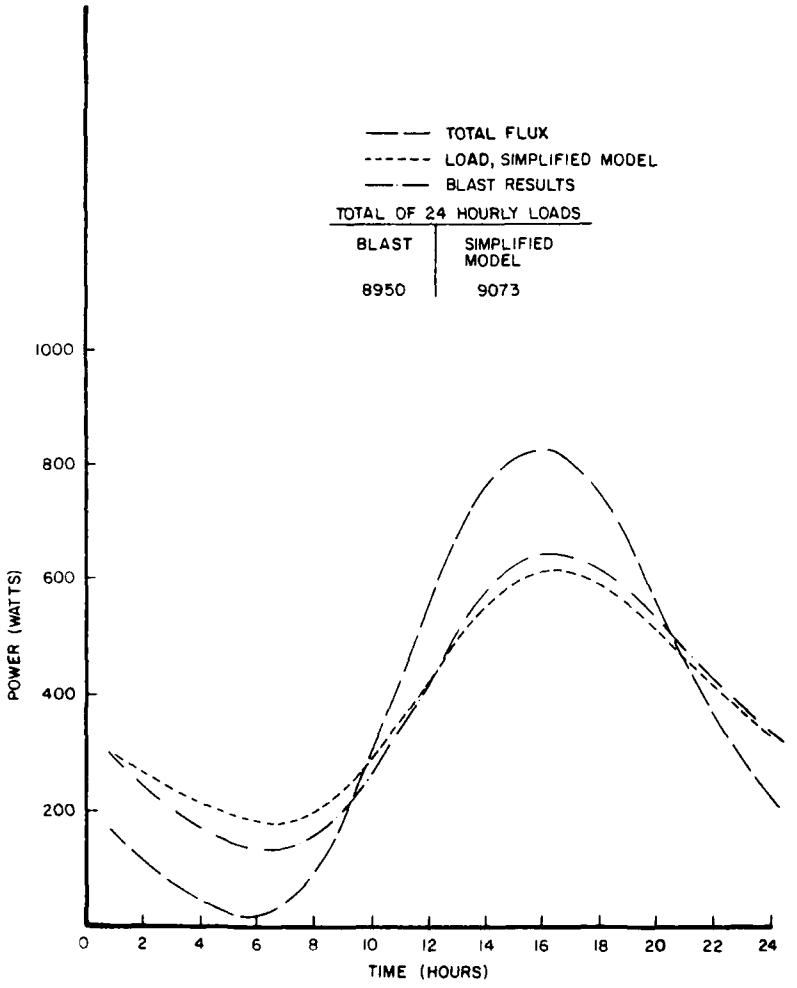

Figure 6-7. Flux and loads for hot sunny day and a wood exterior wall.

"BLAST Results" are the heating or cooling loads calculated by the BLAST energy analysis program.

Figure 6-1 shows the results for a cold sunny day for a room with a heavy conductive wall. While the total of the hourly loads calculated using the simplified model is nearly the same as the BLAST total, the peak load is higher and the minimum load is lower. This discrepancy, which ' not overly severe, was determined to have resulted from the use of pretabulated weighting factors found in the ASHRAE Handbook of Fundamentals. However, these factors do not necessarily apply to the room being studied (ref 22). Adjustment of these weighting factors substantially improved the results, as shown in Figure 6-2. Note that use of the proposed method could not be justified if the weighting factors were adjusted for each different day type analyzed; however, this was not necessary, as shown in Figure 6-3. This curve is for the same zone as Figure 6-2 (heavy conductive exterior wall), but is for a hot day. The same weighting factors were used to calculate loads for both the hot and cold days.

The good agreement between BLAST and the simplified method calculations shows that if we use the correct weighting factors, the proposed method introduces almost no error. Figures 6-4 and 6-5 confirm this result for a heavy insulated exterior wall; Figures 6-6 and 6-7 show similar excellent agreement when the exterior wall is a single sheet of wood.

Notice that we have tabulated the sum of the hourly loads on each figure for both the simplified model and for the BLAST calculation. These results are remarkably close. In the worst case, they differ by only 2 percent.

Conclusions

The preceding analysis shows that application of frequency response techniques produces very good hourly agreement with the response factor and heat balance methods. Recalling from Chapter 5 that the annual agreement between synthesized and actual weather data was also good, we may conclude that the application of frequency response techniques to calculating heating and cooling loads is reasonably precise and uncomplicated, and therefore of great utility for energy analysis programs.

7 CONCLUSIONS AND APPLICATIONS

Conclusions

We now summarize the important conclusions which can be drawn from the preceding six chapters.

1. In Chapter 2, we showed that calculating response factors and conduction transfer functions is tedious and computationally difficult. Their use also requires a substantial amount of record keeping of past temperatures and fluxes in order to calculate heat conduction with precision.

2. As shown in Chapter 3, calculating the frequency response of a multi-layered slab (i.e., calculating heat flow at a boundary of fixed temperature caused by the sinusoidal variation in temperature on the opposite boundary) is much less complicated than calculating response factors and conduction transfer functions. This is particularly true if calculation of the frequency response is required only at a few selected frequencies. Attempts to simplify the calculation of frequency response by using equivalent, single-layer slab models do not appear to be worth the error and risk associated with such simplifications.

3. The use of deterministic plus stochastic modeling techniques, as discussed in Chapter 4, allowed separation of the

deterministic periodic behavior from the stochastic behavior in weather data. Important periodicity exists in the weather data studied only at the annual cycle, the diurnal cycle, and harmonics of the diurnal cycle. These are the only frequencies at which the frequency response for multi-layered slabs need to be calculated.

4. The use of deterministic only (sinusoidal) models for weather data accounts for a large fraction of the variance in the data, but the use of deterministic plus stochastic models accounts for an even larger fraction. Even though we have chosen to ignore the stochastic autoregressive behavior in the proposed simplified model for heating and cooling load calculations, autoregressive behavior is definitely a characteristic of weather data, and it is appropriate to include autoregressive terms in weather data models used for other purposes.

5. We demonstrated in Chapter 5 that the use of synthesized weather data consisting only of the mean, the annual cycle, the diurnal cycle, and the first harmonic of the diurnal cycle as input to the BLAST energy analysis program produces results which are very nearly the same as results produced by using actual weather data for a wide range of cases. We have demonstrated that the differences in calculated results using actual weather data for different years for a particular site are of approximately the same order of magnitude as those resulting from the use of only sinusoidal weather data

components in comparison to actual weather data. We may conclude that ignoring the stochastic component and higher harmonics and side bands in the weather data produces very small errors in calculated building loads and energy consumption.

6. The use of frequency response techniques to calculate conduction through multilayered slabs, combined with the use of weighting factors, produces reasonably accurate results, hour by hour, when compared to the more detailed discrete response factor/heat balance methods for calculating room loads (see Chapter 6).

7. Using the results of Chapters 5 and 6, we may conclude that the use of frequency response techniques instead of the more detailed response factor and heat balance methods for calculating air-conditioning loads produces results which closely agree with the more detailed methods. The procedures are so much simpler that they should be used in lieu of the more detailed techniques.

Applications

The utility of the research described in the preceding chapters is that it establishes the technical adequacy of a load calculation procedure which is simple enough to be implemented on a microcomputer. This method can be combined with existing steady-state fan system and boiler/chiller plant simulation methods (which are already

relatively simple) to produce a microprocessor-oriented energy analysis program.

One approach to such a program is shown schematically in Figure 7-1. The three calculation modules shown could be executed sequentially and overwritten in the microprocessor's memory with the next module as execution progresses. The approach shown also does not require storage of intermediate results which will minimize storage requirements and I/O operations.

Two sets of data must be generated separately in order to implement a microcomputer-based energy analysis program. First, the coefficients for the needed weather data variables must be generated using the methods described in Chapter 4. Second, a much larger set of room weighting factors than are shown in the ASHRAE Handbook of Fundamentals (ref 21) should be tabulated. Detailed energy analysis procedures found in the BLAST program should be used to calculate room weighting factors for a wider variety of room geometries, mass, and glass and exterior wall areas.

The implementation of building energy analysis procedures on microcomputers should greatly increase the number of engineers who will apply these procedures to improve the energy efficiency of the buildings and energy systems they design.

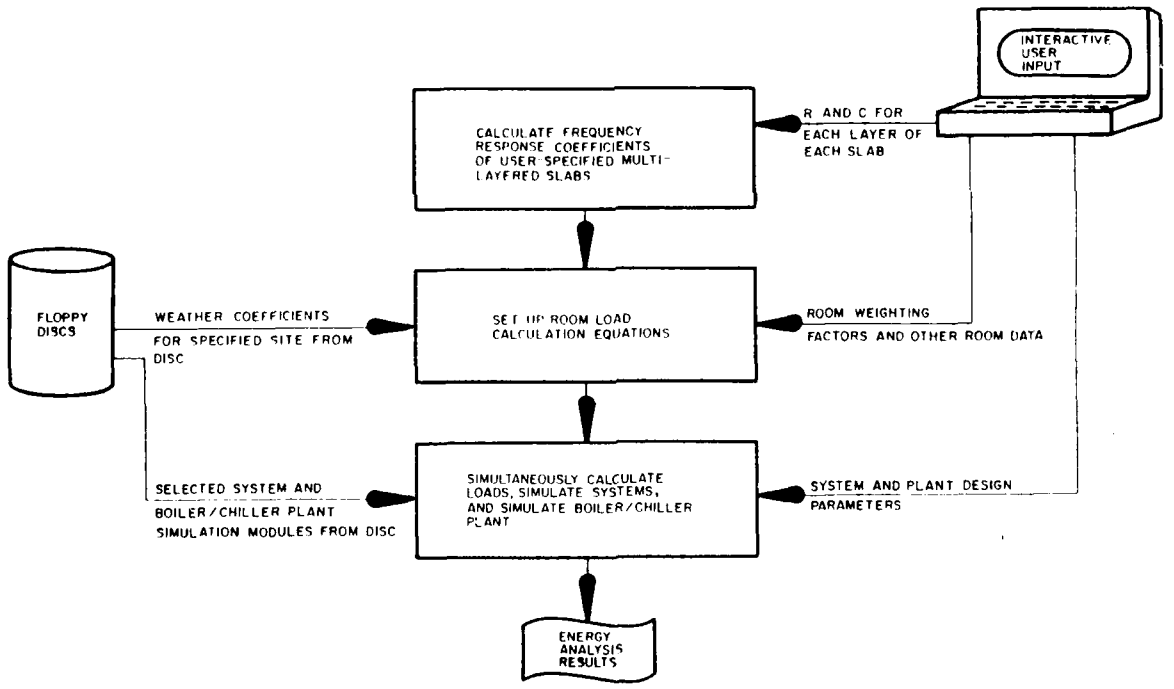

Figure 7-1. Schematic of microprocessor-based energy analysis software.

REFERENCES

1. Gupta, C. L., J. W. Spencer, R. W. R. Muncey: A Conceptual Survey of Computer-Oriented Thermal Calculation Methods, National Bureau of Standards Building Science Series No. 39, Washington, D.C., 1971.

2. Hittle, D. C.: A Comparison of Energy Use Calculated With Actual and Synthesized Weather Data, ASHRAE Trans., 85, part 2, 1979.

3. Mackey, C. O., L. T. Wright: Periodic Heat Flow - Homogeneous Walls and Roof, ASHVE Trans., 50, 1944.

4. Mackey, C. O., L. T. Wright: Periodic Heat Flow - Composite Walls and Roof, ASHVE Trans., 52, 1946.

5. Mackey, C. O., L. T. Wright: The Sol-Air Thermometer - A New Instrument, ASHVE Trans., 52, 1946.

6. Van Gorcum, A.: Theoretical Considerations in the Conduction of Fluctuating Heat Flow, App. Sci. Res., A2, 1951.

7. Muncey, R. W., J. W. Spencer: Calculation of Non-steady Heat Flow: Considerations of Radiation Within the Room, JIHVE, 34, 1966.

8. Muncey, R. W., J. W. Spencer: Calculation of Temperatures in Buildings by the Matrix Method: Some Particular Cases, Bldg. Sci., 3, 1969.

9. Pipes, L. A.: Matrix Analysis of Heat Transfer Problems, J. Franklin Inst., 264, 1957.

10. Gupta, C. L.: A Systems Model for Environmental Design of Buildings, National Bureau of Standards Building Science Series No. 39, Washington, D.C., 1971.

11. Sonderegger, R. C.: Dynamic Models of House Heating Based on Equivalent Thermal Parameters, Doctoral Dissertation, Princeton Univ., NJ, 1977.

12. Nessi, A., L. Nissole: Fonctions d' Influence de Flux de Chaleur des Parois de Construction, Rapport. Comite Tech. Indus. Chauffayes, Paris, 1967.

13. Brisken, W. R., S. G. Reque: Heat Load Calculations by Thermal Response, ASHRAE Trans., 62, 1956.

14. Stephenson, D. G., G. P. Mitalis: Cooling Load Calculations by Thermal Response Factors, ASHVE Trans., 73, 1967.

15. Mitalas, G. P., D. G. Stephenson: Room Thermal Response Factors, ASHRAE Trans., 73, 1967.

16. Mitalas, G. P.: Calculation of Transient Heat Flow Through Walls and Roofs, ASHRAE Trans., 74, 1968.

17. Kusuda, T.: Thermal Response Factors for Multi-Layer Structures of Various Heat Conduction Systems, ASHRAE Trans., 75, 1969.

18. Peavy, B. A.: A Note on Response Factors and Conduction Transfer Functions, ASHRAE Trans., 84, 1978.

19. Hittle, D. C.: Building Loads Analysis and System Thermodynamics (BLAST) Users Manual, Version 2.0, Volumes 1 and 2, Technical Report E-153, US Army Const. Eng. Res. Lab. (CERL), Champaign, IL, 1979.

20. Kusuda, T.: NBSLD, The Computer Program for Heating and Cooling Loads in Buildings, National Bureau of Standards Building Science Series No. 69-R, Washington, D.C., 1978.

21. Handbook of Fundamentals, ASHRAE, New York, NY, 1977.

22. Cumali, Z. O., A. O. Sezgen, R. Sullivan: Passive Solar Calculation Methods, report-contract number EM-78-C-01-5221, Dept. of Energy, Washington, D.C., 1979.

23. Churchill, R. V., J. W. Brown, R. F. Verhey: Complex Variables and Applications, McGraw-Hill, 1974.

24. Mitalis, G. P.: Comments on the Z-Transfer Function Method for Calculating Heat Transfer in Buildings, ASHRAE Trans., 84, 1978.

25. Walton, G. N.: Personal communications, U.S. Army Const. Eng. Res. Lab. (CERL), Champaign, IL.

26. Box, G. E. P., G. M. J. Jenkins: Time Series Analysis for Forecasting and Control, Holden-Day, 1976.

27. Jenkins, G. M. J., D. G. Watts: Spectral Analysis and Its Applications, Holden-Day, 1968.

28. Kapoor, S.: unpublished class notes, University of Illinois, Department of Mechanical and Industrial Engineering, Urbana, IL.

29. Pandit, S. M.: Data Dependent Systems: Modeling Analysis and Optimal Control via Time Series Analysis, Ph.D. Thesis, University of Wisconsin, Madison, WI.

30. Kuo, B. C.: Digital Control Systems, SRL Publishing Co., Champaign, IL, 1977.

31. Franklin, G. F., J. D. Powell: Digital Control of Dynamic Systems, Addeson-Wesley Publishing Co., 1980.

32. Kline, W. A.: A Control System Interpretation of Autoregressive Moving Average Time Series Models, article in preparation.

33. Kline, W. A.: An Evaluation of Dynamic Data System Modeling for the Characterization and Forecasting of Time Series, M.S. Thesis, University of Illinois, Urbana, IL, 1979.

APPENDIX A

COMPARISON OF ENERGY USE PREDICTED USING ACTUAL AND SYNTHESIZED WEATHER DATA

Table A-1

Comparison of Energy Use Predicted Using Actual and Synthesized Weather Data for Charleston, SC, and for a Building With Glass Exterior

Loads

	Heating			Cooling		
Zone No.	Actual	Synthesized	% of Actual	Actual	Synthesized	% of Actual
1	19.26	16.94	88.0	129.32	126.06	97.4
2	31.10	28.88	92.8	126.42	121.48	96.1
3	32.60	30.48	93.5	111.00	106.14	95.6
4	41.97	40.58	96.7	84.18	80.09	95.1
5	0.0	0.0	100.0	362.9	362.9	100.0
6	3.78	3.47	91.9	56.48	55.34	98.0

Fan Systems

	Hot Water			Chilled Water		
System No.	Actual	Synthesized	% of Actual	Actual	Synthesized	% of Actual
1	1327	1324	99.8	2262	2243	99.2
2	866	860	99.3	1185	1061	89.5
3	457	453	99.1	1292	1274	98.6
4	315	309	98.1	810	735	90.7
5	129	120	93.0	881	863	98.0

Boiler/Chiller Plant

	Fuel			Total Electric		
Plant No.	Actual	Synthesized	% of Actual	Actual	Synthesized	% of Actual
1	1901	1903	100.1	1311	1311	100.0
2	1284	1277	99.5	1070	1047	97.8
3	700	690	98.6	1067	1067	100
4	495	487	98.4	956	940	98.3
5	211	203	96.2	939	937	99.8

Table A-2

Comparison of Energy Use Predicted Using Actual and Synthesized Weather Data for Charleston, SC, and for a Building With Heavy Conductive Exterior Walls

Loads

	Heating			Cooling		
Zone No.	Actual	Synthesized	% of Actual	Actual	Synthesized	% of Actual
1	22.40	21.59	96.4	59.98	56.59	94.3
2	27.84	26.89	96.6	61.52	57.63	93.7
3	28.60	27.71	96.9	56.62	53.54	94.6
4	32.03	31.30	97.7	50.08	47.45	94.7
5	0.0	0.0	100.0	362.9	362.9	100.0
6	3.78	3.47	91.9	56.48	55.34	98.0

Fan Systems

	Hot Water			Chilled Water		
System No.	Actual	Synthesized	% of Actual	Actual	Synthesized	% of Actual
1	1489	1500	100.8	2223	2215	99.6
2	1017	1025	100.8	1144	1029	89.9
3	552	559	101.3	1165	1157	99.3
4	365	370	101.4	655	587	89.6
5	115	111	96.5	654	639	97.7

Boiler/Chiller Plants

	Fuel			Total Electric		
Plant No.	Actual	Synthesized	% of Actual	Actual	Synthesized	% of Actual
1	2117	2136	100.9	1304	1305	100.0
2	1471	1478	100.4	1062	1040	97.9
3	910	857	94.1	1041	1042	100.0
4	586	594	101.3	919	905	98.5
5	196	193	98.5	895	894	99.9

Table A-3

Comparison of Energy Use Calculated Using Actual and Synthesized Weather Data for Charleston, SC, and for a Building With Heavy, Insulated Exterior

Loads

	Heating			Cooling		
Zone No.	Actual	Synthesized	% of Actual	Actual	Synthesized	% of Actual
1	6.51	5.95	91.4	67.82	65.90	97.2
2	9.35	8.91	95.3	67.41	65.32	96.9
3	9.65	9.33	96.7	63.46	61.86	97.5
4	11.33	11.12	98.16	57.20	55.92	97.8
5	0.0	0.0	----	362.88	362.88	100.0
6	3.78	3.47	91.9	56.48	55.33	98.0

Fan Systems

	Hot Water			Chilled Water		
System No.	Actual	Synthesized	% of Actual	Actual	Synthesized	% of Actual
1	1396	1403	100.5	2231	2223	99.6
2	926	930	100.4	1143	1028	90.0
3	454	437	100.6	1167	1159	99.3
4	272	274	100.8	654	587	89.8
5	41	39	94.6	683	674	98.7

Boiler/Chiller Plant

	Fuel			Total Electric		
Plant No.	Actual	Synthesized	% of Actual	Actual	Synthesized	% of Actual
1	1990	2005	100.7	1305	1307	100.1
2	1342	1347	100.4	1062	1040	97.9
3	721	727	100.8	1042	1042	100.0
4	464	467	100.5	918	904	98.5
5	78	77	98.3	899	899	100.0

Table A-4

Comparison of Energy Use Predicted Using Actual and Synthesized Weather Data for Madison, WI, and for a Building With Glass Exterior

Loads

	Heating			Cooling		
Zone No.	Actual	Synthesized	% of Actual	Actual	Synthesized	% of Actual
1	92.73	81.13	87.5	98.62	86.70	87.9
2	117.81	113.68	96.5	86.83	75.36	86.8
3	116.99	112.79	96.4	85.13	74.4	87.4
4	132.00	132.36	100.3	53.05	47.99	90.5
5	0.0	0.0	----	353.4	353.08	99.9
6	16.98	16.83	99.1	39.62	38.60	97.4

Fan Systems

	Hot Water			Chilled Water		
System No.	Actual	Synthesized	% of Actual	Actual	Synthesized	% of Actual
1	1838	1845	100.4	1953	1941	99.4
2	1392	1329	95.5	705	587	83.2
3	927	915	98.7	1106	1065	96.4
4	740	720	97.3	463	391	84.4
5	477	457	95.8	698	674	96.6

Boiler/Chiller Plant

	Fuel			Total Electric		
Plant No.	Actual	Synthesized	% of Actual	Actual	Synthesized	% of Actual
1	2560	2578	100.7	1269	1266	[illegible]
2	1991	1909	95.9	956	940	[illegible]
3	1350	1335	98.8	1044	1032	[illegible]
4	1089	1060	97.3	869	855	[illegible]
5	704	676	96.1	917	911	[illegible]

Table A-5

Comparison of Energy Use Predicted Using Actual and Synthesized Weather Data for Madison, WI, and for a Building With Heavy Conductive Exterior

Loads

	Heating			Cooling		
Zone No.	Actual	Synthesized	% of Actual	Actual	Synthesized	% of Actual
1	84.32	82.68	98.1	38.82	33.05	85.1
2	93.51	93.53	100.0	36.96	32.90	96.9
3	93.35	93.16	99.8	36.71	32.31	88.0
4	99.06	99.66	100.6	29.03	26.46	91.1
5	0.0	0.0	---	353.41	353.09	99.9
6	16.98	16.82	99.0	39.62	38.6	97.4

Fan Systems

	Hot Water			Chilled Water		
System No.	Actual	Synthesized	% of Actual	Actual	Synthesized	% of Actual
1	1891	1913	101.2	1936	1928	99.6
2	1316	1336	101.5	536	498	492.9
3	913	925	101.3	992	980	98.8
4	689	699	101.4	313	276	88.2
5	387	386	99.7	537	520	96.9

Boiler/Chiller Plant

	Fuel			Total Electric		
Plant No.	Actual	Synthesized	% of Actual	Actual	Synthesized	% of Actual
1	2655	2684	101.1	1266	1264	99.8
2	1888	1913	101.3	932	924	99.1
3	1340	1357	101.2	1016	1014	99.8
4	1018	1032	101.3	838	829	99.0
5	586	586	100.0	885	882	99.6

Table A-6

Comparison of Energy Use Predicted Using Actual and Synthesized Weather Data for Madison, WI, and for a Building With Heavy, Insulated Exterior

Loads

	Heating			Cooling		
Zone No.	Actual	Synthesized	% of Actual	Actual	Synthesized	% of Actual
1	28.65	27.37	94.9	47.56	45.5	95.6
2	33.82	33.39	98.7	45.04	42.72	94.9
3	33.70	32.98	97.9	44.65	42.23	94.6
4	36.33	36.35	100.0	37.43	35.94	96.0
5	0.0	0.0	---	353.4	353.08	99.9
6	16.97	16.82	99.1	39.62	38.60	947.4

Fan Systems

	Hot Water			Chilled Water		
System No.	Actual	Synthesized	% of Actual	Actual	Synthesized	% of Actual
1	1647	1657	100.6	1960	1949	99.4
2	1078	1084	100.5	525	498	93.1
3	653	656	100.4	1002	990	98.8
4	435	436	100.1	312	279	89.3
5	150	145	96.4	572	563	98.4

Boiler/Chiller Plant

	Fuel			Total Electric		
Plant No.	Actual	Synthesized	% of Actual	Actual	Synthesized	% of Actual
1	2340	2350	100.4	1271	1268	99.8
2	1542	1548	100.4	931	924	99.3
3	979	984	100.5	1018	1016	99.8
4	686	689	100.4	837	830	99.1
5	256	253	98.7	889	887	99.7

Table A-7

Comparison of Energy Use Predicted Using Actual and Synthesized Weather Data for Fort Worth, TX, and for a Building With Glass Exterior

Loads

	Heating			Cooling		
Zone No.	Actual	Synthesized	% of Actual	Actual	Synthesized	% of Actual
1	22.96	15.70	68.4	153.04	151.55	99.0
2	35.50	29.55	83.2	154.29	146.6	95.0
3	36.46	30.65	84.1	139.95	132.8	94.7
4	46.89	42.66	91.0	99.50	93.85	94.3
5	0.0	0.0	---	364.68	364.32	99.9
6	4.38	3.53	80.6	61.88	60.14	97.2

Fan Systems

	Hot Water			Chilled Water		
System No.	Actual	Synthesized	% of Actual	Actual	Synthesized	% of Actual
1	1296	1270	98.0	2299	2255	98.1
2	849	814	95.8	1268	1091	86.0
3	435	417	95.9	1351	1322	97.9
4	312	292	93.5	909	803	88.3
5	146	122	83.6	987	962	97.5

Boiler/Chiller Plant

	Fuel			Total Electric		
Plant No.	Actual	Synthesized	% of Actual	Actual	Synthesized	% of Actual
1	1856	1826	98.4	1316	1313	99.8
2	1267	1217	96.1	1086	1053	97.0
3	658	632	96.1	1079	1078	99.9
4	478	455	95.1	975	956	98.1
5	235	204	86.7	959	958	99.8

Table A-8

Comparison of Energy Use Predicted Using Actual and Synthesized Weather Data for Fort Worth, TX, and for a Building With Heavy Conductive Exterior

Loads

	Heating			Cooling		
Zone No.	Actual	Synthesized	% of Actual	Actual	Synthesized	% of Actual
1	25.17	20.88	83.1	76.85	71.28	92.7
2	30.67	27.00	88.0	80.11	72.90	91.0
3	31.30	27.65	88.3	74.58	68.69	92.1
4	34.97	28.12	80.3	63.33	58.77	92.8
5	0.0	0.0	---	364.7	364.3	99.9
6	4.38	3.53	80.6	61.88	60.14	97.2

Fan Systems

	Hot Water			Chilled Water		
System No.	Actual	Synthesized	% of Actual	Actual	Synthesized	% of Actual
1	1434	1446	100.9	2218	2200	99.18
2	968	976	100.8	1178	1031	87.5
3	516	517	100.2	1192	1170	98.1
4	345	340	98.7	721	624	86.5
5	126	110	87.3	730	704	96.4

Boiler/Chiller Plant

	Fuel			Total Electric		
Plant No.	Actual	Synthesized	% of Actual	Actual	Synthesized	% of Actual
1	2037	2060	101.1	1302	1304	100.1
2	1411	1413	100.1	1069	1041	97.4
3	784	789	100.7	1046	1046	100.0
4	542	541	99.8	933	914	98.0
5	212	194	91.4	909	906	99.7

Table A-9

Comparison of Energy Use Calculated Using Actual and Synthesized Weather Data for Fort Worth, TX, and for a Building With Heavy, Insulated Exterior

Loads

	Heating			Cooling		
Zone No.	Actual	Synthesized	% of Actual	Actual	Synthesized	% of Actual
1	7.70	5.61	72.9	77.97	75.32	96.6
2	10.57	8.99	85.1	78.82	74.82	94.9
3	10.70	9.29	86.8	74.24	71.26	96.0
4	12.53	11.43	91.2	64.11	62.01	96.7
5	0.0	0.0	---	364.68	364.32	99.9
6	4.38	3.53	80.6	61.88	60.14	97.2

Fan Systems

	Hot Water			Chilled Water		
System No.	Actual	Synthesized	% of Actual	Actual	Synthesized	% of Actual
1	1360	1370	100.7	2224	2207	99.2
2	895	900	100.5	1175	1028	87.5
3	428	429	100.2	1181	1162	98.4
4	254	252	99.3	697	604	86.6
5	46	39	84.4	730	716	98.0

Boiler/Chiller Plant

	Fuel			Total Electric		
Plant No.	Actual	Synthesized	% of Actual	Actual	Synthesized	% of Actual
1	1935	1953	100.9	1303	1305	100.1
2	1300	1306	100.5	1068	1041	97.5
3	680	683	100.5	1044	1044	100.0
4	429	428	99.7	927	909	98.1
5	87	76	87.3	907	908	100.1

Table A-10

Comparison of Energy Use Predicted Using Actual and Synthesized Weather Data for Santa Maria, CA, and for a Building With Glass Exterior

Loads

	Heating			Cooling		
Zone No.	Actual	Synthesized	% of Actual	Actual	Synthesized	% of Actual
1	28.01	23.39	83.5	105.17	102.97	97.9
2	41.97	39.81	94.8	76.70	71.82	93.6
3	32.50	28.51	87.7	92.92	82.04	88.3
4	56.27	56.7	100.7	36.18	33.15	91.6
5	0.0	0.0	---	358.12	357.91	99.9
6	5.21	4.98	95.6	42.74	41.87	97.7

Fan Systems

	Hot Water			Chilled Water		
System No.	Actual	Synthesized	% of Actual	Actual	Synthesized	% of Actual
1	2541	2549	100.3	2941	2935	99.8
2	1136	1090	96.0	364	252	69.2
3	610	599	98.3	1082	1062	98.2
4	443	426	96.2	214	152	70.6
5	164	153	93.5	702	688	98.1

Boiler/Chiller Plant

	Fuel			Total Electric		
Plant No.	Actual	Synthesized	% of Actual	Actual	Synthesized	% of Actual
1	3503	3523	100.6	1540	1542	100.1
2	1675	1564	96.3	899	868	96.5
3	913	900	98.6	1049	1045	99.6
4	696	673	96.7	820	809	98.7
5	285	271	96.0	924	921	99.7

Table A-11

Comparison of Energy Use Predicted Using Actual and Synthesized Weather Data for Santa Maria, CA, and for a Building With Heavy, Conductive Exterior Walls

Loads

	Heating			Cooling		
Zone No.	Actual	Synthesized	% of Actual	Actual	Synthesized	% of Actual
1	33.50	31.69	94.6	29.74	27.29	91.7
2	40.89	40.48	99.0	25.70	23.67	92.1
3	36.63	35.81	97.8	27.28	23.82	87.3
4	48.25	48.49	100.5	17.54	16.12	91.9
5	0.0	0.0	---	358.12	357.91	99.9
6	5.21	4.98	95.5	42.74	41.87	97.7

Fan Systems

	Hot Water			Chilled Water		
System No.	Actual	Synthesized	% of Actual	Actual	Synthesized	% of Actual
1	1720	1727	100.4	1972	1969	99.8
2	1173	1179	100.5	183	138	75.6
3	725	730	100.7	940	991	100.1
4	503	505	100.5	98	69.7	71.1
5	165	161	97.8	504	493	97.9

Boiler/Chiller Plant

	Fuel			Total Electric		
Plant No.	Actual	Synthesized	% of Actual	Actual	Synthesized	% of Actual
1	2449	2460	100.4	1284	1284	100.0
2	1654	1656	100.1	861	855	99.3
3	1081	1089	100.8	1031	1031	100.0
4	790	796	100.7	792	789	99.6
5	297	294	98.9	884	882	99.8

Table A-12

Comparison of Energy Use Predicted Using Actual and Synthesized Weather Data for Santa Maria, CA, 1955, and for a Building With Heavy, Insulated, Exterior Walls

Loads

	Heating			Cooling		
Zone No.	Actual	Synthesized	% of Actual	Actual	Synthesized	% of Actual
1	8.40	7.32	87.1	50.80	49.65	97.7
2	11.96	11.64	97.3	45.53	44.32	97.3
3	10.49	9.72	92.6	49.14	46.65	94.9
4	14.89	15.00	100.7	36.94	36.03	94.9
5	0.0	0.0	---	358.12		
6	5.21	4.98	95.5	42.74	41.87	97.7

Fan Systems

	Hot Water			Chilled Water		
System No.	Actual	Synthesized	% of Actual	Actual	Synthesized	% of Actual
1	1541	1546	100.3	1987	1984	99.8
2	997	1000	100.3	183	138	75.6
3	540	542	100.5	1005	1001	99.6
4	335	336	100.3	105	76	72.6
5	51	49	95.4	590	581	98.5

Boiler/Chiller Plant

	Fuel			Total Electric		
Plant No.	Actual	Synthesized	% of Actual	Actual	Synthesized	% of Actual
1	2209	2217	100.3	1287	1287	100.0
2	1414	1427	100.2	861	855	99.3
3	841	844	100.3	1033	1032	99.9
4	557	559	100.4	792	788	99.5
5	102	98	96.4	898	897	99.9

VITA

Douglas C. Hittle was born on April 16, 1947, in Fort Collins, Colorado. He earned a Bachelor of Science degree in Mechanical Engineering in 1969 and a Master of Science degree in Environmental Engineering in 1975, both at the University of Illinois, Urbana-Champaign.

Mr. Hittle has engaged in a full-time engineering career since June 1969, when he joined the Base Civil Engineer's staff at Chanute Air Force Base, Rantoul, Illinois, as a mechanical engineer having design, inspection, and trouble-shooting responsibilities for large air-conditioning and other mechanical systems. In June 1973, he joined the U.S. Army Construction Engineering Research Laboratory (CERL), Champaign, Illinois, where he now serves as a team leader in the Energy Systems Division. At CERL, Mr. Hittle has been responsible for providing technical guidance to research teams performing energy-related research and development including the development of the Building Loads Analysis and System Thermodynamics (BLAST) computer program for simulating energy use in buildings and the development of simplified procedures for predicting the performance of solar energy systems.

Mr. Hittle was named the CERL Researcher of the Year in 1976, received the Department of the Army Research and Development

Achievement Award in 1977, and was awarded a Year of Advanced Study in 1979. He is a member of Sigma Xi research honorary society.

Mr. Hittle is also active in the American Society of Heating, Refrigeration, and Air-Conditioning Engineers, where he serves on the Technical Committee on Energy Calculation, the Subcommittee on Simplified Energy Calculations, Panel 10 of the Standards Committee for Energy Conservation in New Buildings, and as chairman of the Subcommittee on System Simulation. He is also a member of the subgroup on Heating and Climatization of the International Council for Building Research Studies and Documentation (CIB).

Mr. Hittle's publications include:

Hittle, D. C.: A Comparison of Building Energy Use Calculated with Actual and Synthesized Weather Data, ASHRAE Trans., Vol. 85, Part II, 1979.

Hittle, D. C.: The Building Loads Analysis and System Thermodynamics Program--BLAST, Proceedings of the Third International Symposium on the Use of Computers for Environmental Engineering Related to Buildings, May 1978.

Hittle, D. C., and D. L. Herron: Simulation of the Performance of Multizone and Variable Volume HVAC Systems in Four Geographical Locations, ASRAE Trans., Vol. 83, Part I, 1977.

Alereza, T., B. Hinkle, D. C. Hittle, and L. Windingland: Development of a Non-Computerized Method to Determine Energy Utilization in Residential and Commercial Buildings, ASHRAE Trans., Vol. 83, Part I, 1977.

Hittle, D. C., G. N. Walton, and D. F. Holshouser: Method for Estimating Solar Heating and Cooling System Performance, ASHRAE Trans., Vol. 82, Part II, 1976.

Hittle, D. C., and J. J. Stukel: Particle Size Distribution and Chemical Composition of Coal-Tar Fumes, Am. Ind. Hyg. Assoc. J., Vol. 37, No. 4, April 1976.

Terrill, W. R., A. Kirpich, and D. C. Hittle: Solar Heating and Cooling of Army Buildings, Proceedings of the Tenth Intersociety Energy Conversion Engineering Conference, 1975.

CERL DISTRIBUTION

Chief of Engineers
ATTN: Tech Monitor
ATTN: DAEN-ASI-L (2)

Waterways Experiment Station
ATTN: Library

Cold Regions Research Engineering Lab
ATTN: Library

US Government Printing Office
Receiving Section/Depository Copies (2)

Defense Technical Information Center
ATTN: DDA (12)

Engineering Societies Library
New York, NY

FESA, ATTN: Library

ETL, ATTN: Library

Engr. Studies, Center, ATTN: Library

Inst. for Water Res., ATTN: Library

Army Instl. and Major Activities (CONUS)
DARCOM - Dir., Inst., and Services
FORSCOM Engineer, ATTN: AFEN-FE
TRADOC, ATTN: ATEN-FE

US Military Academy
ATTN: Dept of Geography and
Computer Science

USAES, Fort Belvoir, VA
ATTN: Engineer Library

Chief Inst. Div., I&SA, Rock Island

USA ARRCOM, ATTN: Dir., Instl & Svc

TARCOM, Fac. Div.

TECOM, ATTN: DRSTE-LG-F

TSARCOM, ATTN: STSAS-F

NARAD COM, ATTN: DRDNA-F

AMMRC, ATTN: DRXMR-WE

Norton AFB, ATTN: AFRCE-MX/DEE

Fort Belvoir, VA 22060
ATTN: DRDME-G
ATTN: FESA-TSD
ATTN: Canadian Liaison Officer (2)

Naval Civil Engineering Laboratory
ATTN: Code L03AE
ATTN: Code L08A
ATTN: Code L60

Alexandria, VA 22314
ATTN: DLA-W
ATTN: DRCIS

Tyndall AFB, FL 32403, ATTN: RD

Wright-Patterson AFB, OH, 45433, ATTN: POE

WASH, DC
DCNO (Logistics)
ODAS (EE&S)
ODAS (I&H)
HQDA (DALO-TSE-F) (3)
Office of Planning & Development, OFEPM
Director, Bldg Technology & Safety Div
Public Building Service
Ass't Sec for Conservation & Solar Energy
Ass't Sec for Resource Applications
National Institute of Building Sciences
Director, Center for Building Technology
Energy Research and Development Foundation

Dept of Energy
Oak Ridge, TN 37830

G. P. Mitalis
Nat'l Research Council, Ottawa, Canada

Gren Yuel
Unies Ltd., Winnepeg, Canada

Gideon Shavit
Honeywell, Arlington Heights, IL

Dr. Tamami Kusuda
Thermal Engr Section, NBS, WASH, DC

Dave Low, IBM Scientific Center, Los Angeles

Taghi Alereza
ADM Associates, Inc., Sacramento, CA

USA ARRADCOM, ATTN: DRDAR-LCM-SP

Hittle, Douglas C.
Calculating building heating and cooling loads using the frequency response of multi-layered slabs. -- Champaign, IL : Construction Engineering Research Laboratory ; available from NTIS, 1981.
207 p. (Technical manuscript ; E-169)

1. Buildings -- energy consumption-mathematical models. 2. Heating load-mathematical models. 3. Cooling load-mathematical models. I. Title. II. Series: U. S. Army. Construction Engineering Research Laboratory. Technical manuscript ; E-169.

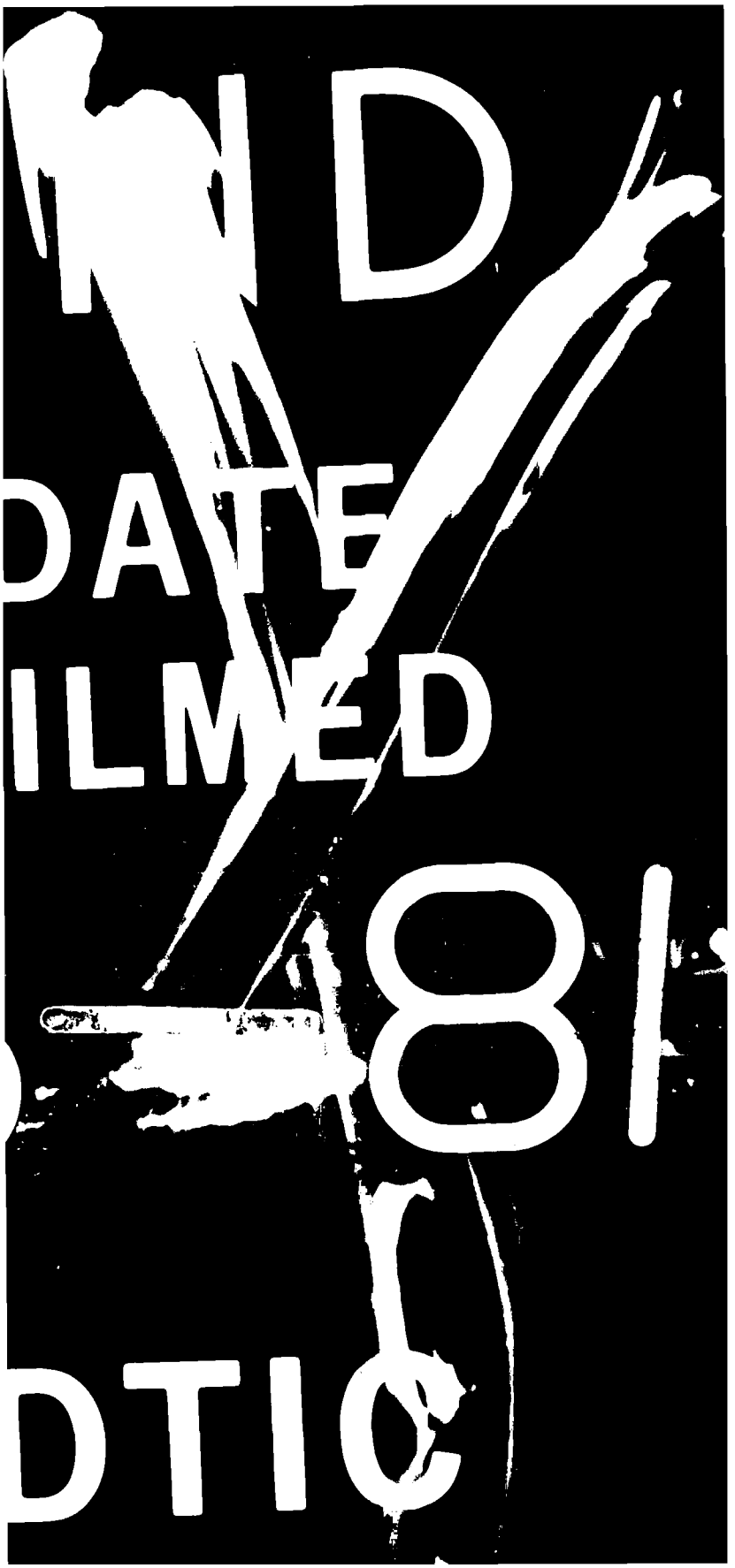
D
DATE
ILMED
81
DTIC

AD-A097 597 NORTHWESTERN UNIV EVANSTON ILL FLD 1
A STUDY OF MALINGERING ON THE CVS ABBREVIATED INDIVIDUAL INTELL--ETC(U)
SEP 51 P P POLLACZEK N60RI15801
UNCLASSIFIED NOFORN

END
DATE FILMED
5-82
DTIC

SUPPLEMENTARY

INFORMATION

ERRATA

Technical Manuscript E-169, *"Calculating Building Heating and Cooling Loads Using the Frequency Response of Multilayered Slabs"*, by D. C. Hittle (February, 1981) ADA097597.

Page 24: [Eq 2-16]

Replace: $B = (\sinh (\ell \sqrt{s/\alpha})) T_2(s) - \frac{\cosh(\ell \sqrt{s/\alpha})}{k \sqrt{s/\alpha}}$

with: $B = (\sinh (\ell \sqrt{s/\alpha})) T_2(s) - \frac{\cosh(\ell \sqrt{s/\alpha})}{k \sqrt{s/\alpha}} q_2(s)$

Page 32: first line:

Replace: $R_n C_{pn}$

with: $R_n C_n$

Page 34: figure 2 - 3

Replace: labels of dashed lines:

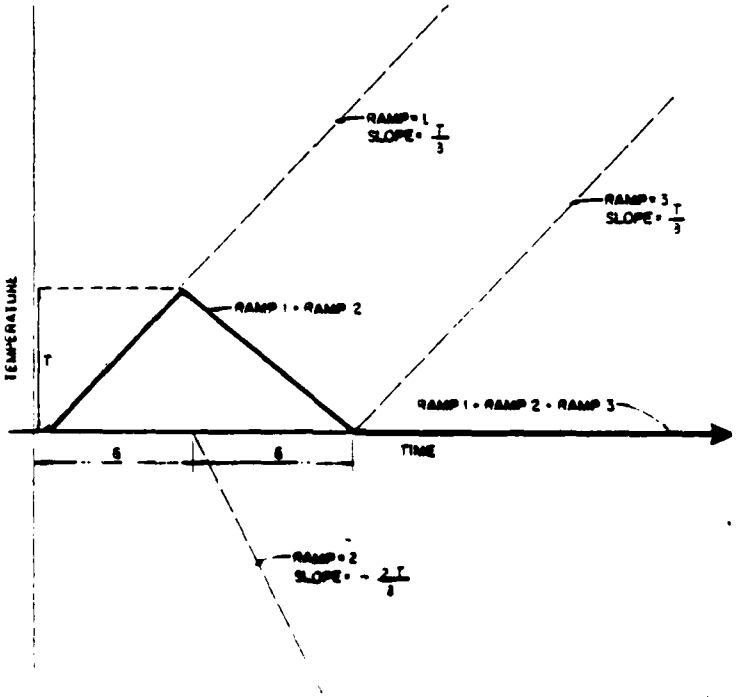

Figure 2-3. The triangular pulse is the sum of the three ramps.

ERRATA for Technical Manuscript E-169 (Cont'd)

Page 37: [Eq 2-42]

Replace:

$$r_n = \left. \frac{-\sqrt{sR_1C_1}\, e^{st}}{\frac{d}{ds}[R_1 s^2 \sinh \sqrt{sR_1C_1}} \right|_{s=\frac{-n^2\pi^2}{R_1C_1}} = \frac{-\sqrt{-n^2\pi^2}\, e^{-tn^2x^2/R_1C_1}}{R_1 \frac{n^4\pi^4}{R_1C_1} \frac{\cosh \sqrt{-n^2\pi^2}}{2\sqrt{-n^2n^2}}}$$

with:

$$r_n = \left. \frac{-\sqrt{sR_1C_1}\, e^{st}}{\frac{d}{ds}[R_1 s^2 \sinh \sqrt{sR_1C_1}} \right|_{s=\frac{-n^2\pi^2}{R_1C_1}} = \frac{-\sqrt{-n^2\pi^2}\, e^{-tn^2x^2/R_1C_1}}{R_1 \frac{n^4\pi^4}{R_1C_1} \frac{\cosh \sqrt{-n^2\pi^2}}{2\sqrt{-n^2n^2}}}$$

Note lower case s^2

Page 37: just after [Eq 2-42] the phrase:

Replace the phrase:

Now, $\cosh \sqrt{-n^2\pi^2} = \cos(jn\pi) = (-1)^n$

with: Now, $\cosh \sqrt{-n^2\pi^2} = \cos(n\pi) = (-1)^n$

Page 39: just after [Eq 2-49]

Replace the phrase:

Similarly, for any incremental time, $m\delta$, where m is greater than or equal to 3:

with: Similarly, for any incremental time, $m\delta$, where m is greater than or equal to 3:*

and add footnote:

*It is actually valid for $m = 2$ also, but the convergence is too slow to make it useful; the remainder, which is dropped, is proportional to $\frac{1}{n^2}$.

ERRATA for Technical Manuscript E-169 (Cont'd)

Page 47: [Eq 2-66]

Replace:

$$q_1(2\delta) = T_i X_2 - T_o X_2$$

with:

$$q_1(2\delta) = T_i X_2 - T_o Y_2$$

Page 49: footnote at bottom

Replace:

$$P(s) = \frac{1}{\delta s^2} \qquad 0 \leq t \leq \delta$$

$$P(s) = (1-2e^{-s\delta})/\delta s^2 \qquad \delta \leq t \leq 2\delta$$

$$P(s) = (1-2e^{-s\delta} + e^{-2s\delta})/\delta s^2 \qquad t \geq 2\delta$$

with:

$$P(s) = (1-2e^{-s\delta} + e^{-2s\delta})/\delta s^2$$

Page 51: first line

Replace: This is the positive X-directed.....

with: This is the positive x-directed....

Page 51: [Eq 2-76]

Replace:

$$B(s) = \ldots\ldots\ldots\ldots\ldots + \frac{R_1}{\sqrt{R_1 C_1}} \cosh \sqrt{sR_2C_2} \sinh \sqrt{sR_1C_1}$$

ERRATA for Technical Manuscript E-169 (Cont'd)

with:

$$B(s) = \cdots\cdots\cdots\cdots\cdots + \frac{R_1}{\sqrt{sR_1C_1}} \cosh \sqrt{sR_2C_2} \sinh \sqrt{sR_1C_1}$$

(Insert s)

Page 53: just above [Eq 2-80]

Replace: The y response .....

with: The Y response .....

Page 55: top line

Replace:

$$\frac{d}{ds}\begin{bmatrix} & \\ & \end{bmatrix} = \begin{bmatrix} \frac{dA(s)}{ds} & \frac{dB(s)}{ds} \\ \frac{dc(s)}{ds} & \frac{dD(s)}{ds} \end{bmatrix} = \begin{bmatrix} & \\ & \end{bmatrix}$$

with:

$$\frac{d}{ds}\begin{bmatrix} & \\ & \end{bmatrix} = \begin{bmatrix} \frac{dA(s)}{ds} & \frac{dB(s)}{ds} \\ \frac{dC(s)}{ds} & \frac{dD(s)}{ds} \end{bmatrix} = \begin{bmatrix} & \\ & \end{bmatrix}$$

Note upper case C

Page 56: [Eq 2-87]

Replace: $q_{o,t} = T_i \sum_{m=1}^{\infty} y_m$ .....

with:

$$q_{o,t} = T_i \sum_{m=1}^{\infty} Y_m \text{ .....}$$

Page 57: mid-page paragraph: (3rd line of)

Replace: Recall that n .....
on the .....
increases .....R_1 = .4 m^2 - $^oK/w$ and

with: Recall that n .....
on the .....
increases .....R_1 = .4 m^2 - $^oK/W$ and

Page 57: last line

Replace:	6	-126.17×10^{-5}	-4.5423	.0149	-9500.7
with:	6	-126.17×10^{-5}	-4.5423	.0106	-9500.7

Page 58: 5th line

Replace: contribution caused ..... $Y_m \simeq g_1 \overset{m}{1} + g_2\lambda_2^m$.

with: contribution caused ..... $Y_m \simeq g_1 \lambda_1^m + g_2\lambda_2^m$.

Page 59: 4th line from the bottom

Replace: Notice that .....T_o, t-m+1

with: Notice that .....T_o, t-m'+1

ERRATA for Technical Manuscript E-169 (Cont'd)

Page 60: [Eq 2-98]

Replace: $q_{i,t} = -\sum_{m=1}^{m'} \ldots\ldots\ldots\ \lambda_1 q_{i,t}$

with: $q_{i,t} = -\sum_{m=1}^{m'} \ldots\ldots\ldots\ \lambda_1 q_{i,t-1}$

Page 61: 5th line

Replace: factors until .....small function of the ...

with: factors until .....small fraction of the ...

Page 64: [Eq 2-112]

Replace:

$$q_{i,t} = \sum_{m=1}^{m''} \ldots\ldots\ldots\ldots\ + (\lambda_1+\lambda_2)q_{i,t-1} - \lambda_1 q_{i,t-2}$$

with:

$$q_{i,t} = \sum_{m=1}^{m''} \ldots\ldots\ldots\ldots\ + (\lambda_1+\lambda_2)q_{i,t-1} - \lambda_1\lambda_2 q_{i,t-2}$$

Page 64: [Eq 2-113]

Replace:

$$q_{o,t} = \sum_{m=1}^{m''} \ldots\ldots\ldots\ldots\ - \lambda_1 q_{o,t-2}$$

with:

$$q_{o,t} = \sum_{m=1}^{m''} \ldots\ldots\ldots\ldots\ - \lambda_1\lambda_2 q_{o,t-2}$$

ERRATA for Technical Manuscript E-169 (Cont'd)

Page 64: [Eq 2-114]

Replace:

$$q_{1,t} = \sum_{m=1}^{M} \ldots\ldots\ldots\ldots + \sum_{m=1}^{k} F_m q_{i,t-k}$$

with:

$$q_{1,t} = \sum_{m=1}^{M} \ldots\ldots\ldots\ldots + \sum_{m=1}^{k} F_m q_{i,t-m}$$

Page 64: [Eq 2-115]

Replace:

$$q_{o,t} = \sum_{m=1}^{M} \ldots\ldots\ldots\ldots + \sum_{m=1}^{k} F_m q_{i,t-k}$$

with:

$$q_{o,t} = \sum_{m=1}^{M} \ldots\ldots\ldots\ldots + \sum_{m=1}^{k} F_m q_{o,t-m}$$

Page 65: next to last line

Replace: The practical ..... transfer function and a ...

with: The practical ..... transfer functions and a ...

Page 68: [Eq 2-126]

Replace:

$$\sum_{m=1}^{M} Y_{k,m} = \sum_{m-1}^{M} Y_{k,m} = \sum_{m=1}^{M} Z_{k,m} = U \prod_{i=1}^{k} (1-\lambda_i)$$

with:

$$\sum_{m=1}^{M} X_{k,m} = \sum_{m=1}^{M} Y_{k,m} = \sum_{m=1}^{M} Z_{k,m} = U \prod_{i=1}^{k} (1-\lambda_i)$$

ERRATA for Technical Manuscript E-169 (Cont'd)

Page 68: last line

Replace: the test of Equation 2-125 is applied for successively increasing

with: the test of Equation 2-126 is applied for successively increasing

Page 69: second line

Replace: made for k < M. As .....Equation 2-125.....

with: made for k < M. As .....Equation 2-126.....


DATE
ILME